

Electronic Thesis and Dissertation Repository

11-21-2022 11:30 AM

The Effect of Oral and Topical Antibiotics on Foreskin Inflammation and HIV Target Cells in Ugandan Men.

Zhongtian (Eric) Shao, *The University of Western Ontario*

Supervisor: Prodger, Jessica L, *The University of Western Ontario*

A thesis submitted in partial fulfillment of the requirements for the Master of Science degree in Microbiology and Immunology

© Zhongtian (Eric) Shao 2022

Follow this and additional works at: <https://ir.lib.uwo.ca/etd>



Part of the [Virus Diseases Commons](#)

Recommended Citation

Shao, Zhongtian (Eric), "The Effect of Oral and Topical Antibiotics on Foreskin Inflammation and HIV Target Cells in Ugandan Men." (2022). *Electronic Thesis and Dissertation Repository*. 9053.
<https://ir.lib.uwo.ca/etd/9053>

This Dissertation/Thesis is brought to you for free and open access by Scholarship@Western. It has been accepted for inclusion in Electronic Thesis and Dissertation Repository by an authorized administrator of Scholarship@Western. For more information, please contact wlsadmin@uwo.ca.

Abstract

Penile circumcision reduces HIV susceptibility by up to 60% in men; however, many men prefer to remain uncircumcised for personal or cultural reasons. Penile circumcision protects against HIV by reducing anaerobic bacteria on the penis. Penile anaerobes cause local inflammation and the recruitment of HIV-susceptible CD4+CCR5+ cells, increasing the likelihood that exposure to HIV during intercourse results in infection. To determine if a non-surgical intervention can reduce penile anaerobes and HIV target cells, we randomized men to antimicrobial treatment prior to circumcision. To be able to quantify the effect of antimicrobials, we developed a novel deep-learning algorithm to quantify HIV target cells in immunofluorescent microscopy images of foreskin. We found that men who received antimicrobials had a lower density of HIV target cells, which correlated with reductions in penile anaerobes and secreted inflammatory mediators. These results suggest that microbiome-based interventions could be a potential tool for HIV prevention.

Keywords

Human Immunodeficiency Virus, Susceptibility, Prevention, Microbiome, Anaerobic Bacteria, Inflammation, T Lymphocytes, Immunofluorescent Microscopy, Deep Learning, Foreskin, Circumcision

Summary for Lay Audience

Male circumcision has been shown to be able to reduce the risk of acquiring HIV by up to 60% in men. Despite these benefits, many at-risk men still choose to not undergo this procedure and it is not completely understood how circumcision can have a protective effect against HIV infection. One way that circumcision protects against HIV is by eliminating specific species of anaerobic bacteria that have been shown to recruit HIV-susceptible cells in the penis. To determine if a non-surgical intervention could similarly eliminate anaerobes from the penis, we completed a clinical trial testing the effect of commonly available antibacterial agents on penile bacteria and the abundance of HIV-susceptible cells in penile tissue. To accomplish this, we developed a machine learning program to automatically analyze and quantify HIV target cells in microscopy images generated from tissues collected after the course of antimicrobials. We found that antibiotic treatments reduced penile bacteria, inflammation, and abundance of HIV-susceptible cells. The results from this study shown that antibiotic treatment could be used as a potential tool for HIV prevention.

Co-Authorship Statement

I hereby declare that this thesis incorporates material that is result of joint research, as follows:

Chapters 1, 2, 3, and 4 include the description of a randomized clinical trial exploring the effect of antimicrobials on the penile microbiota, immunology, and HIV susceptibility in Ugandan men. Tissues and data collected during this trial were the basis for this thesis. The trial was conceived by Rupert Kaul (Departments of Immunology and Medicine, University of Toronto, Canada). Rupert Kaul and Ronald M Galiwango (Departments of Immunology and Medicine, University of Toronto, Canada) initiated and designed the clinical trial. Other co-authors on the published clinical trial protocol include Bernard Bagaya (International Aids Vaccine Initiative, Uganda Virus Research Institute, Uganda), Juliet Mpendo (International Aids Vaccine Initiative, Uganda Virus Research Institute, Uganda), Vineet Joag (Departments of Immunology and Medicine, University of Toronto, Canada), Brenda Okech (International Aids Vaccine Initiative, Uganda Virus Research Institute, Uganda), Annet Nanvubya (International Aids Vaccine Initiative, Uganda Virus Research Institute, Uganda), Ali Ssetaala (International Aids Vaccine Initiative, Uganda Virus Research Institute, Uganda), and Moses Muwanga (Entebbe General Hospital, Uganda). These co-authors contributed to implementation of the study.

Chapter 2 and 4 incorporate unpublished data, from the randomized clinical trial (RCT), generated by other investigators. Soluble inflammatory molecules were measured by R Kaul and RM Galiwango at the University of Toronto, Canada. In vitro HIV pseudovirus entry assays were completed by RM Galiwango at the Uganda Virus Research Institute, Entebbe, Uganda. Penile microbiome data was generated by Cindy M Liu, Dan Park, Tony Pham, and Juan Salazar (all at the Department of Environmental and Occupational Health, George Washington University, USA). Data analysis, graphing, interpretation, and writing of results incorporating this data (soluble inflammatory molecules, HIV pseudovirus entry, and microbiome) was completed by myself (100%) under the supervision of my supervisor Jessica L Prodder.

Chapters 2, 3, and 4 contain data generated by immunofluorescent microscopy of tissues samples collected during the RCT, Lane B Buchanan (PhD Candidate, Department of Microbiology and Immunology, The University of Western Ontario, Canada) designed the protocols used for immunofluorescent staining (100%). I generated the protocol for staining RCT samples and performed all sectioning, staining, and microscopy image acquisition (100%).

Chapters 2, 3, and 4 describe two methods for the quantification of HIV target cells in foreskin tissue: (1) pixel-based automated analysis algorithms and (2) machine learning algorithms for cell counting. The pixel-based algorithms were previously described in a book chapter authored by myself and the following other co-authors: LB Buchanan, Yuan Chung Jiang (Department of Microbiology and Immunology, The University of Western Ontario, Canada), Abbie Lai (Department of Medicine, McMaster University, Canada), Thomas J Hope (Department of Cell and Developmental Biology, Northwestern University, USA), Ann M Carias (Department of Cell and Developmental Biology, Northwestern University, USA),

and JL Prodger. In all cases only my primary contributions towards these publications are included in this thesis. LB Buchanan and I are the primary authors of the book chapter. LB Buchanan and I contributed to the writing of the manuscript. YC Jiang, A Lai, and I contributed to the development of the algorithms described in the book chapter. JL Prodger oversaw the development of the algorithms and provided feedback on refinement of ideas for the writing. My contribution to the portions of the book chapter included in this thesis is 90%. The machine learning algorithm was designed in collaboration with Ali Khan (Department of Medical Biophysics, The University of Western Ontario, Canada). My contribution to the design and writing of scripts for this algorithm is 30%. I completed all the training for the algorithm and generated all images used for training (100%).

I am aware of the University of Western Ontario Senate Policy on Authorship, and I certify that I have properly acknowledged the contribution of other researchers to my thesis and have obtained written permission from each of the co-author(s) to include the above material(s) in my thesis. I certify that, with the above qualification, this thesis, and the research to which it refers, is the product of my own work. This thesis includes 2 original papers that have been previously published/submitted to journals for publication, as follows:

Thesis Chapter	Publication title/full citation	Publication Status
Chapter 1, 2, 3, 4	Galiwango RM, Bagaya B, Mpendo J, Joag V, Okech B, Nanvubya A, Ssetaala A, Muwanga M, Kaul R. Protocol for a randomized clinical trial exploring the effect of antimicrobial agents on the penile microbiota, immunology and HIV susceptibility of Ugandan men. <i>Trials</i> . 2019 Jul 19;20(1):443. doi: 10.1186/s13063-019-3545-7. PMID: 31324206; PMCID: PMC6642556.	Published
Chapter 2, 3	Buchanan LB, Shao Z, Jiang YC, Lai A, Hope TJ, Carias AM, Prodger JL. Quantitative Immunofluorescent Imaging of Immune Cells in Mucosal Tissues. <i>Methods Mol Biol</i> . 2022;2440:143-164. doi: 10.1007/978-1-0716-2051-9_9. PMID: 35218538.	Published

I certify that I have obtained a written permission from the copyright owner(s) to include the above published material(s) in my thesis. I certify that the above material describes work completed during my registration as a graduate student at the University of Western Ontario.

I declare that, to the best of my knowledge, my thesis does not infringe upon anyone's copyright nor violate any proprietary rights and that any ideas, techniques, quotations, or any other material from the work of other people included in my thesis, published or otherwise, are fully acknowledged in accordance with the standard referencing practices. Furthermore, to the extent that I have included copyrighted material that surpasses the bounds of fair dealing within the meaning of the Canada Copyright Act, I certify that I have obtained a written permission from the copyright owner(s) to include such material(s) in my thesis. I declare that this is a true copy of my thesis, including any final revisions, as approved by my thesis committee and the Graduate Studies office, and that this thesis has not been submitted for a higher degree to any other University or Institution.

Acknowledgments

I would like to acknowledge the staff at Entebbe General Hospital and UVRI-IAVI for their help with the implementation of the randomized clinical trial described in this thesis. I would like to thank Dr. Rupert Kaul and Dr. Ronald Galiwango for providing the raw data for the soluble inflammatory mediator analysis and in vitro pseudovirus entry analysis described in this thesis. I would like to thank Dr. Cindy Liu, Mr. Dan Park, Mr. Tony Pham, and Mr. Juan Salazar for providing the raw data for the penile microbiome analysis described in this thesis. I would like to thank my supervisor Dr. Jessica Prodger and my advisory committee members Dr. Ryan Troyer, Dr. Eric Arts, and Dr. Rupert Kaul for their help in editing this thesis and providing advice on experimental design and data analysis. I would like to thank my fellow lab members Mr. Lane B. Buchanan, Dr. David Zuanazzi, Ms. Hannah Wilcox, and Ms. Shirley Constable for their advice on experimental design and data analysis.

Table of Contents

Abstract.....	ii
Summary for Lay Audience.....	iii
Co-Authorship Statement.....	iv
Acknowledgments.....	vi
Table of Contents.....	vii
List of Tables (where applicable)	xi
List of Figures.....	xii
List of Abbreviations	xiv
Chapter 1.....	1
1 Introduction.....	1
1.1 HIV prevention strategies	1
1.2 Voluntary penile circumcision for HIV prevention	1
1.3 Immunopathogenesis of HIV in the foreskin.....	2
1.4 Mucosal inflammation is critical to acquiring HIV	3
1.5 Penile anaerobes are associated with HIV seroconversion, inflammation, and immune cells.....	4
1.6 Proving the role of the foreskin microbiome in HIV susceptibility.....	5
1.7 Objectives	6
Chapter 2.....	8
2 Randomized Clinical Trial Methods	8
2.1 Study Overview	8
2.2 Study Design.....	8
2.2.1 Study sites:	8
2.2.2 Study population:	9
2.2.3 Randomization and blinding.....	9

2.2.4	Treatment group assignment.....	11
2.2.5	Study procedures, visits, and sampling.....	12
2.2.6	Lost to follow-up status and reimbursement.....	13
2.2.7	Study outcomes.....	13
2.2.8	Trial status and summary.....	13
2.3	Biological sample processing.....	14
2.3.1	Blood collection and processing.....	14
2.3.2	Genital swab collection and handling.....	14
2.3.3	Urine collection and handling.....	14
2.3.4	Foreskin collection and processing.....	15
2.4	Laboratory assays completed by collaborators.....	16
2.4.1	Penile microbiome characterization.....	16
2.4.2	Multiplex ELISA for soluble inflammatory molecule quantification.....	17
2.4.3	Pseudovirus cell entry assay.....	17
2.5	Statistical and ethics considerations.....	18
2.5.1	Sample size.....	18
2.5.2	Ethics and Patient involvement.....	18
Chapter 3	20
3	Comparison between a deep-learning and a pixel-based approach for the automated quantification of HIV target cells in foreskin tissue.	20
3.1	Introduction.....	20
3.1.1	Understanding HIV infection at the site of exposure.....	20
3.1.2	Using immunofluorescent microscopy to quantify immune cells in the genital mucosa.....	21
3.1.3	Existing strategies for automated cell segmentation in immunofluorescent microscopy images of mucosal tissue.....	25
3.2	Materials and Methods.....	29

3.2.1	Tissue Source	29
3.2.2	Immunofluorescence microscopy	29
3.2.3	Manual counting of HIV Target Cells	32
3.2.4	Pixel-based cell counting using Fiji and CellProfiler	32
3.2.5	Annotation of images for StarDist model training in Labkit	36
3.2.6	StarDist model training	37
3.2.7	StarDist model validation	38
3.2.8	StarDist model performance in high autofluorescence or high cell density areas	39
3.2.9	Statistical Analysis.....	40
3.3	Results.....	41
3.3.1	Automated HIV target cell segmentation using StarDist is comparable to manual counting and more accurate than pixel-based cell segmentation .	41
3.3.2	StarDist does not have issue with systematic overcounting or undercounting in different tissue regions.....	46
3.3.3	Automated cell segmentation with StarDist is robust in areas with high cell density or high autofluorescence.	49
3.3.4	Accuracy of custom StarDist model rapidly improves with additional training images.....	53
3.4	Discussion.....	56
Chapter 4.....		61
4	Effect of antimicrobial treatments on the penile microbiome, inflammation, and HIV target cells	61
4.1	Introduction.....	61
4.2	Methods.....	62
4.2.1	Quantification of HIV target cell availability using immunofluorescence microscopy	62
4.2.2	Pixel-based quantification of HIV target cells by determine the percent coverage of tissue area	64
4.2.3	Statistical analysis.....	67

4.3 Results.....	68
4.3.1 Effect of antimicrobial treatments on the abundance of penile bacteria... 68	
4.3.2 Effect of antimicrobial treatments on the density of HIV target cells in the foreskin	70
4.3.3 HIV target cell density is higher in the inner foreskin.....	75
4.3.4 Soluble inflammatory molecules correlate with HIV target cells density	77
4.3.5 High absolute abundance of BASIC species, but not overall bacterial load, is associated with HIV target cell density.....	83
4.4 Discussion.....	88
Chapter 5.....	95
5 Overall Summary and Future Directions	95
References or Bibliography	98
Curriculum Vitae	114

List of Tables (where applicable)

Table 1: Inclusion and exclusion criteria	10
Table 2: List of microscope filters and their designations	31
Table 3: Input parameters for pre-processing workflow used to improve accuracy of automated HIV target cell segmentation in foreskin tissue scans.....	35
Table 4: Input parameters for thresholding and segmentation for pixel-based quantification of HIV target cells in foreskin tissue scans	35
Table 5: Performance of StarDist deep-learning model surpasses the performance of a previous validated pixel-based method for HIV target cell segmentation.....	45
Table 6: StarDist is less likely to have issues with cell merging, cell splitting, or misidentification of autofluorescence as cells in tissue regions with high cell density or high autofluorescence when compared to automated pixel-based cell segmentation.....	52
Table 7: Proportion of CD3+ cell subsets in the inner foreskin of study participants.....	74

List of Figures

Figure 1: Visualization of the epidermis and dermis in foreskin tissue..... 23

Figure 2: Representative images of inner and outer foreskin tissue sections stained for the identification of HIV target cells. 24

Figure 3: Common methods used for automated cell segmentation in immunofluorescent microscopy images of mucosal tissue..... 28

Figure 4: Automated segmentation of HIV target cells in foreskin tissue images stained for CD3, CD4, CCR5 and nuclei using a pixel-based workflow and StarDist..... 43

Figure 5: Comparison of automated counts generated using StarDist with manual counting and automated counts generated using a pixel-based workflow..... 44

Figure 6: Automated cell segmentation using StarDist does not result in major overcounting or undercounting in different tissue regions. 48

Figure 7: Comparison of automated cell segmentation using StarDist and a pixel-based workflow in tissue regions with high cell density or high autofluorescence..... 51

Figure 8: Training images rapidly improve the accuracy of a custom StarDist model used for the quantification of HIV target cells in foreskin tissue. 55

Figure 9: Tissue area used for HIV target cell quantification in immunofluorescent microscopy images of foreskin tissue..... 63

Figure 10: Overview of pixel-based approach for the quantification of tissue area available for HIV entry (CD4+CCR5+ area) in foreskin tissue section scans..... 66

Figure 11: Topical antimicrobial treatments reduce total bacteria absolute abundance and BASIC species absolute abundance but not control taxa absolute abundance. 69

Figure 12: Effect of antimicrobial treatments on the abundance of HIV target cells in the foreskin. 73

Figure 13: Higher abundance of HIV target cells in found in the inner foreskin.	76
Figure 14: Inner foreskin CD3+ cell density is correlated with soluble inflammatory mediator levels in the coronal sulcus.	79
Figure 15: Inner foreskin CD3+CD4+CCR5+ cell density is correlated with soluble inflammatory mediator levels in the coronal sulcus.	80
Figure 16: Inner foreskin CD3-CD4+CCR5+ cell density is correlated with soluble inflammatory mediator levels in the coronal sulcus.	81
Figure 17: Percent coverage of inner foreskin CD4+CCR5+ tissue area is not correlated with soluble inflammatory mediator levels in the coronal sulcus.....	82
Figure 18: Men in the top quartile for abundance of BASIC species and men in the top quartile for abundance of control taxa have similar total bacterial abundance but differ in abundance for BASIC species.	85
Figure 19: High abundance of BASIC species is associated with recruitment of HIV target cells to the inner foreskin without alterations in T cell subset distribution.	87

List of Abbreviations

ART	Antiretroviral therapy
BASIC	A group of 6 bacterial species previously identified to be associated with HIV seroconversion, inflammation, and immune cells (<i>Peptostreptococcus anaerobius</i> , <i>Prevotella bivia</i> , <i>Prevotella disiens</i> , <i>Dialister propionificaciens</i> , <i>Dialister micraerophilus</i> , and a genetic near neighbor of <i>Dialister succinatiphilus</i>).
BlaM-Vpr	Beta-lactamase-Vpr Chimeric Protein
BP	Base pair
BV	Bacterial vaginosis
CCF2-AM	Lipophilic, esterified form of CCF2 substrate (substrate consisting of cephalosporin core linking 7-hydroxycourmarin to fluorescein).
CCR5	C-C chemokine receptor type 5
CD3	Cluster of differentiation 3
CD4	Cluster of differentiation 4
CUDA	Compute unified device architecture
DAPI	4',6-diamidino-2-phenylindole
DC-SIGN	Dendritic cell-specific intercellular adhesion molecule-3-grabbing non-integrin
DNA	Deoxyribonucleic acid
ELISA	Enzyme-linked immunosorbent assay
FBS	Fetal bovine serum
FDR	False Discovery Rate
FN	False negative
FNR	False negative rate
FOV	Field of view
FP	False positive
FRET	Fluorescence resonance energy transfer
HIV	Human Immunodeficiency virus
HPV	Human papillomavirus
HSV-2	Herpes simplex virus 2

IF	Immunofluorescence microscopy
IL-1 α	Interleukin-1 alpha
IL-1 β	Interleukin-1 beta
IL-8	Interleukin 8
LL-37	Human cathelicidin LL-37
MIG	Monokine induced by gamma interferon
MIP-1	Macrophage inflammatory protein 1
MMP-9	Matrix metalloproteinase 9
NMS	Non-maximum suppression
OCT	Optimal cutting temperature compound
PBS	Phosphate buffered saline
PC	Penile Circumcision
PCR	Polymerase chain reaction
PIPES	Piperazine-N,N'-bis(2-ethanesulfonic acid)
PPV	Positive predictive value
PrEP	Pre-exposure prophylaxis
qPCR	Quantitative polymerase chain reaction
R5 HIV	Strain of HIV that uses CCR5 as a co-receptor and CD4 as the main receptor to infect host cells
RANTES	Regulated upon activation, normal T cell expressed and secreted (also known as CCL5)
RCT	Randomized controlled trial
RNA	Ribonucleic acid
ROI	Region of interest
RPMI	Roswell Park Memorial Institute 1640 Medium
rRNA	Ribosomal ribonucleic acid
SLPI	Secretory leukocyte peptidase inhibitor
STI	Sexually transmitted infection
Th1 Cells	T helper 1 cells
Th17 Cells	T helper 17 cells
TIMP1	Tissue inhibitor of metalloproteinase 1
TP	True positive

TPR	True positive rate
T _{RM}	Resident memory T cells
UNAIDS	Joint united nations programme on HIV/AIDS
VEGF	Vascular endothelial growth factors
V _{pr}	HIV viral protein R

Chapter 1

1 Introduction

1.1 HIV prevention strategies

Over the past 4 decades, considerable progress has made in implementing HIV prevention strategies and improving the life expectancy of HIV infected individuals (1,2). While there is currently no cure for HIV, providing early and effective antiretroviral therapy (ART) for individuals infected with HIV significantly reduces the risk of further transmission to their partner and allows infected individuals to live long healthy lives. Furthermore, consistent use of antiretroviral drugs as prophylaxis (PrEP) by uninfected individuals can reduce their risk of acquiring HIV by up to 95% (3,4). However, despite the wide range of effective HIV prevention strategies that are available, according to estimates from UNAIDS, over 670,000 people acquired HIV in 2020 alone (5). HIV continues to be a major public health issue. While there has been a large scale-up of HIV treatment, the current rate of ART and PrEP provision is still outstripped by the global rate of new infections occurring each year (6,7). The effectiveness of current treatments in key populations is further threatened by the lack of political will to invest in and systematically implement HIV prevention programs in endemic countries and the emergence of antiretroviral drug resistance in eastern and southern Africa (8–11). The development of new strategies and continued adoption of other effective prevention tools tailored to reach key populations is essential for achieving steep reductions in new HIV infections (2,12,13).

1.2 Voluntary penile circumcision for HIV prevention

Voluntary penile circumcision (PC) has been recommended by UNAIDS and the WHO since 2007 as a part of a broader strategy for reducing new HIV infections in men. As demonstrated through three large randomized controlled trials, PC decreases HIV susceptibility in men by at least 60%. Safe PC remains the only one-time HIV prevention

method to date (14–16). PC campaigns are actively implemented in 15 priority countries in sub-Saharan Africa with high HIV prevalence and low PC rates (17,18). In addition to reducing HIV risk, PC has also been found to reduce acquisition of classical sexually transmitted infections (STI), such as herpes simplex virus type 2 (HSV-2) and high-risk strains of human papillomavirus (HR-HPV), and to reduce the prevalence of genital ulcerations among men (14–16,19–21). Asymptomatic HSV-2 infection is associated with a three-fold increase in HIV acquisition and the presence of genital ulcers is associated with an five-fold increase in HIV acquisition (22–24). PC is also associated with reduced acquisition of HR-HPV, BV, trichomoniasis, and genital ulcerations in the female partners of heterosexual men (25–27). Despite the benefits of PC, many eligible men still choose to not undergo this surgical procedure and PC programs are falling well short of their targets (1,5,18). The foreskin has previously been shown to be the main site of HIV acquisition in heterosexual men during sexual transmission (28–32). Due to the important role that the foreskin plays in HIV acquisition and the incomplete uptake of PC among at-risk men, it is important to develop new non-surgical prevention tools that can be offered to at risk men who choose to remain uncircumcised.

1.3 Immunopathogenesis of HIV in the foreskin

Sexual transmission of HIV occurs across the anogenital mucosa (penile, cervical, vaginal, rectal) exclusively through HIV strains that use CCR5 and CD4 as receptors for entry (33,34). In most cases of sexual HIV transmission, initial infection is typically acquired from a single virus genotype despite the diversity of HIV genotypes found in an infected partner's genital secretions (35,36). Sexual transmission of HIV is surprisingly inefficient (HIV is only transmitted in ~1/100 of penile-vaginal sex acts where the female partner is viremic) (24,37). A wide variety of factors contributes to risk of HIV transmission. Among these factors, the availability of CCR5+/CD4+ target cells in the at-risk partner's genital mucosa is a critical determinant of an individual's risk for HIV infection (38). A variety of immune cells present in the mucosa express these two receptors. Two dendritic cell subsets (epidermal Langerhans' cells and dermal DC-SIGN+ dendritic cells) can express CD4 and CCR5 and are abundant in the mucosa.

While human dendritic cells are resistant to productive infection with HIV-1, they can efficiently transmit intact, infectious virus particles to CD4⁺/CCR5⁺ T cells through a process called trans-infection (39,40). Among the two dendritic cell subsets, Langerhans' cells are especially important due to the proximity of these cells to the mucosal surface (39,41). In addition to dendritic cells, CCR5⁺/CD4⁺ T cells are critical to establishing HIV infection, and HIV pathogenesis and AIDS is caused by the progressive depletion of CD4 T cells systemically (42). Mucosal CD4 T cells subsets, including Th17 cells, Th1 cells, and CD4 T cell subsets that express the integrins $\alpha 4\beta 7$ or $\alpha 4\beta 1$, have been shown to be more susceptible to HIV infection than other CD4 T cell subsets (43–49). In animal models, in vivo HIV susceptibility has been associated with the number of mucosal CCR5⁺ CD4 T cells and/or $\alpha 4\beta 7$ ⁺ CD4 T cells (50,51). Previous work by our group has shown that men who remain seronegative despite regular unprotected sex with a viremic partner have reduced abundance of Th17 and activated CD4 T cells in their foreskin tissue (52). This suggests that the availability of specific highly susceptible HIV target cells is a key determinant of HIV susceptibility.

1.4 Mucosal inflammation is critical to acquiring HIV

In the absence of inflammation, dendritic cells are generally much more abundant than CD4 T cells in the genital mucosa. However, when the genital mucosa is inflamed, CCR5⁺ CD4 T cells are recruited into the mucosa, providing additional target cells for HIV that results in a state of increased HIV susceptibility. HIV preferentially infects and replicates in activated CD4 T cells and so inflammation may facilitate the establishment of productive mucosal infection by increasing both the density and the permissiveness of mucosal CD4 T cells available for infection (36,53–57). Additionally, local immune activation in the genital mucosa can also promote the maturation of dendritic cells, and dendritic cells that have been exposed to bacterial antigens are more proficient at facilitating trans-infection (39,58,59). All together, these findings emphasize the importance of the inflammatory state of the genital mucosa in the early stages of HIV acquisition. Bacterial STIs are strongly related to the transmission and acquisition of HIV infection. In women, vaginal levels of pro-inflammatory cytokines/chemokines IL-1 β , IL-

8 and RANTES, as well as innate immune factors such as α -defensins, LL-37 and lactoferrin which have pro-inflammatory properties, has been correlated with increased density of HIV target cells in the genital mucosa and HIV acquisition (60–63). In men, increase in penile levels of chemotactic cytokine IL-8 and MIG are directly associated with increased risk of HIV acquisition. Penile levels of IL-8 are correlated with the tissue density of CCR5+CD4 T cells and highly HIV-susceptible CD4 T cell subsets such including Th17 cells (64). Increased levels of antimicrobial peptides including α -defensins and secretory leukocyte protease inhibitor (SLPI), which are normally associated with innate immune response to bacterial pathogens, are also associated with HIV seroconversion (65).

1.5 Penile anaerobes are associated with HIV seroconversion, inflammation, and immune cells

Epidemiologic data suggest a link between genital anaerobes and HIV risk. Bacterial vaginosis (BV), which is characterized by the overgrowth of facultative and anaerobic bacteria in the vagina, has consistently been linked to increased HIV susceptibility in women and also to increased risk of transmission of HIV from HIV-positive females to their male partners (66–68). Bacterial vaginosis is a highly prevalent condition which affects almost one-third of women in the United States and even more women in sub-Saharan African countries (69,70). In most women, a healthy vaginal microbiome consists of predominantly of lactobacilli. Previous studies have shown that in sub-Saharan African women, whose vaginal microbiome were not dominated by lactobacilli, were 2-3 times more likely to acquire HIV after accounting for other HIV risk factors (66,71,72). The dysbiosis of the vaginal microbiome in BV is thought to contribute to HIV susceptibility by inducing the production of pro-inflammatory cytokines in the vaginal mucosa and disrupting normal mucosal barrier function. While information about the association between penile microbiome and HIV risk is limited, recent studies by our group show the anaerobes associated with BV and HIV risk in women can be found on the penis and suggest transmission between heterosexual couples (73,74). In men, absolute abundance of BV-associated anaerobes (e.g., *Prevotella*,

Prophyromonas, *Dialister*) on the penis has been associated with IL-8 levels in the sub-preputial space and density of HIV susceptible CD4+ T cell subsets, such as Th17 cells, in the foreskin (64). In a case-control study of uncircumcised men who acquired HIV during a randomized-controlled trial of male circumcision in Uganda, the absolute abundances of penile anaerobes at enrollment were associated with risk of acquiring HIV during the 2-year follow-up period of the trial. Every 10-fold increase in anaerobes, such as *Prevotella*, *Dialister*, *Fingoldia*, and *Peptoniphilus*, was associated with an increased odds of HIV acquisition of 54 to 63%, after controlling for other known HIV risk factors. Many of the anaerobes found to be associated with HIV seroconversion in the uncircumcised men were also associated with BV and HIV risk in women (73,74). However, anaerobes are highly co-occurrent in the penile microbiome, and therefore it is difficult to infer which species are causal of HIV risk. To address this, our group also assessed which species were associated with an increased density of HIV target cells, and identified six species, which we named “bacteria associated with HIV seroconversion, inflammation, and immune cells” (BASIC) (75). The reduction of these six species (*Peptostreptococcus anaerobius*, *Prevotella bivia*, *Prevotella disiens*, *Dialister propionicifaciens*, *Dialister micraerophilus*, and a genetic near neighbour of *Dialister succinatiphilus*) using a microbiome-based non-surgical intervention could be a potential HIV prevention strategy for men in endemic areas who choose to remain uncircumcised.

1.6 Proving the role of the foreskin microbiome in HIV susceptibility

Voluntary male circumcision has been shown to be able to significantly alter the composition of the penile microbiome, including substantially reducing the abundance of BASIC species, suggesting that PC may reduce susceptibility to HIV by reducing penile anaerobes, which in turn reduces local inflammation and the abundance of HIV target cells in the foreskin (38,73,75,76). As an alternative to PC, elimination BASIC anaerobes using topical or oral antimicrobial therapies may reduce local foreskin tissue inflammation and the recruitment of HIV target cells. Thus, modification of the penile microbiome could constitute a new, non-surgical method for HIV prevention for men at

risk of HIV (31,75). However, it is not known which antimicrobial agents can eliminate BASIC species and whether this change will result in a reduction of foreskin inflammation and HIV susceptibility. We hypothesize that oral and/or topical antimicrobials will reduce the abundance of BASIC species and the density of HIV-susceptible CCR5+CD4+ cells in the foreskin. To test this hypothesis, we used samples collected during a randomized clinical trial (RCT) of licensed antibacterial agents, where the intervention was administered for three weeks preceding PC (77). HIV-negative Ugandan men (n=125) requesting voluntary PC were randomized to receive either no intervention (controls) or a treatment course with one of four commonly available antibacterial agents prior to elective PC. The density of HIV susceptible CCR5+CD4+ cells in excised foreskin collected from the RCT was then quantified, using immunofluorescent (IF) microscopy and a novel automated deep-learning IF image analysis algorithm, to determine the effect of antimicrobial treatments on foreskin abundance of HIV-susceptible CCR5+ CD4+ cells. In this thesis project, I have three objectives.

1.7 Objectives

1. **Objective 1:** Develop, validate, and apply automated deep-learning IF microscopy image analysis algorithms to measure HIV target cell density in whole foreskin tissue sections.
 - **Hypothesis:** The automated deep-learning algorithm will be able to segment HIV target cells with accuracy comparable to manual identification and better than the automated pixel-based cell segmentation workflow in the image processing software, ImageJ.
2. **Objective 2:** Determine the effect of antimicrobial treatments on HIV target cell density.

- **Hypothesis:** HIV target cell density will be lower in the inner foreskin of men in the treatment groups when compared to the men in the control group.
3. **Objective 3:** Determine if the relationship between antimicrobial treatments and HIV target cell density is mediated by changes in the penile microbiome.
- **Hypothesis:** HIV target cell density in the inner foreskin will be associated with the abundance of BASIC species at the time of PC (i.e., post-treatment, in participants randomized to the treatment arms).

Chapter 2

2 Randomized Clinical Trial Methods

**NB* None of the methods described in Chapter 2 were performed by the candidate (Z Shao). They are provided here for background on RCT design and sample collection.*

2.1 Study Overview

This study is based on a randomized, open-label clinical trial examining the effect of antimicrobials on HIV susceptibility in Ugandan men (77). HIV-uninfected men (n=125) seeking voluntary PC were randomly assigned to one of five treatment arms (n=25). Men in the control group were circumcised without delay while men in the other 4 intervention groups were asked to use either oral tinidazole, penile topical metronidazole, penile topical clindamycin, or penile topical hydrogen peroxide for one month prior to circumcision. These antimicrobial agents were selected as they are licensed and commonly used for the treatment of BV in women or management of conditions associated with microbial imbalance such as gingivitis/periodontitis (78–82,82). The impact of these interventions on the availability of HIV target cells in the foreskin was determined via immunofluorescent microscopy. The impact of the interventions on HIV target cell availability in the foreskin was further correlated with impact of interventions on the composition of the penile microbiome and the abundance of penile inflammatory cytokines assessed by 16S rRNA sequencing and multiplex enzyme-linked immunosorbent assay, respectively.

2.2 Study Design

2.2.1 Study sites:

Participant enrollment and sample collection was completed at the Entebbe General Hospital in Uganda. Biological samples were first processed at the Uganda Virus Research Institute – International Aids Vaccine Initiative (UVRI-IAVI) laboratory prior to being shipped to the University of Western Ontario (London, Canada), the University

of Toronto (Toronto, Canada), George Washington University (Washington, D.C, USA), and Johns Hopkins University (Baltimore, USA) for further analysis.

2.2.2 Study population:

A total of 125 HIV-negative Ugandan men (aged ≥ 18 years) seeking voluntary PC at Entebbe General Hospital were enrolled in the study (77). Men were invited to participate in the study during the health education and HIV counseling/testing session routinely held at the clinic. Potential participants were screened for eligibility (**Table 1**), confirmed to be general healthy and without symptomatic genital infections, and willing to undergo HIV testing. Only men who agreed to provide written informed consent and demonstrated an understanding of the study (in the opinion of the study team clinical staff) were invited to participate.

2.2.3 Randomization and blinding

Eligible men (**Table 1**), who have provided written consent to participate in the trial were assigned to any of the treatment arms in an open-label fashion using computer generated randomized numbers. At enrollment, each participant chooses a single envelope from a pile of sealed-opaque envelopes that have been shuffled by the clinical staff in the presence of the participant. Each envelope contained a randomly generated number which determined the participant's treatment arm assignment.

Table 1: Inclusion and exclusion criteria

Inclusion Criteria

Aged \geq 18 years

Male

Uncircumcised

HIV-negative

Willing to give written informed consent

Willing and able to answer a short social-behavior questionnaire

Wiling to comply with study protocol requirements including randomization and study drug usage

Available for planned duration of randomization group

Exclusion criteria

HIV-infected

Already circumcised

Self-reported or physician noted genital itching/burning, penile discharge, genital ulceration or other possible sexually transmitted infection symptoms

Participating in other research studies that might compromise the outcomes of this study

2.2.4 Treatment group assignment

At enrollment, study participants were randomly assigned to one of five study groups (n=25 participants per group), as follows:

1. **Control group:** Participants received no antimicrobial treatment and immediately underwent circumcision, as per the normal Entebbe General Hospital protocol.
2. **Oral tinidazole group:** Participants were asked to defer circumcision by 4 weeks and were provided with oral tinidazole 2g once daily for 2 days. Tinidazole is commonly used for the treatment of several conditions including amebiasis, giardiasis, trichomoniasis, and BV. Tinidazole belongs to the imidazole family of antibiotics, which prevent the growth of Gram-positive and Gram-negative anaerobic bacteria via disruption of bacterial DNA synthesis (83–85).
3. **Topical metronidazole group:** Participants were asked to defer circumcision by 4 weeks and were asked to apply 0.75% metronidazole cream topically underneath the foreskin twice daily for 1 week and then twice weekly for 3 weeks. This formulation of metronidazole is commonly used for the treatment of BV in women. Metronidazole also belongs to the imidazole family (80,81).
4. **Topical clindamycin group:** Participants were asked to defer circumcision by 4 weeks and were asked to apply 2% clindamycin cream topically underneath the foreskin twice daily for 1 week and twice weekly for 3 weeks. Topical clindamycin is commonly used for the treatment of acne vulgaris and BV. Clindamycin prevents the growth of many aerobic Gram-positive cocci and several anaerobic Gram-positive and Gram-negative bacteria by impairing bacterial protein synthesis (81,86).
5. **Topical hydrogen peroxide group:** Participants were asked to defer circumcision by 4 weeks and were asked to apply 1% hydrogen peroxide gel topically underneath the foreskin twice daily for 1 week and then twice weekly

for 3 weeks. Hydrogen peroxide gel is a common oral/skin disinfectant typically used for the treatment of gingivitis/periodontitis. It primarily affects anaerobic bacteria and kills both Gram-positive and Gram-negative bacteria through the release of reactive oxygen species that results in the damage of bacterial DNA (82,87).

2.2.5 Study procedures, visits, and sampling

Potential participants who had clinically apparent symptoms for STIs (genital ulcerations, urethral discharge, dysuria) were deferred from enrolment and offered treatment as specified by the Uganda Ministry of Health guidelines. Symptomatic STIs are also a contraindication for PC, so these individuals were asked to return upon resolution of symptoms, when they would be eligible for both study participation and PC. Treatment was also offered for study participants who were found to have asymptomatic gonorrhoea or chlamydia later by polymerase chain reaction (PCR) urine screening. Prior to randomization, all participants received HIV counseling and testing via rapid diagnostic tests. A brief social behavioral questionnaire, including sexual history, was administered and condoms were also provided to all participants. Peripheral venous blood, urine, and genital swabs from the coronal sulcus, inner foreskin, and urethral meatus were collected as baseline biological samples. All men in intervention groups (tinidazole, metronidazole, clindamycin, hydrogen peroxide) had a visit after the intensive phase of their treatment, on day 3 for men in the tinidazole group (administered orally) and day 8 for men in the metronidazole, clindamycin, and hydrogen peroxide groups (administered topically). Men in the metronidazole, clindamycin and hydrogen peroxide groups received phone call reminders about product use twice a week. A follow-up visit was scheduled for the men in the intervention groups at 4 weeks after enrollment. The men were interviewed about product use, tolerability, and sexual practices. During the visit, repeat blood, urine, and penile swab samples were taken, and the men were circumcised. The excised foreskin tissues were used for the immunofluorescent microscopy analysis described in this thesis and were also used by study collaborators in flow cytometry-based assays.

2.2.6 Lost to follow-up status and reimbursement

Participants enrolled in the study were “lost to follow-up” if they did not present to the clinic within three days of a scheduled date/visit. Participants were reimbursed for their time of study participation at the end of each clinic visit. Time compensation worth 20,000 UGX (~\$7 USD) were provided to each study participant per study visit.

2.2.7 Study outcomes

The overarching objective of the RCT is to determine the impact of antimicrobials on foreskin HIV susceptibility, penile immunology, and penile microbiota (77). The main objective of this thesis, which represents one endpoint of the RCT, is to assess the effect of antimicrobial intervention on foreskin tissue density of HIV susceptible cells (cells bearing the two receptors used for HIV entry: CD4 and CCR5) based on immunofluorescence microscopy. Other endpoints of the RCT, which will be investigated by study collaborators, include determining the effect of the antimicrobial interventions on (1) viral entry into foreskin-derived CD4+ T cells using a validated primary clade A, R5 tropic pseudovirus entry assay; (2) proportional abundance of CD4+ T cell subsets (including Th17 cells) based on flow cytometry of digest foreskin tissue; (3) levels of soluble immune mediators on the penis, assayed by enzyme-linked immunosorbent assay (ELISA); and (4) composition of the foreskin microbiome using 16S rRNA sequencing (52,64,73,74,88–90). Foreskin tissue density of HIV target cells will be correlated with (1) the abundance of BASIC species and (2) levels of soluble immune mediators as a part of this thesis project.

2.2.8 Trial status and summary

Study participant enrollment began in December 2017 and was completed in January 2019. Out of the 125 participants enrolled, 9/125 participants were lost to follow-up; therefore, the analysis population includes 116/125 participants.

2.3 Biological sample processing

2.3.1 Blood collection and processing

For each blood draw, clinical staff collected peripheral venous blood from participants into two 8.5ml BD Vacutainer acid citrate dextrose tubes (Becton, Dickson & Company, NJ, USA), and blood samples were centrifuged at 2000 x g at 4°C for 20 minutes to isolate plasma. The plasma samples collected were first stored at -80°C then later used for testing of HIV and STIs including herpes simplex virus type 2 (HSV-2) and syphilis at the UVRI-IAVI laboratory.

2.3.2 Genital swab collection and handling

Genital swab samples were collected in the Entebbe General Hospital circumcision clinic by rotating pre-moistened Dacron swabs (COPAN Diagnostics Inc., CA, USA) on the coronal sulcus (2 swabs), the inner foreskin (2 swabs), and urethral meatus (1 swab). Immediately after collection, all swabs were placed in clean microtubes and transported to the UVRI-IAVI laboratory on ice. One swab from the inner foreskin and one swab from the coronal sulcus was frozen at -80°C without processing. Each of the other swabs (1x urethral meatus, 1x inner foreskin, 1x coronal sulcus) were resuspended in two aliquots 250µl phosphate-buffered saline (PBS) mixed with a protease inhibitor and buffer before being stored at -80°C. Swab samples were later shipped to George Washington University, USA for microbiome analysis and the University of Toronto, Canada for soluble inflammatory molecule analysis (52,64,73,88,90).

2.3.3 Urine collection and handling

During the first visit and at the 4-week follow-up, study participants were asked to self-collect urine in a urine container. Urine samples were transported on ice to the UVRI-IAVI laboratory and aliquoted into PCR urine tubes (Cobas, Roche Molecular Systems, Inc) for PCR testing for *Neisseria gonorrhoeae* and *Chlamydia trachomatis*.

2.3.4 Foreskin collection and processing

As previously described, the inner aspect of the foreskin is marked with a suture during surgery to assist with tissue orientation during processing (91). The inner foreskin is defined as the portion of the foreskin tissue that covers the glans and coronal sulcus on the nonerect penis and the outer foreskin is the portion of the foreskin tissue that is exposed to air on the non-erect penis. After circumcision, foreskin samples were immediately transported to the UVRI-IAVI laboratory at ambient temperature for processing. Excess connective tissue and obvious blood clots were first trimmed off from the tissue before the tissue was cut into 0.25cm^2 sections. One 0.25cm^2 section from each of the inner and outer foreskin was separately snap frozen into cryomolds in optimal cutting temperature compound (OCT) media (Thermo Fisher Scientific Inc., MA, USA). These samples were shipped to the University of Western Ontario, Canada for the immunofluorescent microscopy analysis described in this thesis project. One section from each of the inner and outer foreskin was cryopreserved in 10% dimethyl sulfoxide in FBS freezing media at -150°C .

Other tissue sections are digested for flow cytometry analysis. First, 0.25cm^2 inner and outer foreskin sections were separately soaked in RPMI 1640 media with 500U/ml collagenase type 1 (Gibco #17100) and 42.5U/ml deoxyribonuclease (Invitrogen, MA, USA). The soaked tissues were mechanically disrupted using scissors and then enzymatically digested at 37°C for 30 minutes at 900rpm on a shaker (Eppendorf Thermo mixer, Hamburg, Germany). The resulting cell suspensions were then added to 3ml cold fetal bovine serum (FBS) and filtered through a $100\mu\text{m}$ cell strainer (BD Biosciences, NJ, USA). Deoxyribonuclease (30U/ml) was added to the filtrate and then the cells are washed and resuspended in R10 media (RPMI 1640 media with 10% heat-inactivated FBS, 10U/ml penicillin, $10\mu\text{g/ml}$ streptomycin, 250 ng/ml amphotericin B, and 2mM L-glutamine; Gibco, Invitrogen, Carlsbad, CA, USA) before being rest overnight at 37°C under 5% CO_2 . The rested cells were counted using trypan blue exclusion and $\sim 10 \times 10^6$ cells were plated in 500 μl R10 media. Plated cells were

stained for 30 minutes at 4°C with labelled monoclonal antibodies for flow cytometry analysis on-site at the UVRI-IAVI laboratory (49,89).

2.4 Laboratory assays completed by collaborators

2.4.1 Penile microbiome characterization

Penile microbiome characterization was completed using penile swab samples collected at study enrollment, at one-week post-treatment, and at the time of circumcision. This analysis was completed by study collaborators at George Washington University, USA and exact details of the methods used for this analysis are outside of the scope of this thesis project. Briefly, the penile microbiome was characterized by using amplicon sequencing and broad-range real-time PCR of the V3V4 hypervariable region of the 16S rRNA gene as previously described (73,88,90). Barcoded universal primers specific for the V3V4 hypervariable region were used for sequencing. Amplicons were purified, quantified, and pooled prior to sequencing on the Illumina MiSeq platform using the 300bp paired-end protocol. Sequence read quality was assessed using a standardized bioinformatics pipeline implemented in accordance with standard operating procedures from the National Institutes of Health Human Microbiome Project. The `-utax` function in the USEARCH sequence analysis tool in QIIME (open source microbiome bioinformatics platform) was used to assign taxonomy and cluster operational taxonomic units against the Greengenes reference database (92). For each sample, vectors of phylotype proportions were clustered into community state types, by calculating Jensen-Shannon distances between all pairs of community states and generating a hierarchical clustering using the Jensen-Shannon distance data and Ward linkage (73,74,88). Through combining sequencing and qPCR data, the absolute abundance of penile bacterial genus and species of interest was calculated as follow: absolute abundance of a taxon per swab = total penile bacterial load per swab (measure as total copied of 16S rRNA gene per swab by qPCR) x proportional abundance of the given taxon (measure as the number of 16S rRNA gene sequences assigned to a taxon in a given sample, divided by the total number of 16S rRNA sequences obtained for the sample).

For the purposes of this thesis, we decided to focus on 1) total bacterial abundance, 2) BASIC species abundance, and 3) the abundance of bacteria belonging to two non-inflammatory “control” taxa (*Corynebacterium* and *Staphylococcus*), previously found to be unchanged/increased after circumcision and not previously associated with HIV seroconversion or inflammation (75). Only five of the six BASIC species were included in analyses (*Peptostreptococcus anaerobius*, *Prevotella bivia*, *Prevotella disiens*, *Dialister propionicifaciens* and *Dialister micraerophilus*) as the genetic near neighbour of *Dialister succinatophilus* was excluded due to incomplete data processing. (73,75).

2.4.2 Multiplex ELISA for soluble inflammatory molecule quantification

Measurement of penile levels of soluble inflammatory molecules was completed using penile swab samples collected at study enrollment, at one-week post-treatment, and at the time of circumcision. This analysis was completed by study collaborators at the University of Toronto, Canada and exact details of the methods used for this analysis are outside of the scope of this thesis project. Briefly, inflammatory molecule levels will be measured using a chemiluminescent multiplex ELISA assay (MesoScale Discovery). This assay was selected due to the ability of providing optimal sensitivity and reproducibility for low abundance mucosal sample. It has previously been validated for use with foreskin swab samples (52,73,76).

2.4.3 Pseudovirus cell entry assay

A HIV pseudovirus assay is used to determine the effect of the interventions on HIV entry into inner foreskin T cells. The assay was completed by study collaborators on site at the UVRI-IAVI laboratory in Uganda using CD4+ T cells isolated from inner foreskin samples obtained from circumcision. The exact details on the methods for this assay are outside of the scope of this project but have been well characterized in previous studies (49,89). The virus used for this assay contains a β -lactamase-viral protein R

(BLaM-Vpr) and is pseudotyped with an envelope from an early transmitted, CCR5-tropic, subtype A virus. When the pseudovirus enters target cells, BLaM-Vpu is delivered into the cytosol. After target cells have been incubated with the pseudovirus, the substrate CCF2-AM is added. CCF2 is a membrane-permeant form of the fluorescent molecule CCF which contains 2 fluorophores (7-hydroxy-coumarin and fluorescein) linked by a β -lactam bond. Cells that were not infected by the pseudovirus will not have β -lactamase in the cytosol. In these cells, excitation of 7-hydroxy-coumarin at 409nm leads to fluorescent resonance energy transfer (FRET) to fluorescein and green light emission at 520nm. Infected cells will have β -lactamase in the cytosol (via delivery from BLaM-Vpu) that will cleave the β -lactam bond in CCF2-AM and prevent FRET. This results in blue emission at 447nm by 7-hydroxy-coumarin when 7-hydroxy-coumarin is excited. The ratio of blue to green emission can thus be used as a measure of viral fusion and cytosolic entry of HIV.

2.5 Statistical and ethics considerations

2.5.1 Sample size

The sample size of 25 participants per treatment group for the RCT was based on the primary endpoint, which was the HIV pseudovirus assay. Previously defined pseudovirus entry parameters into inner foreskin-derived CD4⁺ T cells suggested that a sample size of 25 participants per group would provide statistical power of 80% to identify clinical approaches that reduce virus entry by $\geq 33\%$. This was the efficacy threshold that was deemed as sufficient to inform future intervention strategies. All available samples (n=116) were used for the IF analysis presented in this thesis.

2.5.2 Ethics and Patient involvement

The RCT protocol was reviewed and approved by the Ugandan Virus Research Institute's Research and Ethics Committee (UVRI SEC), the Ugandan National Council for Science and Technology (UNCST), and the University of Toronto HIV Research Ethics Board. The data and biological samples collected from study participants were

labelled with a unique study identification number. All clinical events that were directly related to the study were referred to and managed by the UVRI-IAVI clinical team according to the Ugandan Ministry of Health guidelines. Participants in the study were not directly involved in the design of this study and did not directly assess the effect of the interventions. Participants did play a role in contributing to peer referral of potential participants. The Community Advisory Board for UVRI-IAVI meets quarterly and provided advice to the study team on study design and recruitment. The protocol for analysis of frozen tissue sections by IF (and correlation with data generated by collaborators) was approved by the Research Ethics Board at The University of Western Ontario.

Chapter 3

3 Comparison between a deep-learning and a pixel-based approach for the automated quantification of HIV target cells in foreskin tissue.

3.1 Introduction

3.1.1 Understanding HIV infection at the site of exposure

Sexual transmission of HIV, which occurs at the anogenital mucosa, accounts for the vast majority of new HIV infections worldwide (93,94). After HIV virions penetrate the genital epithelium, the availability of target cells bearing the HIV co-receptors CD4 and CCR5 becomes the critical determinant of productive infection in mucosal tissue (**Figure 1**) (30,38,95,96). The inner foreskin is enriched in T cell populations that are highly susceptible to HIV, such as activated T cells and Th17 cells, compared to the bloodstream (28,30,32). Non-T cell types that are abundant in the foreskin, such as macrophages, dermal dendritic cells, Langerhans cells and fibroblasts, are also thought to facilitate the spread of viral infection, either by direct infection or by transferring viral particles to susceptible T cells through trans-infection (**Figure 1**) (97,98). The genital mucosa is also inhabited by diverse polymicrobial communities of bacteria that shape the local immune environment. The composition of the genital microbiome has been shown to be associated with both the availability and activation status of HIV target cells, and with an individual's risk of acquiring HIV during sex with an infected partner (73,75,95,99). Achieving an optimal balance between the diverse immune cell subsets of the genital mucosa promotes tolerance to commensal bacteria while maintaining the ability to rapidly respond to pathogens. An inflammatory environment in the genital mucosa promotes productive infection with HIV, while a tolerogenic environment is associated with relative protection (100,101). The genital mucosa is in constant contact with antigens, antimicrobial factors, hormones, and commensal bacteria that can

modulate the local environment of genital mucosa to a pro-inflammatory state and in turn modulate and individual's risk to HIV infection (24,37,64,73–75). When testing new prevention modalities or determining best practices to prevent HIV transmission, it is essential to develop ways to quantify immune cells in mucosal tissue, to better understand how behaviours, medications, etc. influence the abundance of HIV target cells in the mucosa.

3.1.2 Using immunofluorescent microscopy to quantify immune cells in the genital mucosa

High-parameter flow cytometry has been actively used in studies focused on HIV detection, susceptibility, prevention, and pathogenesis. Advancements in CD4 T cell laboratory testing and the detection of HIV-infected mononuclear cells in the bloodstream were critical developments for the care and management of HIV infected individuals (102,103). Flow cytometry is highly useful for understanding immune cell populations and HIV infection in peripheral blood as it allows quantification of multiple target cell types of interest and the simultaneous detection of a large variety of different cell markers on single cells. While flow cytometry is advantageous for the study of immune cells in blood, it is less suitable for mucosal tissues (104–107). Due to the nature of flow cytometry, tissues must be mechanically or enzymatically disrupted into single cell suspensions so information on the spatial location of cells within tissue is lost. This is a disadvantage in the context of susceptibility to viral infection, as the closer target cells are to the apical surface of the epithelium the less distance a virion needs to traverse to access susceptible cells (42,52). Information on the proximity of immune cell subsets to one another is also lost, which is important for understanding immunological events such as immune cell activation, antigen presentation, and trans infection of HIV (64,75,108,109). In addition to losing spatial information, the viability of delicate sprawling cells that are abundant in the foreskin mucosa, such as dendritic cells and Langerhans cells, is reduced due to the disruption process. Tissue disruption may also alter expression of cell surface markers relevant to activation and viral entry. Lastly, flow

cytometry provides information on the relative abundance of immune cell subsets but is ill suited for measuring the density of immune cells in tissue.

Immunofluorescent (IF) imaging overcomes the limitations imposed by tissue disruption but introduces new challenges in quantification. Structural proteins and collagen fibers, which are abundant in genital mucosal tissue, exhibit high levels of autofluorescence that can obscure positive staining and make cell identification difficult (**Figure 2**). Autofluorescence is highly variable in different tissue regions in the same sample and among samples from different individuals (28,30,110). Due to the difficulty of cell quantification and the high level of variability in IF images, manual counting is still a common practice despite its lack of efficiency and issues with bias. A single 8 μ m thick section of a 5mm x 5mm piece of genital tissue contains thousands of immune cells. In many cases, instead of quantifying whole tissue section images, randomly selected field-of-views (FOV) that are a fraction of the size of each whole image are quantified instead. However, by reducing the “sample size” of tissue analyzed precision is lost and random noise introduced into the data, reducing statistical power. Furthermore, manual counting also suffers from reproducibility issues, investigator bias, and inter-investigator variability which becomes highly problematic in clinical studies where large numbers of samples are involved. To overcome these issues, significant effort has been made to automate image processing and cell segmentation in recent years.

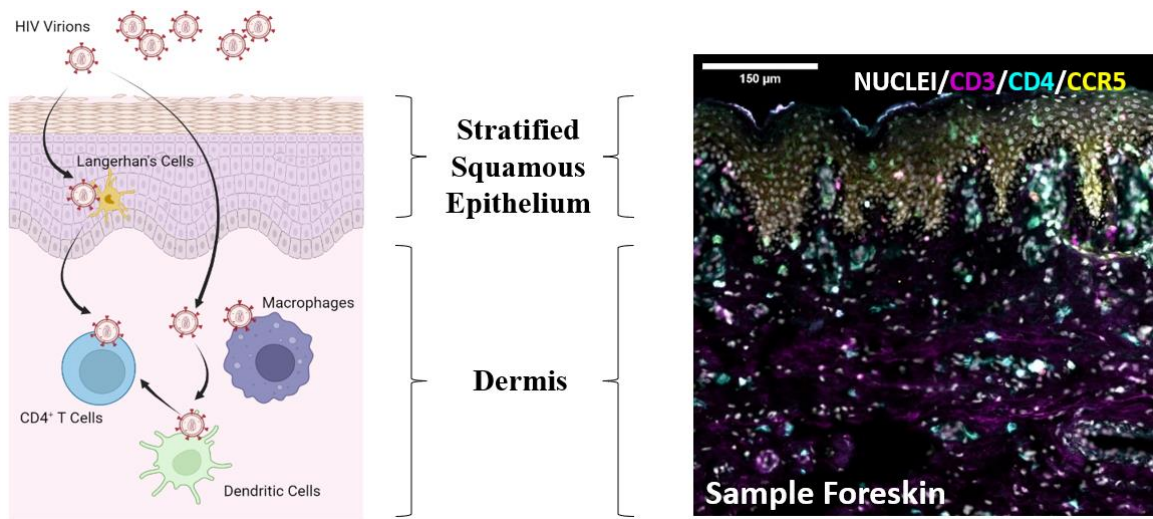


Figure 1: Visualization of the epidermis and dermis in foreskin tissue. The epidermis is characterized by a very high density of nuclei staining which represents tightly packed epithelial cells while cells are more dispersed in the dermis. HIV susceptible immune cells can be found in both the epidermis and dermis. However, they are usually more abundant in the dermis, particularly in areas of the dermis that are close to the basal edge of the epidermis.

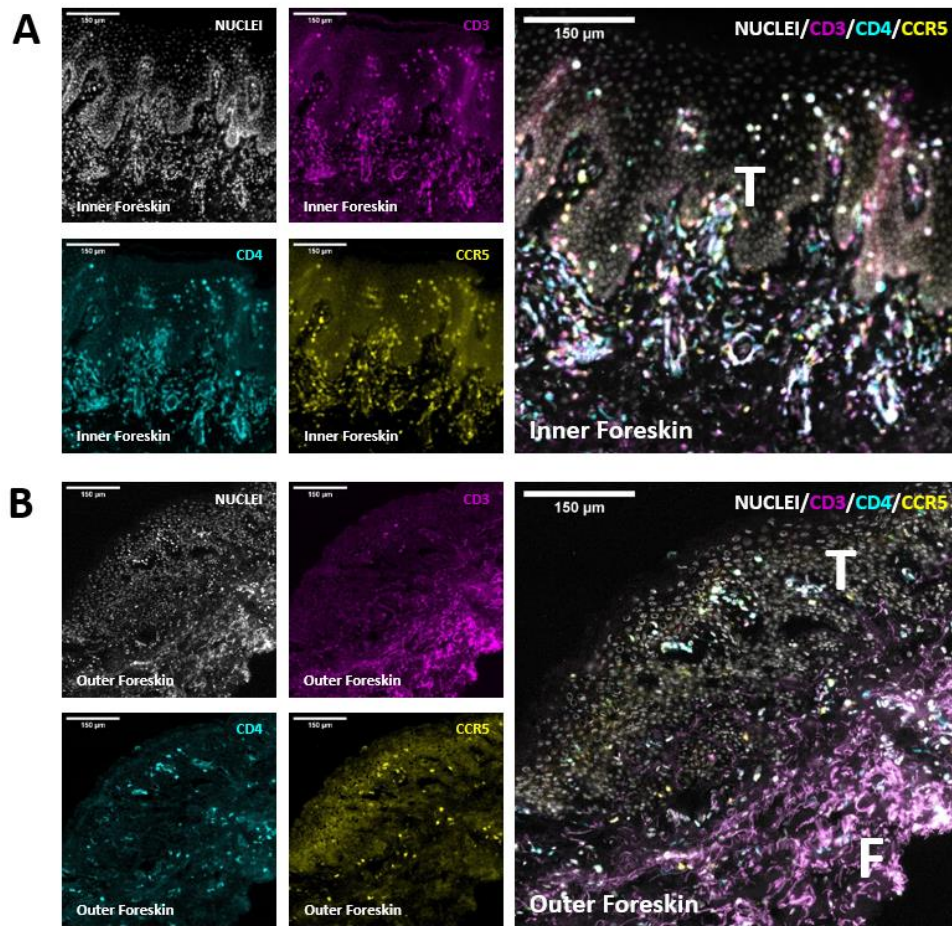


Figure 2: Representative images of inner and outer foreskin tissue sections stained for the identification of HIV target cells. Images were obtained from foreskin tissue sections from HIV-negative men in a randomized controlled trial assessing the effect of antimicrobials on the penile microbiome, penile inflammation, and foreskin HIV susceptibility. Foreskin tissue sections were stained for CD3, CD4, CCR5, and nuclei to identify HIV susceptible cell populations. Whole (A) inner and (B) outer foreskin tissue imaged at 200x total magnification. Individual staining for CD3, CD4, CCR5, and nuclei is shown on the left while merged composite of positive staining from all channels is shown on the right. White letters mark areas containing cell clusters that are likely to contain (T) HIV-susceptible CD4+CCR5+ T cells and areas with (F) significant autofluorescence.

3.1.3 Existing strategies for automated cell segmentation in immunofluorescent microscopy images of mucosal tissue

Several medical image analysis companies offer software products that can perform automated cell counting in IF images. However, these products are limited by poor flexibility for modification by the user and high cost (111,112). Custom cell counting workflows based on free open-source image analysis software programs such as ImageJ/Fiji, CellProfiler and QuPath are commonly used for cell segmentation in a large variety of tissue types (**Figure 3**) (113–115). Workflows based on these programs are highly flexible as these programs contain many image processing functions with adjustable input parameters. Furthermore, only basic programming knowledge is required to automate workflows built on these programs to achieve high-throughput processing of images.

Traditional cell segmentation workflows typically use a “bottom-up” pixel-based strategy. In these pixel-based approaches, a threshold is applied so that every pixel is classified as positive staining or background (i.e., converted to a binary, or black-and-white image). Images may also undergo additional processing before or after thresholding to improve pixel classification. Separate clusters of positive pixels are then identified as individual cells (**Figure 3B**) (116–118). While this basic approach is very easy to implement and generates good results in cases where cells are very clearly isolated from one another, it struggles with images that have variable brightness (e.g., variable expression of the target protein between cells/regions), densely packed or irregularly shaped cells, or high levels of autofluorescence (119). All these features are common in IF images of genital mucosal tissue. In many cases, it is very difficult or impossible to find a combination of parameters that will accurately detect cells across all areas of the tissue and all tissues in the study (120). When image processing is not aggressive enough, closely packed cells may be merged and large amounts of autofluorescence could be incorrectly identified as positive staining. Aggressive image processing is effective in eliminating autofluorescence but can also result in elimination of true cell staining and result in splitting of whole cells into several fragments.

Advances in deep learning have enabled “top-down” object-based approaches for cell segmentation. In these approaches, a prediction is made to identify individual cells (objects) with rough shape representations that are progressively refined to fit cells more closely. These approaches use training input to develop segmentation parameters which correspond to features. Initial attempts at using machine learning for cell segmentation used bounding boxes to create cell selections. (121–123). In the prediction phase of these approaches, a cell is identified with several overlapping instances of bounding boxes representing all possible ways the cell could be identified (**Figure 3C**). The best fitting box out of all the bounding boxes is then selected using a technique called non maximum suppression (NMS) (124). This approach is good at distinguishing between autofluorescence and positive cell staining, however, it is inaccurate in areas with densely packed cells. In these areas, bounding boxes can be incorrectly eliminated by NMS when there is overlap between bounding box selections for different cells (**Figure 3C**).

Recent studies have proposed better shape representations to replace bounding boxes. For instance, the deep learning segmentation method StarDist uses star-convex polygons to identify cells (125). Star-convex polygons are well suitable for approximating the shape of important HIV target cells. It can match the blob-like shape of CD4+ T cells and also maintain enough flexibility to outline sprawling cells like macrophages and dendritic cells. The sophisticated prediction process used by StarDist enables more accurate prediction of cell boundaries and better performance in areas with high cell density (**Figure 3D**). Implementation of StarDist deep learning models into existing IF image analysis workflows is also user-friendly. While training new StarDist models requires knowledge of python, no programming experience is required to use existing StarDist models. Software plugins allow existing StarDist models to be used in image processing programs such as ImageJ/Fiji and QuPath (113,115,125).

The StarDist method has previously been validated for nuclei segmentation and cell detection in different tissues. However, StarDist has not previously been used to identify immune cells in IF microscopy images of genital mucosal tissue. In this chapter,

we describe the training and validation of a StarDist model to identify HIV target cells in foreskin tissue. Specifically, we introduce a reusable workflow that can be used to train custom StarDist models. This workflow uses multi-channel IF microscopy images as input and is not limited by the tissue type or markers used for staining. We describe the training of a custom StarDist model used to identify HIV target cells in foreskin tissue stained for CD3, CD4, CCR5, and nuclei. The accuracy of this StarDist model was compared to manual counting and automated counting using a previously established pixel-based algorithm. The training workflow, training dataset and StarDist model used in this thesis have been made available in the public domain (<https://github.com/prodgerlab/stardist>).

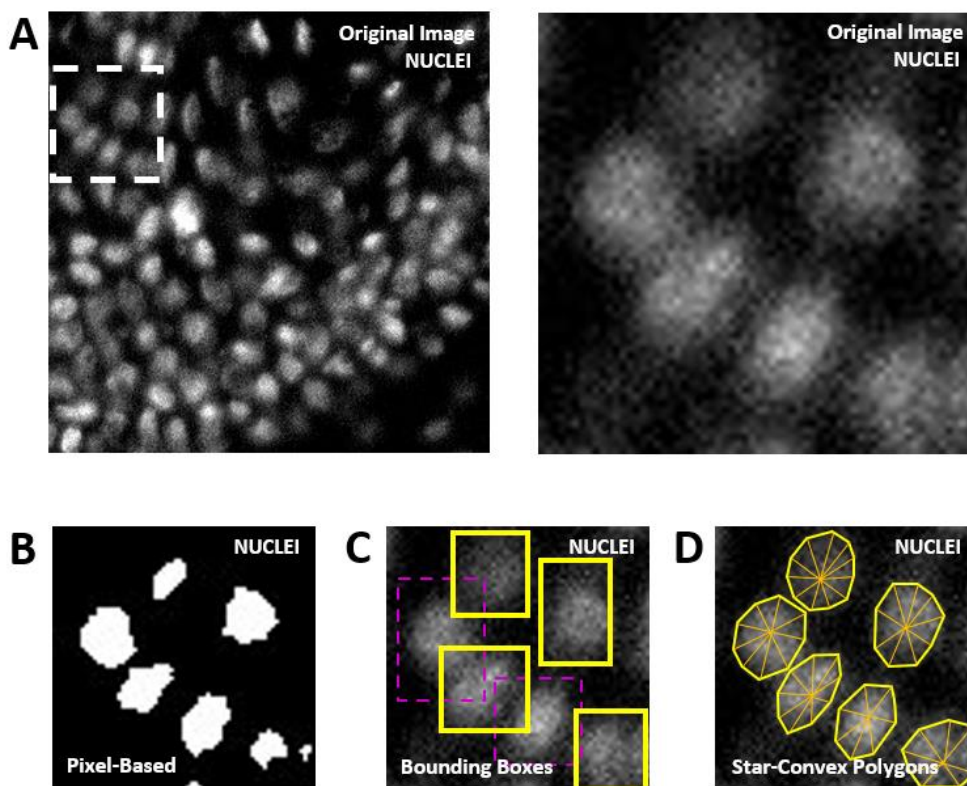


Figure 3: Common methods used for automated cell segmentation in immunofluorescent microscopy images of mucosal tissue. (A) Sample immunofluorescent microscopy image of nuclei staining in a tissue area with high cell density. Early methods of automated cell segmentation utilize (B) pixel-based bottom-up approach where cells are defined by pixels that are above a certain intensity threshold. These methods tend to be very crude and can result in cell merging or splitting. (C) The first deep learning approaches utilize bounding boxes to first localize cells. This approach does not rely on a bottom-up approach. However, bounding boxes can overlap in areas where cells are closely packed and result in the suppression of valid cell instances during the process of non-maximum suppression. Boxes in yellow represent correctly placed bounding boxes, boxes in purple represent valid cell instances that were suppressed. (D) Deep learning cell segmentation with StarDist utilizes star-convex polygons instead of boxes to create predictions.

3.2 Materials and Methods

3.2.1 Tissue Source

Foreskin samples were collected as a part of a randomized clinical trial (RCT) examining the effect of antimicrobials on the penile microbiome, foreskin inflammation, and foreskin HIV target cell density (77). Detailed information on the RCT methodology can be found in Chapter 2 in sections 2.2.1 to 2.2.8. In brief, a total of 125 HIV-negative men (≥ 18 years) seeking voluntary male circumcision were enrolled and randomly assigned to 1 of 5 treatments (topical clindamycin, topical hydrogen peroxide, topical metronidazole, oral tinidazole) or no treatment, prior to circumcision.

3.2.2 Immunofluorescence microscopy

Tissue samples from the study were separately stained using two different antibody panels to investigate the effect of the interventions on: 1) foreskin tissue integrity and 2) foreskin HIV target cell density, respectively. Staining, imaging, and analysis for the assessment of tissue integrity was completed as a part of another study and is outside the scope of this project. Staining and imaging of tissue samples to quantify target cell populations was completed according to previously published methods and are described below (126).

Cell markers of interest captured by the antibody panel used to quantify HIV target cell populations include CD3, CD4, and CCR5. Foreskin samples from 116/125 participants enrolled in the RCT were available for immunofluorescent microscopy analysis. One inner foreskin sample and one outer foreskin sample was analyzed for each participant meaning a total of 232 foreskin tissue samples were analyzed as a part of this project. Frozen tissue blocks were prepared in the UVRI-IAVI laboratory in Uganda immediately after circumcision and then shipped to the University of Western Ontario in Canada for immunofluorescent microscopy analysis. Frozen tissue blocks were sectioned at a thickness of $8\mu\text{m}$ using a CM1850 cryostat (Leica, Wetzlar, Germany) and two sections from each tissue block were adhered to a microscopy slide for staining. Slides

were stored at -80 °C for up to 1 month in an air-tight box. Prior to staining, slides were thawed and air-dried for 30 minutes. Each tissue section was fixed by applying 100µl of 3.7% formaldehyde in PIPES (100mM PIPES, 2mM MgCl₂, 1mM EGTA in PBS, pH 6.8) buffer and incubation for 5 minutes at room temperature. Slides were washed 3 times in 1x PBS between all subsequent blocking and staining steps. Each tissue section was blocked by applying 100µl of a solution consisting of 10% normal donkey serum, 0.1% Triton X-100, and 0.01% sodium azide diluted in 1x PBS (henceforth referred to as blocking solution) for 30 minutes at room temperature. Each section was incubated with 100µl of undiluted anti-human primary CD3 antibody (Abcam, Cambridge, United Kingdom) for 1 hour at 37 °C, followed by incubation with 100 µl of donkey anti-rabbit Alexa Fluor 488-conjugated secondary antibody (diluted to 0.25% in blocking solution) (Abcam, Cambridge, United Kingdom) in the dark for 30 minutes at room temperature. Next, sections were each incubated with 100µl of mouse anti-human CCR5 primary antibody (diluted to 5% in blocking buffer) (a gift from Dr. Matthias Mack, University of Regensburg, Germany) for 1 hour at 37 °C, followed by incubation with 100 µl of donkey anti-mouse Alexa Fluor 647-conjugated secondary antibody (diluted to 0.25% in blocking solution) (Abcam, Cambridge, United Kingdom) in the dark for 30 minutes at room temperature. Finally, sections were each incubated with 100 µl goat anti-human CD4 primary antibody (diluted to 5% in blocking buffer) (Abcam, Cambridge, United Kingdom) overnight at room temperature then incubated with 100 µl of donkey anti-goat Alexa Fluor 568-conjugated secondary antibody (diluted to 0.25% in blocking buffer) (Abcam, Cambridge, United Kingdom) in the dark for 30 minutes at room temperature. Coverslips were mounted onto stained slides by applying 100 µl Fluoromount G mounting media with DAPI (Thermo Fisher Scientific, MA, USA) per slide. Slides were stored at 4 °C for up to one week prior to imaging. Tiled images for whole tissue sections were scanned with a DM5500B fluorescence microscope (Leica, Wetzlar, Germany) using the 20x objective lens for CCR5 (Y5 filter set, referred to as far-red channel), CD4 (DSR filter set, referred to as red channel), CD3 (GFP filter set, referred to as green channel), and cell nuclei (CFP filter set, referred to as blue channel). Excitation and emission filters are listed in **Table 2**.

Table 2: List of microscope filters and their designations

Fluorophore	Leica Filter Designation	Absorbance λ	Excitation Filter*	Emission λ	Emission Filter*	Emission Colour
DAPI	CFP	358	436/20	461	480/40	Blue
Alexa Fluor 488	GFP	494	425/60	517	480/LP	Green
Alexa Fluor 546	DSR	556	545/30	573	620/60	Red
Alexa Fluor 647	Y5	650	620/60	665	700/75	Far-Red

Note: LP (long pass filter), λ (wavelength in nanometers)

*peak wavelength of light that passes through the filter and filter bandwidth

3.2.3 Manual counting of HIV Target Cells

All possible cell type combinations from the foreskin tissue sections stained for CD3, CD4, CCR5, and nuclei were counted individually (all cells, CD3+ cells, CD4+ cells, CCR5+ cells, CD3+CD4+ cells, CD3+CCR5+ cells, CD4+CCR5+ cells, and CD3+CD4+CCR5+ Cells). Total cell count was determined by counting all positive stained nuclei. Counting of specific cell types was completed using composite images containing staining for nuclei and the marker(s) of interest. First, composite images containing the staining for the markers of interest were generated from raw 4-channel (channels: CD3, CD4, CCR5, Nuclei) images. For each 4-channel sample image, 7 different composites corresponding each of the cell types of interest were generate (CD3+ cells, CD4+ cells, CCR5+ cells, CD3+CD4+ cells, CD3+CCR5+ cells, CD4+CCR5+ cells, CD3+CD4+CCR5+ cells). As mentioned, each composite image is created from merging the channel image(s) for the marker(s) of interest with the channel image for nuclei staining. For example, the composite image for CD3+ cells was created by merging the CD3 channel with the nuclei channel. Counting was completed by a single trained lab member using the Cell Counter plugin for Fiji. A cell is positive for a marker of interest when positive marker staining directly overlaps/surrounds positive nuclei staining. Positive marker staining that are unassociated with nuclei were ignored.

3.2.4 Pixel-based cell counting using Fiji and CellProfiler

A pixel-based cell counting algorithm used to quantify HIV target cells in immunofluorescent microscopy images of foreskin tissue stained for CD3, CD4, CCR5, and nuclei was previously validated by our group (126). This algorithm was is based on the open-source image analysis programs Fiji and CellProfiler (113,114). Image processing functions in Fiji were used to pre-process images. Both Fiji and CellProfiler were used for thresholding and cell segmentation after pre-processing (113,114). The epidermis and dermis of foreskin tissue are very different in terms of cell density and level of autofluorescence. To improve the accuracy cell segmentation using the pixel-

based workflow, the epidermis and dermis underwent pre-processing, thresholding and segmentation using different parameters.

Prior to pre-processing, full tissue section scans were split into the dermis and epidermis sections via manual tracing in Fiji and saved as separate files. The epidermis and dermis images were then split into individual channel images (CD3, CD4, CCR5, nuclei) by applying the “Stack to Images” function in Fiji. All individual channel images were pre-processed by applying the “Subtract Background”, “Brightness/Contrast”, and “Minimum Filter” functions successively. The “Subtract Background” function and “Minimum Filter” functions were applied using the corresponding pre-optimized parameters as listed in **Table 3**, the “Auto” setting was used for all “Brightness/Contrast” adjustments.

Image processing functions in Fiji and CellProfiler were used successively in order to automatically quantify HIV target cells in the pre-processed images (113,114). Fiji was used to threshold pre-processed images and select positive staining. CellProfiler was used to quantify cells of interest by determining the number of instances where each combination of positive marker staining for CD3, CD4, and CCR5 overlapped with positive staining of nuclei. In Fiji, pre-processed images were converted to 8-bit format and the “Adaptive Thresholding” plugin for ImageJ was used in Fiji to threshold images (113,127). The “Fill Holes”, “Despeckle”, “Erode”, and “Watershed functions were then applied successively in Fiji to further process the images. Positive marker staining selection was completed by applying the “Analyze Particles” function with the options for “Display Results”, “Clear Results” and “Add to Manager” checked and the “Circularity” setting set from 0.00 to 1.00 to detect all objects. The regions-of-interest (ROIs) generated after applying the “Analyze Particles” function were saved and overlaid with a black 8-bit image with the same dimensions as the image being analyzed to create a binary image representing positive marker signal. The number of regions-of-interest for nuclei staining represents the total cell count of the image. The steps described above were applied to all pre-processed images with pre-optimized

parameters listed in **Table 4**. Specifically, predetermined values were used for the “Block Size” and “Subtraction Value” parameters for “Adaptive Thresholding” and predetermined values were used for the “Particle Size” parameters for “Analyze Particles”. The binary black and white images of positive marker staining were imported into CellProfiler using the “ConvertImageToObjects” function. The “RelateObjects” function was then applied to determine positive marker staining for CD3 and/or CD4 and/or CCR5 that overlaps with positive nuclei staining (113,114). Through this process, the number of each type of cell of interest (CD3+ cells, CD4+ cells, CCR5+ cells, CD3+CD4+ cells, CD3+CCR5+ cells, CD4+CCR5+ cells, CD3+CD4+CCR5+ cells) was quantified. Scripts for high-throughput pre-processing and automated counting of images has been made available in the public domain (<https://github.com/prodgerlab/pixel-based-quantification>).

Table 3: Input parameters for pre-processing workflow used to improve accuracy of automated HIV target cell segmentation in foreskin tissue scans

		Image Type							
		EPIDERMIS				Dermis			
Function	Input Parameter	Nuclei	CD3	CD4	CCR5	Nuclei	CD3	CD4	CCR5
Subtract Background	Rolling Ball Radius	10	14	12	10	25	15	15	15
	Minimum Filter	0	2	1	0.5	2	2.5	1.5	1.5

Table 4: Input parameters for thresholding and segmentation for pixel-based quantification of HIV target cells in foreskin tissue scans

		Image Type							
		EPIDERMIS				Dermis			
Function	Input Parameter	Nuclei	CD3	CD4	CCR5	Nuclei	CD3	CD4	CCR5
Adaptive Thresholding	Block Size	100	100	100	100	100	100	100	100
	Subtraction Value	-5	-45	-10	-25	-30	-40	-35	-20
Analyze Particles	Particle Size	5 to ∞	7 to ∞	10 to ∞	7 to ∞	5 to ∞	10 to ∞	5 to ∞	10 to ∞

3.2.5 Annotation of images for StarDist model training in Labkit

Manual annotation of field-of-view (FOV) images for StarDist model training was completed using the Labkit plugin (version 0.3.7) for Fiji (113,128). Manual annotation was completed by 2 different trained lab members following the instructions listed in the StarDist GitHub repository (<https://github.com/stardist/stardist>).

A total of 40 FOVs were randomly generated from the whole tissue section scans from the randomized controlled trial for training. We randomly selected 40 out of the 232 whole tissue section scans for FOV generation and created a random crop (600x600 μ m, 1500x1500 pixels) from each selected image. Prior to annotation, all FOVs were visually assessed to ensure that none of the FOVs included any areas with tissue folding from improper adherence of tissue sections to microscopy slides during cryosectioning. The 40 FOVs included inner and outer foreskin images from all 5 groups in the randomized controlled trial. The full thickness of the epidermis is included in each FOV image (both the apical and basal edge of the epidermis is clearly identifiable) while at least half of the full thickness of the dermis is included. All FOVs underwent manual counting prior to annotation. This counting process was completed to ensure the accuracy of annotation. All possible cell type combinations were annotated individually in each FOV. From each 4-channel raw FOV image, 7 composite images were generated and annotated separately. The 7 different composite images corresponded to the 7 different cell types that are identified by our StarDist model (CD3+ cells, CD4+ cells, CD3+CD4+ cells, CD3+CCR5+ cells, CD4+CCR5+ cells, CD3+CD4+CCR5+ cells). The channel image for nuclei staining was annotated to train the model to determine total cell count. This means that a total of 320 (280 composite images, 40 raw nuclei staining images) were annotated with 40 images corresponding to each of the cell types of interest.

FOVs were opened in the Labkit plugin (version 0.3.7) for Fiji for annotation (113,128). All cells, which included cells on the image border, were manually traced and assigned an individual label with the override option selected to prevent overlapping cells. Completed annotation images were saved as separate tiff files. Each annotated set

used for training included 1 raw 4-channel FOV image and 8 annotated images (considered as ground truth for training).

3.2.6 StarDist model training

Training of the custom StarDist model was completed using a CUDA enabled Windows 10 workstation computer running a Window Subsystem for Linux with the Ubuntu (version 22.04) distribution of Linux installed. This workstation computer was equipped with an NVIDIA GeForce RTX 3090 graphics card to accelerate model training. The training environment, all scripts, and all additional software packages used for model training were operated in the Ubuntu distribution of Linux (version 22.04). The training environment was set up using the Mambaforge (version 0.24.0) distribution of Python (version 3.10.5) for Linux and TensorFlow (version 2.10.0) through a custom workflow created using Snakemake (version 7.12.0). Snakemake is a popular workflow management system commonly used for data analysis (129). It uses a simple specification language on top of Python to organize data analysis. Configuration of the necessary software packages, initialization of the training environment, running the training/validation scripts, and export of the trained StarDist model was streamlined with Snakemake through a Snakefile. The Snakemake workflow used to set up the training environment was adapted from instructions from the StarDist GitHub repository (<https://github.com/stardist/stardist>) which originally described set-up of a Python training environment using the Anaconda distribution of Python. Our full Snakemake workflow, which includes all scripts used for model training and export, has been made available in the public domain (<https://github.com/prodgerlab/stardist>).

The scripts used for model training and export were also adapted from example Jupyter notebooks from the StarDist repository, which provided instruction for 2D (U-Net-based) StarDist model training. Adjustments were made so that immunofluorescent microscopy images with 4 channels can be used as input. We also adapted the image augmentation functions included in the example Jupyter notebook and included these functions in our training script. Data augmentation includes random flipping and intensity

modification to training images, this process improves the accuracy of the StarDist model without the need for additional training images and annotation. Training was completed with the `n_rays` parameter for Config2D set to 32 and all other parameters were left to their default value in accordance with the Jupyter notebook in the StarDist GitHub repository (<https://github.com/stardist/stardist>). The full dataset used for training has been made available in the public domain (<https://zenodo.org/record/7030912#>).

Model training was performed for 400 epochs with steps per epoch set to 100. The model was exported after the probability and overlap parameters for non-maximum suppression post-processing were optimized. These optimized NMS parameters were used when using the model in the StarDist plugin (version 0.6.0) for Fiji (113,125). When using the model for prediction, images fed into the model were first normalized with the percentile range for image normalization was set from 1.7 to 99.8. The model was then run with the probability/score threshold set to 0.50, the overlap threshold set to 0.70. number of tiles was set to 16 and boundary exclusion was set to 2. Our trained StarDist model with optimized parameter pre-loaded has been made available in the public domain (<https://zenodo.org/record/7030912#>).

3.2.7 StarDist model validation

We compared the performance of our StarDist model against manual counting and pixel-based automated cell counting using 10 FOV images. The FOV images used for validation were randomly generated from the randomized controlled trial sample images in the same fashion as the FOVs used for StarDist model training. Both inner foreskin images and outer foreskin images were used to make validation FOVs and each of the validation images were derived from RCT sample images that were not used to make model training FOVs. Like the model training FOV images, validation FOVs were 600x600 μm (1500x1500 pixels) in size, excluded areas with tissue section folding, included the full thickness of the epidermis (apical and basal edge could both be clearly identified), and included at least half of the thickness of the dermis. Manual counting of

the validation images was completed by one trained lab member following the instructions described in section 3.2.3.

The percent difference between 1) manual counting and pixel-based automated counting, and the percent different between 2) manual counting and StarDist deep-learning automated counting was determined. The total number of true positive, true negative, false positive, and false negative counts were determined from the pixel-based and StarDist counts through comparison with manual counts. Key metrics such as sensitivity, precision, false negative rate, and false discovery rate was determined for the pixel-based counting algorithm and StarDist deep-learning counting algorithm.

3.2.8 StarDist model performance in high autofluorescence or high cell density areas

Four image crops containing an area with high autofluorescence ($70 \times 70 \mu\text{m}$, 175×175 pixels) and Four image crops containing an area with high cell density ($70 \times 70 \mu\text{m}$, 175×175 pixels) was created from each of the 10 validation FOV images ($600 \mu\text{m}$, 1500×1500 pixels). Image crops were created such that there was no overlap between the image crops generated from the same validation FOV. This means that none of the high autofluorescence image crops overlapped with each other and none of the high cell density image crops overlapped with each other. A total of 40 high autofluorescence image crops were analyzed and a total of 40 high cell density image crops were analyzed. High autofluorescence image crops and high cell density image crops were analyzed using both the StarDist algorithm and pixel-based algorithm. Performance of the StarDist counting method and pixel-based counting method in areas of high autofluorescence was visually assess by determining the number of image crops where autofluorescence was inaccurately counted as a cell (113,125,126). Performance of the StarDist counting method and pixel-based counting method in areas of high cell density was visually assessed by determining the number of instances of where cells were falsely merged in all 40 high cell density image crops.

3.2.9 Statistical Analysis

Results are presented as mean \pm SDs. Difference between number of counts between pixel-based automated counting and manual counting and difference between number of counts between StarDist automated counting and manual counting was assessed using paired T tests. Statistical analysis was performed using Prism 9 (GraphPad software, La Jolla, CA, USA). All figures were also generated using Prism 9. Results were statistically significant if the p-value was less than 0.05.

3.3 Results

3.3.1 Automated HIV target cell segmentation using StarDist is comparable to manual counting and more accurate than pixel-based cell segmentation

To determine if the performance of our custom StarDist model is comparable to manual counting and exceeds the performance of a previously validated pixel-based workflow, we completed manual counting, automated segmentation using StarDist, and automated segmentation using a pixel-based method for 10 FOV images (600x600 μ m each) of foreskin tissue stained for HIV target cells (staining for CD3, CD4, CCR5, and nuclei) (**Figure 4**). Pairwise comparison of manual counts with counts generated with our StarDist model showed that total cell count and counts for all cell types of interest (CD3+ cells, CD4+ cells, CCR5+ cells, CD3+CD4+ cells, CD3+CCR5+ cells, CD4+CCR5+ cells, CD3+CD4+CCR5+ cells) were not significantly different between the 2 methods ($p>0.05$) (**Figure 5**). Automated counts generated with the pixel-based workflow were not significantly different ($p>0.05$) from manual counts for total cell count, CD3+ cells, and CD4+ cells. However, automated counts generated using the pixel-based method for all other cell types were significantly different from manual counts. Specifically, automated counts for CCR5+ cells ($p=0.0043$), CD3+CD4+ cells ($p=0.0058$), CD3+CCR5+ cells ($p=0.0004$), CD3+CD4+CCR5+ cells ($p=0.0005$) were significantly lower than manual counts while automated counts for CD4+CCR5+ cells ($p=0.0245$) were significantly higher than manual counts (**Figure 5**).

Overall, based on pooled counts from all 10 validation FOVs, the percent difference of StarDist counts from manual counts was less than 5% for all cell types except for CD4+CCR5+ cells (11.32%) and CD3+CD4+CCR5+ cells (13.59%). Meanwhile, percent difference of counts generated using the pixel-based approach from manual counts was less than 5% only for total cell count and CD3+ cell count. The percent difference of CCR5+ cell count, CD3+CD4+ cell count, CD3+CCR5+ cell count, CD4+CCR5+ cell count, and CD3+CD4+CCR5+ cell count from manual counts for were all over 12%. In particular, the percent difference of CD3+CD4+CCR5+ cell counts from

manual counts was 24.9%. Generally, the percent difference from manual counts of automated counts generated with the pixel-based approach ranged between 1.25 (CD4+CCR5+ cells) to 8.4 times (CCR5+ cells) greater than automated counts generated with StarDist (**Table 5**). Automated cell segmentation of HIV target cells in foreskin tissue using our custom StarDist model had higher sensitivity and precision than automated cell segmentation using a pixel-based approach for all cell types. The sensitivity of our custom StarDist model was over 94% for counts of all cell types and over 97.5% for CD3+CCR5+ cell counts, CD4+CCR5+ cell counts, and CD3+CD4+CCR5+ cell counts. Meanwhile the sensitivity of the pixel-based workflow was less than 85% for all cell types except for counts for total cell count (93.58%) and CD3+ cells (91.10%). In particular, the sensitivity of the pixel-based approach for CD3+CD4+CCR5+ cells was only 60.70%. Precision wise, both StarDist and the pixel-based method had over 90% precision for all cell types except for CD4+CCR5+ cells and CD3+CD4+CCR5+ cells (87.94% and 85.19% respectively for StarDist, 69.77% and 77.96% respectively for the pixel-based workflow) (**Table 6**).

StarDist also had a lower false negative rate and lower false discovery rate than the pixel-based approach for counts all cell types. The false negative rate of automated cell segmentation using the StarDist model was under 5.2% for all cell types while the false negative rate for the pixel-based workflow was between 6.42% (total cell count) and 39.30% (CD3+CD4+CCR5+ cells). Overall, the false discovery rate for the pixel-based workflow was 1.7 (CD3+ cells) to 16.4 (CD3+CD4+CCR5+ cells) times higher than automated cell segmentation using our custom StarDist model. The false discover rate of both methods of automated cell segmentation was under 10% for all cell types except for CD4+CCR5+ cells and CD3+CD4+CCR5+ cells (12.06% and 14.81% respectively for StarDist, 30.23% and 22.04% respectively for the pixel-based approach) (**Table 5**).

Quantification of HIV target cells using StarDist appeared to be comparable to manual counting and the performance of the StarDist model exceeded the performance of pixel-based cell segmentation by all metrics we examined.

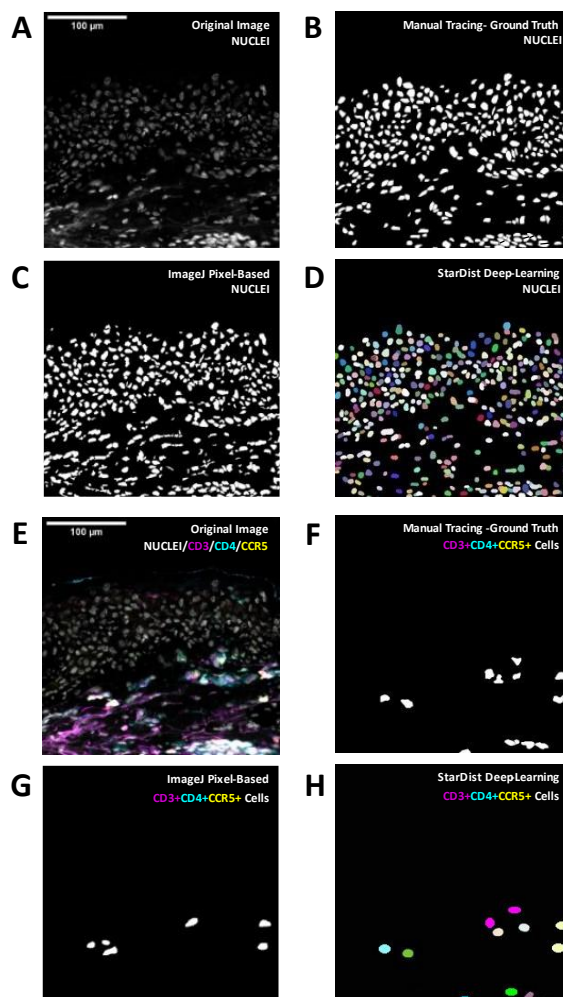


Figure 4: Automated segmentation of HIV target cells in foreskin tissue images stained for CD3, CD4, CCR5 and nuclei using a pixel-based workflow and StarDist. (A, E) Representative image of (A) nuclei staining and (E) composite image of staining for CD3, CD4, CCR5, and nuclei were generated from a cropped image of a full tissue section scan of foreskin tissue imaged at 200x total magnification. Visual representation of (B-D) counting of all positively stained nuclei and (F-H) counting of all CD3+CD4+CCR5+ cells in the representative image. Methods of cell segmentation presented include (B, F) Manual counting of cells, (C, G) automated counting using a pixel-based approach, and (D, H) automated segmentation using a custom StarDist deep-learning model.

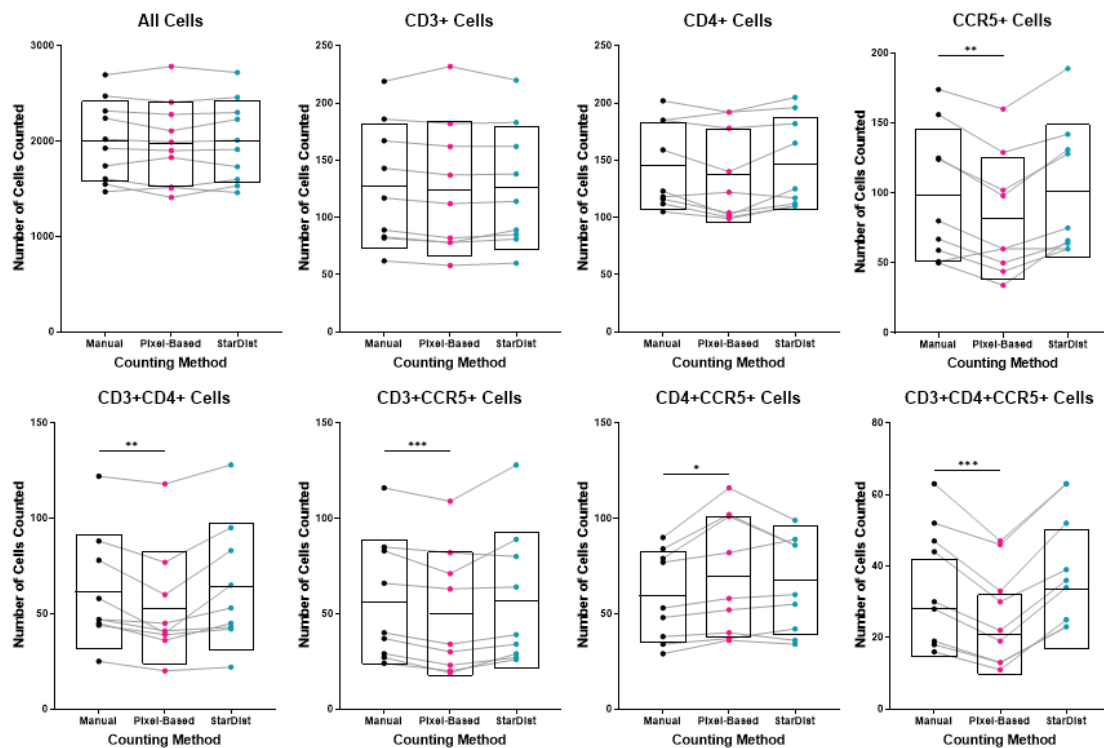


Figure 5: Comparison of automated counts generated using StarDist with manual counting and automated counts generated using a pixel-based workflow. Cell counting was completed on 10 validation field-of-view images (600x600 μ m) randomly generated from a set of 232 full foreskin tissue section scans stain for CD3, CD4, CCR5, and nuclei to identify HIV susceptible cells in the tissue. Full tissue section scan images were originally imaged at 200x total magnification. The 10 validation images include both inner foreskin and outer foreskin images. Manual counting of images was completed by 1 observer. Manual counts are represented by black dots while automated counts produced using a pixel-based workflow and StarDist are represented by pink and cyan dots respectively. Gray lines connect counts from the same validation image. Black center line and box represents mean \pm SD. Difference between manual counts and automated counts produced by the pixel-based workflow of StarDist was assess using two-tailed paired T-tests. Significant differences are indicated by asterisks (* $p \leq 0.05$, ** $p \leq 0.01$, *** $p \leq 0.001$).

Table 5: Performance of StarDist deep-learning model surpasses the performance of a previous validated pixel-based method for HIV target cell segmentation

		Cell Types							
		All Cells	CD3+ Cells	CD4+ Cells	CCR5+ Cells	CD3+ CD4+ Cells	CD3+ CCR5+ Cells	CD4+ CCR5+ Cells	CD3+ CD4+ CCR5+ Cells
Total Counts*	Manual	20037	1697	1843	1231	939	800	792	542
	Pixel-Based	19736	1651	1726	1019	796	704	1013	422
	StarDist	19956	1673	1866	1259	978	825	887	621
% Difference from Manual Counts	Pixel-Based	1.51%	2.75%	6.56%	18.84%	16.48%	12.77%	14.19%	24.90%
	StarDist	0.41%	1.42%	1.24%	2.25%	4.07%	3.08%	11.32%	13.59%
% Change from Manual Counts	Pixel-Based	-1.50%	-2.71%	-6.35%	-17.22%	-15.23%	-12.00%	15.28%	-22.14%
	StarDist	-0.40%	-1.41%	1.25%	2.27%	4.15%	3.13%	11.99%	14.58%
True Positives (TP)	Pixel-Based	18750	1546	1554	918	754	639	637	329
	StarDist	19720	1609	1780	1185	903	788	780	529
False Positive (FP)	Pixel-Based	986	105	172	101	42	65	276	93
	StarDist	236	64	86	74	75	37	107	92
False Negative (FN)	Pixel-Based	1287	151	289	313	185	161	155	213
	StarDist	317	88	63	46	36	12	12	13
Sensitivity/ True Positive Rate (TPR)	Pixel-Based	93.58%	91.10%	84.32%	74.57%	80.30%	79.88%	80.43%	60.70%
	StarDist	98.42%	94.81%	96.58%	96.26%	96.17%	98.50%	98.48%	97.60%
Precision/ Positive predictive value (PPV)	Pixel-Based	95.00%	93.64%	90.03%	90.09%	94.72%	90.77%	69.77%	77.96%
	StarDist	98.82%	96.17%	95.39%	94.12%	92.33%	95.52%	87.94%	85.19%
False negative rate (FNR)	Pixel-Based	6.42%	8.90%	15.68%	25.43%	19.70%	20.13%	19.57%	39.30%
	StarDist	1.58%	5.19%	3.42%	3.74%	3.83%	1.50%	1.52%	2.40%
False discovery rate (FDR)	Pixel-Based	5.00%	6.36%	9.97%	9.91%	5.28%	9.23%	30.23%	22.04%
	StarDist	1.18%	3.83%	4.61%	5.88%	7.67%	4.48%	12.06%	14.81%

*Generated from 10 FOV images (600x600 μm) of foreskin tissue stained for CD3, CD4, CCR5, and nuclei.

3.3.2 StarDist does not have issue with systematic overcounting or undercounting in different tissue regions

The epidermis and dermis regions of the foreskin are very different in terms of cell density and level of autofluorescence (**Figure 1&2**). To improve the accuracy of automated cell segmentation, many pixel-based workflows process the epidermis and dermis region of tissues using different image analysis parameters. However, even with specialized image processing for different tissue regions, systematic undercounting and overcounting can still occur. To determine if our StarDist model is also affected by systematic counting errors in different tissue regions, we manually split the 10 validation images described in section 3.3.1 into epidermis and dermis regions and determined the total number of manual counts, automated counts from the pixel-based method, and automated counts from StarDist for each of the regions. We compared the percent change of automated counts generated using the pixel-based method and automated counts generated using StarDist from manual counts in the epidermis or dermis to determine if systematic overcounting or undercounting was occurring. Percent change was selected as the metric used for assessment as it provided information on the directionality of differences between automated counts and manual counts (**Figure 6**).

For full tissue sections (before splitting into separate tissue regions) the percent change of StarDist counts from manual counts was within $\pm 5\%$ for all cell types except for CD4+CCR5+ cells (12.0%) and CD3+CD4+CCR5+ cells (14.6%). Automated segmentation with the pixel-based workflow was less accurate when looking at full tissue section counts as the percent change from manual counts was only with $\pm 10\%$ for total cell count, CD3+ cell counts, and CD4+ cell counts. The percent change for all other cell counts were outside of $\pm 12\%$ and specifically for CD3+CD4+CCR5+ cells at -22.1%. Overall, the percent change of automated counts from manual counts in the epidermis showed that both the pixel-based method and StarDist method were overcounting. This was much more dramatic for the pixel-based method. There was a positive percent change from manual counts for all cell types. In particular, the percent change from manual counts was over +25% for CD4+ cells, CCR5+ cells, CD3+CD4+ cells,

CD4+CCR5+ cells, and CD3+CD4+CCR5+ cells (**Figure 6**). Overcounting by the StarDist model in the epidermis was very minimal. There was a positive percent change for counts for all cell types except for CD3+ cells (-3.2%), however, all percent change values were within $\pm 10\%$. In the dermis, the pixel-based method displayed systematic undercounting as counts for all cell types had a negative percent change from manual counts. In particular, the percent change from manual counts for CD4+ cells, CCR5+ cells, CD3+CCR5+ cells, and CD3+CD4+CCR5+ cells were below -20%. The StarDist model had a negative percent change from manual counts for cell counts for total cell count, CD4+ cells, CCR5+ cells, CD3+CD4+ cells and CD3+CCR5+ cells but the percent change values for all cell types except for CD4+CCR5+ cells (12.2%) and CD3+CD4+CCR5+ cells (11.6%) were within $\pm 10\%$ (**Figure 6**). Overall, these results show that our StarDist model does not have issue with systematic overcounting or undercounting in different tissue regions.

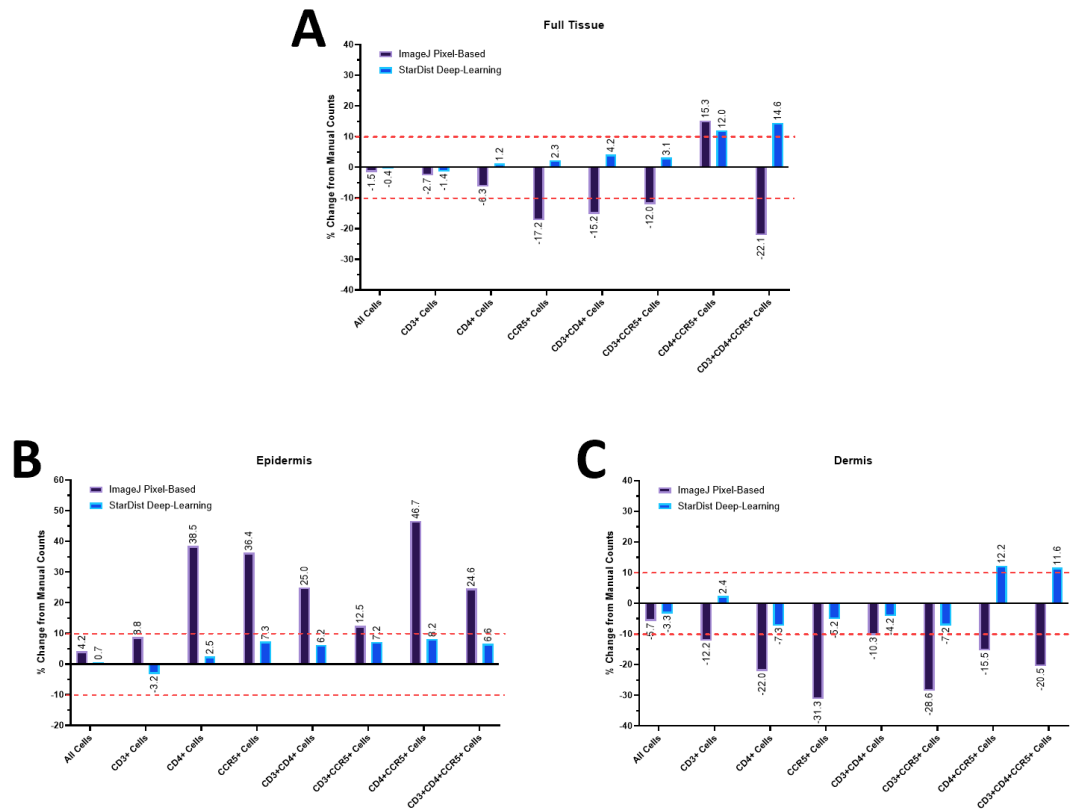


Figure 6: Automated cell segmentation using StarDist does not result in major overcounting or undercounting in different tissue regions. Cell counting was completed on 10 validation field-of-view images (600x600 μ m) randomly generated from a set of 232 full foreskin tissue section scans stain for CD3, CD4, CCR5, and nuclei to identify HIV susceptible cells in the tissue. The 10 validation images include both inner foreskin and outer foreskin images. Cell segmentation was completed on the full field-of-view images before images were manually divided into the epidermis and dermis sections. (A-C) Difference between automated counts and manual counts in (A) full tissue, (B) epidermis, and (C) dermis is shown as percent change of automated counts from manual counts. Percent difference of counts generated using a pixel-based approach is represented by purple bars while percent difference of counts generated using StarDist is represented by blue bars. Red dotted lines mark $\pm 10\%$ change of automated counts from manual counts.

3.3.3 Automated cell segmentation with StarDist is robust in areas with high cell density or high autofluorescence.

Pixel-based approaches for automated cell segmentation often struggle in areas with high cell density or high autofluorescence. Thresholding in areas with high cell density can often result in cell merging or splitting. Collagen fibers found in the dermis of foreskin tissue are highly autofluorescent and are often misidentified as cells with pixel-based cell segmentation methods. Due to the high prevalence of areas with densely packed cells and autofluorescence in foreskin tissue, it is critical that automated cell segmentation methods used to quantify HIV target cells are robust in these areas. While deep-learning methods for automated cell segmentation are designed to be less affected by noise, it was unclear if automated segmentation of HIV target cells using our custom StarDist model would be more effective than a pixel-based approach in difficult tissue regions with high cell density or high autofluorescence.

To compare the performance of our StarDist model with the performance of pixel-based approach in tissue regions with high cell density or high autofluorescence, we created 4 image crops (70x70 μ m) containing areas with high cell density and 4 image crops (70x70 μ m) containing areas with high levels of autofluorescence from each of the 10 validation images mentioned in section 3.3.1. This resulted in a total of 40 images crop containing areas with high cell density and 40 image crops containing areas with high levels of autofluorescence (**Figure 7**). High autofluorescence areas were characterized by the abundance of autofluorescent collagen fibers (**Figure 7A2**). Each of these image crops contained less than 30 cells and were meant to represent problematic areas that would challenge conventional pixel-based automated cell segmentation. We applied the StarDist model and pixel-based workflow on the image crops. Based on the image crops with high cell density, we determined the total number of images where cell merging or splitting occurred during the cell segmentation process for StarDist or the pixel-based approach (**Figure 7A3, B3, C3, D3**). Based on the image crops with high autofluorescence, we determined the total number of images where autofluorescent

collagen fibers were misidentified as cells by StarDist or the pixel-based approach (**Figure 7A2, B2, C2, D2**).

Cell merging and cell splitting occurred in ≥ 2 out of the 40 high cell density images when processed by the pixel-based approach for any cell type. There were over 10/40 images where cell splitting or merging occurred for nuclei, CD3+ cells, CD4+ cells, and CCR5+ cells for the pixel-based approach. In general, the number of image crops where cell merging occurred was 2 (CD4+CCR5+ cells) to 7 times (CD4+ cells) more for the pixel-based approach compared to processing with StarDist. In fact, cell merging and splitting only occurred in ≤ 6 images tested out of 40 for all cell types when processed using StarDist. No cases of cell merging occurred for CD3+CD4+ cells or CD3+CD4+CCR5+ cells and cell splitting was only seen for the segmentation of nuclei when using StarDist to process the 40 high cell density image crops (**Table 6**). Cell merging and cell splitting was most common for the segmentation of nuclei, likely due to the high number of nuclei compared to the number for the other individual cell types. Misidentification of autofluorescence as cells occurred ≥ 10 out of 40 high autofluorescence image crops tested for all cell types except for CD4+CCR5+ cells and CD3+CD4+CCR5+ cells when using the pixel-based approach for analysis. Conversely, misidentification of autofluorescence as cells occurred in ≤ 5 out of 40 high autofluorescence image crops when using StarDist for analysis. For both the pixel-based approach and StarDist, misidentification of autofluorescence as cells was most prevalent for CD3+ cell segmentation (35/40 image crops for pixel-based, 5/40 image crops for StarDist) (**Table 7**). Overall, these results suggest that StarDist is less likely to have problems with cell merging/splitting and misidentification of autofluorescence as cells. Automated cell segmentation with StarDist appears to be robust in areas that would normally challenge pixel-based automated cell segmentation workflows (**Figure 7**).

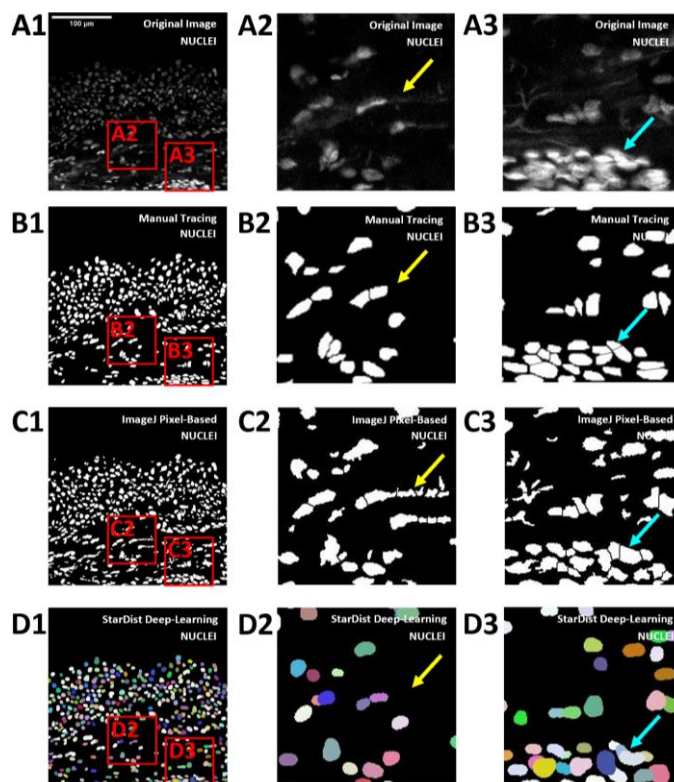


Figure 7: Comparison of automated cell segmentation using StarDist and a pixel-based workflow in tissue regions with high cell density or high autofluorescence.

Four image crops ($70 \times 70 \mu\text{m}$) representing areas of high cell density and four image crops representing areas with autofluorescence was generated from each of the 10 “validation” field-of-view images ($600 \times 600 \mu\text{m}$) generated from full foreskin tissue scans stained for CD3, CD4, CCR5 and nuclei (imaged at 200x total magnification). Cell segmentation was completed on the full field-of-view images before cropping. Less cell merging/splitting and misidentification of autofluorescence as cells was seen with the StarDist approach. Images shown in figure represent: **(A1-A3)** Unprocessed image of nuclei staining, **(B1-B3)** manual tracing of nuclei representing the ground truth, **(C1-C3)** automated segmentation using a pixel-based approach, **(D1-D3)** automated segmentation using StarDist. **(A1, B1, C1, D1)** Processing of validation field-of-view without cropping. **(A2, B2, C2, D2)** Processing of a tissue region with high autofluorescence. **(A3, B3, C3, D3)** Processing of a tissue region with high cell density. Yellow arrows point to autofluorescent collagen fibers while cyan arrows point to tightly packed cells.

Table 6: StarDist is less likely to have issues with cell merging, cell splitting, or misidentification of autofluorescence as cells in tissue regions with high cell density or high autofluorescence when compared to automated pixel-based cell segmentation

	Cell Types							
	All Cells	CD3+ Cells	CD4+ Cells	CCR5+ Cells	CD3+ CD4+ Cells	CD3+ CCR5+ Cells	CD4+ CCR5+ Cells	CD3+ CD4+ CCR5+ Cells
Cell Merging*								
Pixel-Based	32	13	14	17	5	8	8	2
StarDist	6	6	2	4	0	1	2	0
Cell Splitting*								
Pixel-Based	22	12	10	11	2	2	3	2
StarDist	5	0	0	0	0	0	0	0
Misidentification of Autofluorescence as Cells **								
Pixel-Based	27	35	16	15	11	14	7	2
StarDist	2	5	3	3	3	2	3	0

*Number of images (out of 40 images of tissue regions with high cell density) where cells were inaccurately merged or split during automated cell segmentation.

**Number of images (out of 40 images of tissue regions with high abundance of autofluorescent collagen fibers) where autofluorescence was misidentified as cells.

3.3.4 Accuracy of custom StarDist model rapidly improves with additional training images

Manual annotation of training images is by far the most time-consuming step of the training process of deep-learning models, and it can be hard to determine the optimal balance between improvements in model accuracy and time-investment for training. In this section, we show the improvement of our StarDist model in segmentation of nuclei (all cells), CD3+ cells, CD4+CCR5+ cells and CD3+CD4+CCR5+ cells after training with 10, 20, 30, and 40 images (**Figure 8**). The cell types that were chosen as points of focus for this analysis were selected based on their relevance to HIV susceptibility. Cells that are CD3 positive represent T cells, cells that are positive for CD4/CCR5 represent cells that HIV can attach to for entry, and cells that are positive for CD3/CD4/CCR5 represent CD4+CCR5+ T cells, which are the main reservoir for productive HIV infection in sexual transmission. Furthermore, the cell types selected are also relevant in terms of the number of image channels that are used as input. The segmentation of CD3+ cells, CD4+CCR5+ cells, and CD3+CD4+CCR5+ cells require 2, 3, and 4 image channels respectively as input for detection. Pooled cell counts were generated using the 10 validation images described in section 3.3.1 as input and percent difference from manual counts was used as a metric to measure accuracy. Overall, these results can serve as a guide for the training of new custom models to quantify other types of immune cells in genital mucosal tissue.

As expected, the percent difference of automated counts generated by StarDist from manual counts for all cell, CD3+ cells, CD4+CCR5+ cells and CD3+CD4+CCR5+ cells decreased with each of addition of 10 annotated images for training. The percent difference from manual counts for CD3+ cell counts, CD4+CCR5+ cell counts, and CD3+CD4+CCR5+ cell counts was reduced by 65-75%, 30-55%, 30-45% respectively with every additional 10 images used for training (**Figure 8D**). All versions of the StarDist model, except for the model trained with only 10 images, was the most accurate in segmentation nuclei (all cells), followed by segmentation of CD3+ cell, CD4+CCR5+ cells, and CD3+CD4+CCR5+ cells (ordered by lowest percent difference from manual

counts to highest percent difference from manual counts). The percent difference of automated StarDist counts from manual counts was below 10% for all cells (all nuclei) after training with 10 images and below 10% for CD3+ cells after training with 20 images. While automated segmentation of CD4+CCR5+ cells and CD3+CD4+CCR5+ cells did not manage to achieve a percent difference less than 10% after training with 40 images, the percent difference was very close to 10% at 11.32% and 13.59% respectively (**Figure 8D**).

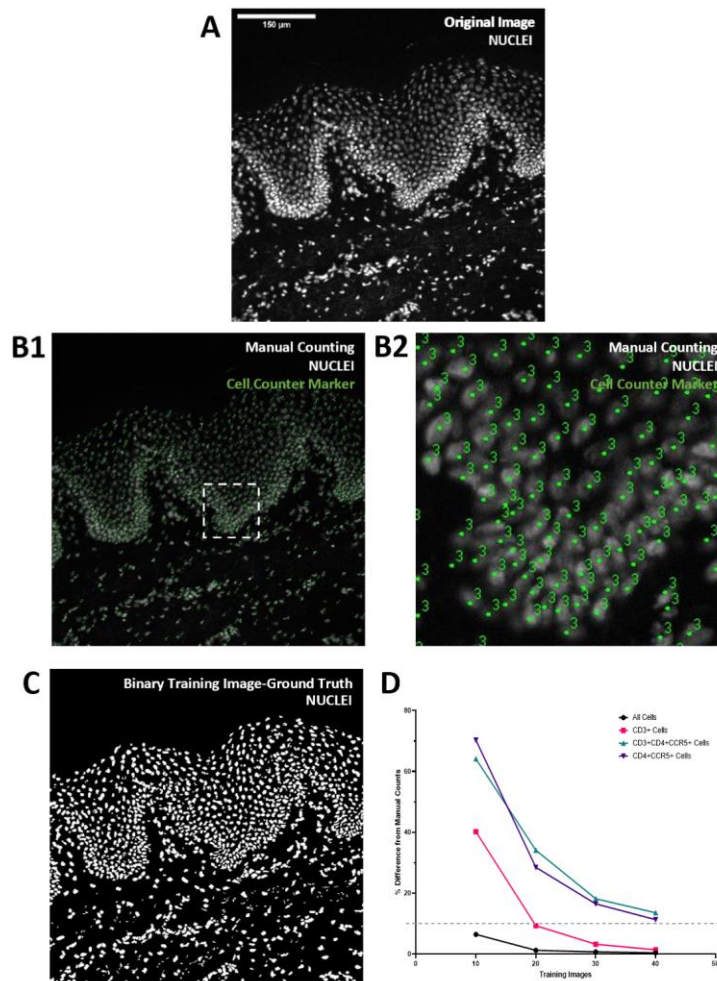


Figure 8: Training images rapidly improve the accuracy of a custom StarDist model used for the quantification of HIV target cells in foreskin tissue. (A-C) Workflow of annotating foreskin tissue stained for CD3, CD4, CCR5, and nuclei for StarDist model training. **(A)** Raw image of nuclei staining. **(B1-B2)** Manual cell counting using the Cell Counter plugin for Fiji. **(C)** Tracing of cells in the LabKit plugin for Fiji to produce annotated images for training. **(D)** Percent difference of automated counts generated by StarDist from manual counts for nuclei (all cells), CD3+ cells, CD4+CCR5+ cells, and CD3+CD4+CCR5+ cells after training with 10 images, 20 images, 30 images, and 40 images. Counting was completed on 10 validation field-of-view images (600x600μm) randomly generated from a set of 232 full foreskin tissue section scans stain for CD3, CD4, CCR5, and nuclei to identify HIV susceptible cells in the tissue.

3.4 Discussion

In this chapter we described the development and validation of a deep-learning approach to quantify HIV target cells in foreskin tissues. Using the Snakemake workflow management system and the StarDist plugin for Fiji, we trained a custom StarDist deep-learning model that can be used to identify HIV target cells in multi-channel immunofluorescent microscopy images of foreskin tissue (113,125,129). The accuracy of this deep-learning model was compared to manual counting and a conventional automated cell segmentation algorithm which utilizes a pixel-based approach (126). The reliability of the deep-learning model was also further tested in tissue regions with high cell density or high autofluorescence.

Most new HIV infections worldwide are still acquired via sexual transmission. In men, the availability of target cells in the foreskin is a critical determinant of HIV susceptibility in men during sex (38,41,54,91). Immunofluorescent microscopy is an excellent tool for understanding the spatial distribution of immune cells in genital mucosal tissues, however, cell segmentation in IF microscopy images can be difficult. Previous studies have relied on manual counting to quantify cells of interest; however, this approach is very time consuming and is vulnerable to bias due to the subjective nature of manual counting. Overall, manual counting is not feasible especially when full tissue section scans from large study cohorts need to be analyzed. Studies that use an automated approach for cell segmentation in immunofluorescent microscopy images often use a pixel-based workflow that relies on thresholding to identify positively stained cells (120,130). However, the reliability of this method is poor in regions with high cell density and high autofluorescence.

To address the issues related to automated immune cell segmentation in IF microscopy images of genital mucosal tissue, we developed and validated a deep-learning approach to quantify HIV target cells in the foreskin (113,125). This approach can replace conventional pixel-based methods for immune cell quantification and can be easily adapted to accommodate the detection of a wide variety of immune cell subsets in

different types of genital mucosal tissue. Our approach utilizes multi-channel IF microscopy images as input and enable the detection of multiple cell types (based on combination of marker staining) simultaneously. We decided to use StarDist and its plugin for Fiji as the backbone for the development of our deep-learning model because of its accessibility (113,125). StarDist is open source and use of StarDist models can easily be incorporated into existing image analysis workflows. Plugins that allow StarDist models to be run without any programming knowledge requirements are available for popular open-source software such as ImageJ/Fiji, Napari, QuPath, Icy, and KNIME (113,115,131,132). Results from utilizing StarDist models are also highly reproducible since trained StarDist models and training datasets can be easily shared.

The performance of our StarDist model against manual counting and automated segmentation using a conventional pixel-based approach using 10 validation images. Based on our validation, our custom StarDist model exceeded conventional pixel-based cell segmentation in performance metrics including percent difference from manual counts, sensitivity, precision, false negative rate, and false discovery rate (**Table 5**). Most notably, our custom StarDist model achieved over 94% sensitivity and over 85% precision for all cell types we examined. Automated counts with StarDist were also highly comparable to manual counts. There was no significant difference between StarDist counts and manual counts for all cell types examined for the 10 validation images (**Figure 5**). The percent difference of StarDist counts from manual counts was also less than 5% for all cell types except for CD4+CCR5+ cells (11.32%) and CD3+CD4+CCR5+ cells (13.59%). However, the percent difference of counts for these cell types are likely to decrease with more training. These cell types were the rarest among all cell types we examined, thus fewer instances were available for training compared to other cell types (**Table 5**). Detection of these cell types is also more complex as image information from 3 channels are used to detect CD4+CCR5+ cells and image information from 4 channels are used to detect CD3+CD4+CCR5+ cells. Cell detection using our StarDist model also appears to be robust in challenging tissue areas with high cell density or high levels of autofluorescence (**Figure 7**). Performance of

conventional automated cell segmentation can struggle in both the epidermis and dermis region of foreskin tissue for different reasons. In the epidermis, thresholding can be difficult due to high cell density. In the dermis, thresholding can be difficult due to high abundance of autofluorescent collagen fibers. In contrast to conventional automated cell segmentation that relies on thresholding, StarDist did not systematically overcount or undercount in the epidermis or dermis (**Figure 6**). StarDist also managed to detect cells with high accuracy in isolated cases of high cell density or high autofluorescence (**Table 6**). Based on these results, we conclude that the performance of our StarDist model is comparable to manual counting and StarDist is a suitable replacement for conventional pixel-based approaches for HIV target cell quantification.

A limitation of our custom StarDist model is that the images used for the training and validation were all acquired using the same microscope with the same imaging settings. The differences resulting from acquiring images with different microscopes may impact the accuracy of our model. While it might be possible to rescale images and to normalize the properties of images acquire from different microscopes, it is possible that our StarDist model will not perform reliably using images from other microscopes. Furthermore, our StarDist model is trained using foreskin tissue stained for CD3, CD4, CCR5, and nuclei. It cannot be reliably used to analyze foreskin tissues stained for different markers. The use of this algorithm with other tissue types such as cervical tissue has also not been validated. However, an easy solution for all these limitations is training with new images. New StarDist models can quickly be trained using our Snakemake framework (113,125,129).

An advantage of the StarDist approach for cell segmentation is that star-convex polygons are very good at identifying blob-like objects like nuclei or T cells. However, star-convex polygons are also bad at fully approximate the irregular shape of sprawling cells such as Langerhans cells. Deep-learning methods based on other shape approximation strategies might be needed to accurately segment irregularly shaped immune cells (133). Recent work by Mandal et al. described using planar parametric

spline curves for cell segmentation in a method called SplineDist (134). This method was shown to be capable of being incorporated into the StarDist architecture to accurately capture non-star-convex objects. Discrete cell segmentation methods, including StarDist, are also limited in the sense that positive cell surface marker staining that is unassociated with nuclei is unaccounted for in the segmentation process. The appendages of sprawling HIV target cells such as Langerhans cells and dendritic cells can often span through multiple tissue sections, resulting in cell membrane area that is positively stained for CD4 and CCR5 but unassociated with nuclei. Not accounting for these areas ignores a large amount of tissue area that HIV virions can use for cell entry. While pixel-based methods for image analysis are problematic for discrete cell segmentation, they are good for measuring the total amount of tissue area that is positively stained for a particular marker. Thus, pairing StarDist HIV target cell counting results with results from pixel-based quantification of CD4+CCR5+ tissue area could be beneficial in terms of gaining a more holistic understanding of HIV susceptibility in foreskin tissue.

To our knowledge, this study is the first to describe deep-learning methods for the identification of HIV target cells in multi-channel IF microscopy images of genital mucosal tissue. Previous studies have extensively described deep-learning methods for segmentation of CD3+ cells but these methods are mostly on histology images (135–138). Among the existing studies that use deep learning to segment cells in IF microscopy images, the vast majority are exclusively focused on nuclei segmentation. Existing methods for deep-learning cell segmentation in IF microscopy images are not designed to enable simultaneous quantification of multiple cell types. This limits understanding of both the distribution and composition of immune cells. Implementation and reproducibility of these models compared to StarDist are also more limited as they require a higher-level understanding of convolutional neural networks and software packages related to neural network construction (139,140).

Manual annotation of training images is one of the most time-consuming steps for the development of any supervised deep-learning models of cell segmentation. To work

around the problem of generating training images, recent studies have focused on developing generalist methods for cell segmentation that does not require new training data. These models were designed for nuclei segmentation; however, it is possible that these approaches can be adapted to work with T cells and other rounded cells have defined cell borders (139,141–143). Other previous attempts at improving the ease of adopting custom deep learning methods includes the creation of shared repositories of training sets with various tissue types and trained models. However, these repositories mainly contain IF images of nuclei or histology images. Improving the diversity of training images in these repositories would greatly improve the adoptability of deep-learning methods for cell segmentation (144–147).

In conclusion, in this chapter we showed that deep learning is an accurate and time saving approach that can be used to analyze immune cell composition in full mucosal tissue section scans. We trained and validated a custom StarDist model that produces highly accurate counts of HIV target cells in foreskin tissue. This model is robust in regions of high cell density and autofluorescence. Overall, this model can be easily applied and incorporated into existing ImageJ workflows which makes it an appropriate replacement for conventional pixel-based methods for automated HIV target cell segmentation.

Chapter 4

4 Effect of antimicrobial treatments on the penile microbiome, inflammation, and HIV target cells

4.1 Introduction

While many effective strategies are now available for HIV prevention, the reduction in the annual number of new HIV infections among adults has stalled since 2016 (1,13). Between 2010 and 2020, the total of new infection globally has only declined by 31%, which is far short of the 2020 UNAIDS target of 75%. Implementation of existing HIV prevention strategies has proven to be inefficient, and many countries have yet to sufficiently implement effective prevention measures for individuals who are most at risk of infection (18,148–150). Thus, a rework of current HIV prevention strategies and new tools for HIV prevention could be needed to increase the current pace of reducing new HIV infections globally.

Circumcision can reduce a heterosexual man's risk of acquiring HIV by up to 60% (14–16). However, many men at high risk of HIV acquisition still choose to remain uncircumcised and the biological mechanisms behind how circumcision modifies HIV risk is not completely understood. The abundance of certain species of anaerobic bacteria which are reduced by circumcision, was previously associated with HIV seroconversion, penile inflammation, and the abundance of HIV target cells in the foreskin in uncircumcised men (64,73,75,76). It is possible that these penile bacteria may be causing local inflammation which results in the recruitment of HIV target cells in the foreskin (31). If this is the case, modification of the penile microbiome in uncircumcised men using antimicrobial agents may represent a novel method of reducing the HIV susceptibility of men who choose to remain uncircumcised. However, it is not known if or which antimicrobial agents can optimally reduce penile anaerobes associated with HIV risk and if the reduction in the anaerobes will reduce foreskin inflammation and HIV susceptibility. In this chapter, we present select results from an open-label randomized controlled trial which examined the effect of commonly available antibacterial agents on

the foreskin microbiome, inflammation, and HIV susceptibility in Ugandan men (77). Specifically, men were either circumcised immediately without delay (control group) or asked to use topical clindamycin, topical metronidazole, topical hydrogen peroxide, or oral tinidazole for 4 weeks prior to circumcision. Using foreskin tissue collected at time of circumcision we compared the foreskin HIV target cell abundance between treatment group and control group men. We also correlated the abundance of HIV target cells in the foreskin with the abundance of BASIC species bacteria and soluble inflammatory markers in the coronal sulcus at time of circumcision. Detailed description of the randomized controlled trial can be found in chapter 2.

4.2 Methods

4.2.1 Quantification of HIV target cell availability using immunofluorescence microscopy

HIV target cells were quantified in IF microscopy images of foreskin tissue using (1) the automated deep-learning cell segmentation algorithm described in Chapter 3; (2) an automated pixel-based algorithm, that measures the total tissue area positive for both CD4 and CCR5 (as opposed to the pixel-based cell segmentation algorithm described in Chapter 3). The deep-learning cell segmentation algorithm was used to measure the number of HIV target cells per unit area of foreskin tissue. The pixel-based algorithm was used to quantify the total tissue area that is positive for both CD4 and CCR5. While the pixel-based algorithm is a simplified method for HIV target cell quantification, it complements the deep-learning algorithm since irregularly shaped target cells that are not captured effectively by discrete cell segmentation methods can be accounted for using this method (125).

We focused our image analysis only on the tissue area that was within 300 μ m of the apical surface of the epithelium (**Figure 9**). This was done as the total amount of dermis tissue in tissue sections varied greatly between study participants. The threshold of 300 μ m from the apical surface of the epithelium was selected as this area contained

the vast majority of HIV target cells in the tissue sections and would be most relevant for comparing HIV susceptibility between treatment groups (**Figure 9**).

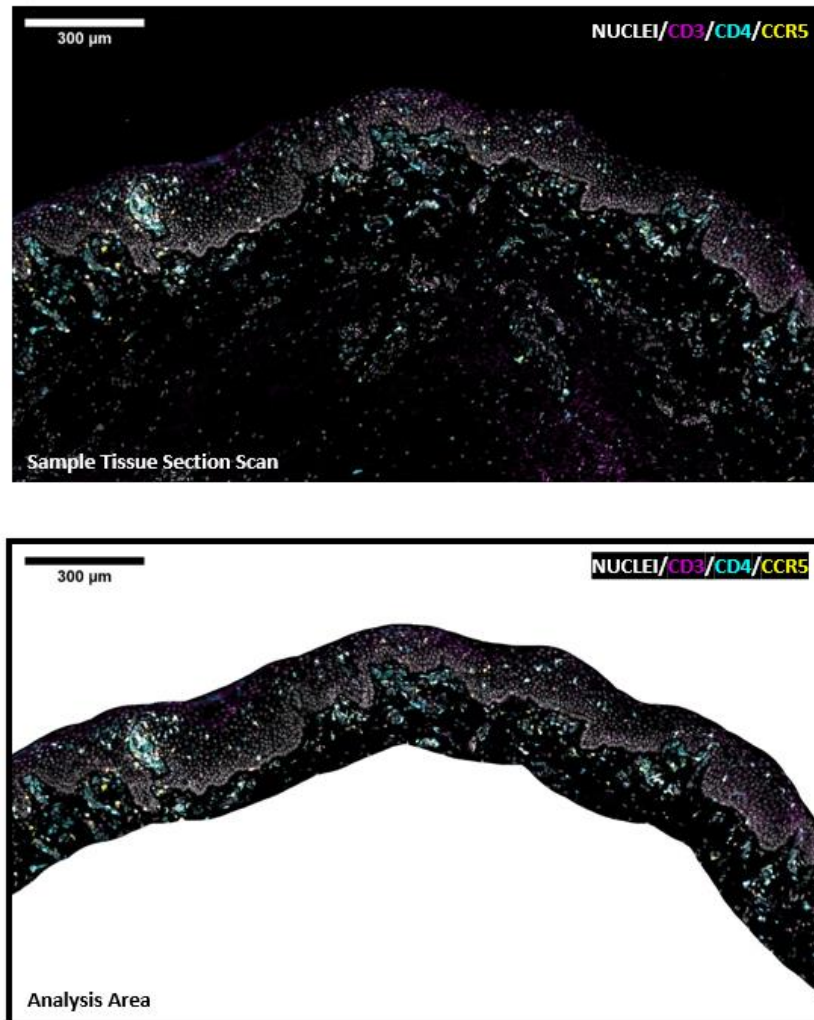


Figure 9: Tissue area used for HIV target cell quantification in immunofluorescent microscopy images of foreskin tissue. Full tissue section scans of foreskin tissue stained for CD3, CD4, CCR5, and nuclei were captured at 200x total magnification. The area within 300µm of the apical edge of the epidermis in each image was manually cropped out and saved for automated image analysis. HIV target cells in the 300µm region were quantified using a deep-learning cell segmentation algorithm and a pixel-based algorithm

was applied to determine the percent coverage of tissue area susceptible for HIV entry (CD4+CCR5+ tissue area) in the 300 μ m region.

4.2.2 Pixel-based quantification of HIV target cells by determine the percent coverage of tissue area

The workflow for this algorithm is built on image processing functions in the Fiji distribution of ImageJ2 (version 2.6.0) and the Adaptive Thresholding plugin (version 2019.06.24) for ImageJ (113,127). This approach for quantifying HIV target cells has been published by our group (126).

- (1) The total size of the tissue section was measured by applying the “Analyze Particles” function in Fiji with the parameters for “Circularity” set from 0.00 to 1.00, “Size” set from 0 to infinity, and options for “Display Results” and “Summarize” checked. Tissue section size measurement was completed on composite images of the tissue section scans with contains all channels merged (**Figure 10A**).
- (2) CD4 and CCR5 channel images undergo thresholding to eliminate background noise and isolate positive staining signal (**Figure 10B1, 10B2**). The CD4 and CCR5 channel images were first converted to 8-bit format and then the “Adaptive Thresholding” plugin is used with the parameters for “Block Size” and “Subtraction Value” set at 100 and -5 respectively for CD4 and 100 and -40 respectively for CCR5 (**Figure 10C1, 10C2**).
- (3) Positive staining for CCR5 is outlined and saved as “Regions of Interest” files using the “Analyze Particles” function in ImageJ with the parameters for “Circularity” set from 0.00 to 1.00, “Size” set from 0 to infinity, and options for “Overlay” and “Add to Manager” checked.
- (4) To determine the tissue area that is positive for both CD4 and CCR5, the CCR5 “Region of Interest” files were overlayed on top of a corresponding CD4 channel

image and then the “Clear Outside” function in Fiji is applied to eliminate any CD4 positive staining that is not within a CCR5 “Region of Interest” outline (**Figure 10D1, 10D2**). The remaining CD4 positive staining represents tissue area that is positive for both CD4 and CCR5 (**Figure 10E**).

- (5) The total area of this CD4 and CCR5 positive staining was measured by applying the “Analyze Particles” function in ImageJ with the parameters for “Circularity” set from 0.00 to 1.00, “Size” set from 0 to infinity, and options for “Display Results” and “Summarize” checked.
- (6) This area was divided by the total tissue section area to determine the percent signal coverage for CD4 and CCR5 for each tissue section.

The validity of this algorithm was assessed by comparison to manual assessment of CD4/CCR5 expression levels. Five randomly selected images (600 μ m by 600 μ m) were ranked by visual inspection from lowest to highest percent signal coverage for CD4 and CCR5. The percent signal coverage for CD4 and CCR5 were calculated by the pixel-based algorithm, and these numbers were used to generate rankings, which were compared to manual ranking.

Pre-written script for batch processing for the pixel-based quantification algorithm described above has been made available in the public domain (<https://github.com/prodgerlab/pixel-based-quantification>).

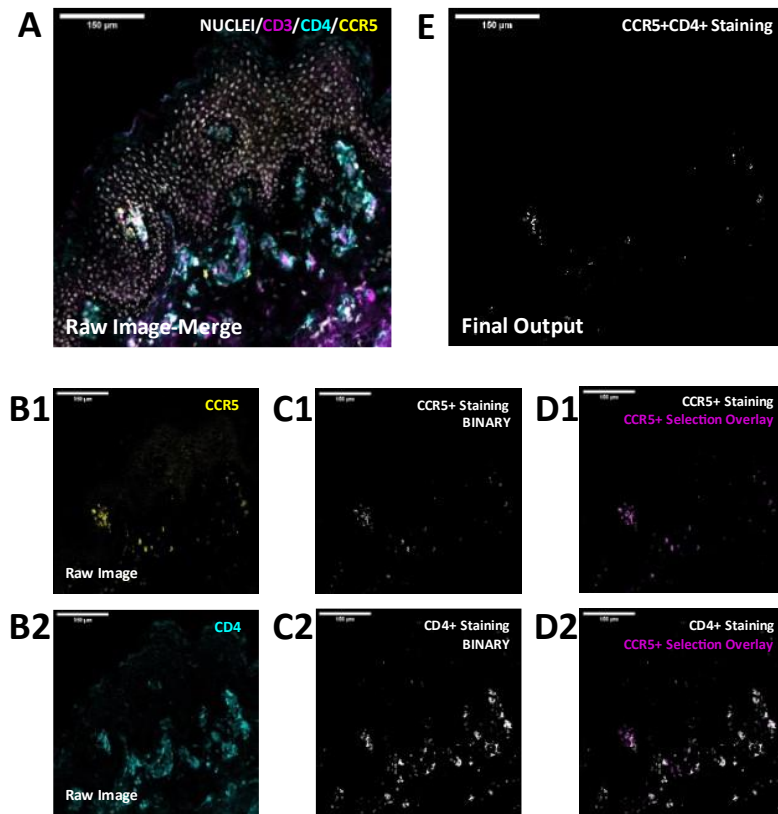


Figure 10: Overview of pixel-based approach for the quantification of tissue area available for HIV entry (CD4+CCR5+ area) in foreskin tissue section scans.

Analysis was completed using only the tissue area that was within 300 μ m of the apical surface of the epidermis of adult foreskin tissue (both inner and outer foreskin) stained for CD3, CD4, CCR5, and nuclei and imaged at 200x total magnification. (A) Representative image of foreskin tissue stained for the identification of HIV target cells. Image is a composite representing positive staining from all channels merged together. Raw, unprocessed staining for (B1) CCR5 and (B2) CD4 in the representative image. Binary image of (C1) CCR5+ staining and (C2) CD4+ staining after adaptive thresholding. (D1) Isolation and selection of CCR5+ staining and (D2) overlay of CCR5+ staining on CD4+ staining. (E) Elimination of CD4+ positive staining that does not overlap with CCR5+ positive staining to determine area that is positively stained for both CD4 and CCR5. Tissue area available for HIV entry is quantified by determine the percent coverage of CD4+CCR5+ staining over the tissue section.

4.2.3 Statistical analysis

Statistical analysis was completed using Prism v9 (GraphPad Software). The impact of antimicrobial agents on the density of HIV target cells in the foreskin based on immunofluorescent microscopy was assessed by comparing each antimicrobial intervention group with the untreated control group using a two-tailed Mann-Whitney tests. The difference in HIV target cell density between the inner foreskin and outer foreskin in all participants will be compared using a Wilcoxon matched pairs signed rank tests. The relationship between the penile absolute abundance of bacterial species of interest (i.e. bacterial species previously associated with HIV seroconversion, inflammation, and HIV target cell recruitment to the inner foreskin) and the density of HIV target cells in the inner foreskin will be determined as follows. First, participants will be organized from lowest to highest penile abundance of BASIC species and control taxa at the time of circumcision. Next the HIV target cell density of participants with no detectable amounts of BASIC species will be compared with the HIV target cell density of participants in the top quartile in terms of absolute abundance of BASIC species and control taxa using a Kruskal-Wallis test followed by a Dunn's multiple comparisons test. Correlation between penile levels of inflammatory cytokines/chemokines and the density of HIV target cells in the inner foreskin at the time of circumcision will be assessed with a simple linear regression.

4.3 Results

4.3.1 Effect of antimicrobial treatments on the abundance of penile bacteria

Penile microbiome data collection and bacteria swab sample processing was completed by study collaborators at George Washington University. Analysis was completed only for men who had available swab samples at all timepoints and were not lost to follow-up: clindamycin group (n=22), hydrogen peroxide group (n=25), metronidazole group (n=22), tinidazole group (n=23) (**Figure 11**).

Although not a part of this thesis, the effect of treatment on penile bacteria is presented here for context.

Both the total bacteria absolute abundance and pooled BASIC species absolute abundance was significantly reduced ($p < 0.05$) by topical antimicrobial treatments (topical clindamycin, topical hydrogen peroxide, topical metronidazole) after 1-week and 4-weeks of treatment while the pooled absolute abundance of control taxa bacteria was either not significant changed ($p > 0.05$) or was significantly increased ($p < 0.05$) after 1- or 4- weeks of treatment (**Figure 11**). For all treatments, the median total bacteria absolute abundance and median of pooled BASIC species absolute abundance was lower at the 1-week timepoint when compared to the 4-week timepoint. The most reduction in total bacteria absolute abundance and pooled BASIC species absolute abundance after 1 week of treatment was seen in the topical clindamycin group and then followed by the topical metronidazole group (**Figure 11**).

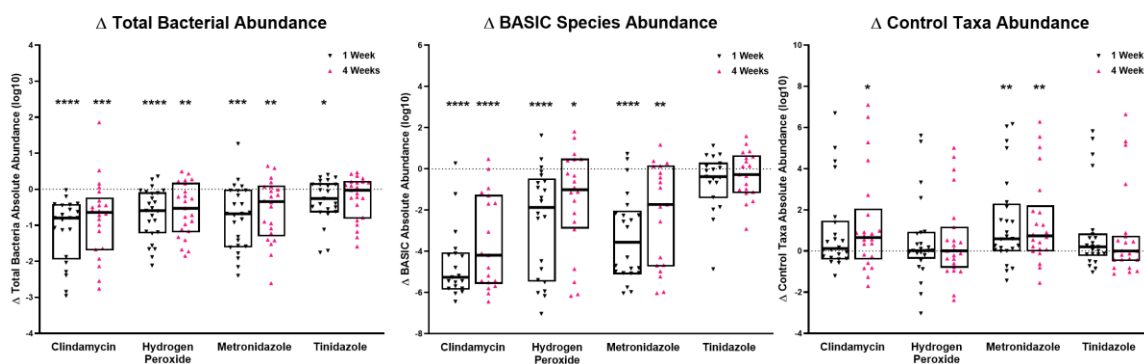


Figure 11: Topical antimicrobial treatments reduce total bacteria absolute abundance and BASIC species absolute abundance but not control taxa absolute abundance. The penile microbiome of study participants was characterized via amplicon sequencing and qPCR of the V3V4 hypervariable regions of the 16S rRNA gene using coronal sulcus swabs collected at baseline, 1-week of treatment and at the time of circumcision (4-weeks of treatment). Analysis was completed only for men who had available swab samples at all timepoints: clindamycin group (n=22), hydrogen peroxide group (n=25), metronidazole group (n=22), tinidazole group (n=23). Total bacteria absolute abundance and BASIC species absolute abundance were significantly lower ($p \leq 0.05$) at 1- and 4-weeks of treatment when compared to baseline for all topical antimicrobial treatment groups. Control taxa absolute abundance was not significantly different ($p > 0.05$) or was significantly increased ($p \leq 0.05$) after any treatment for 1-week or 4-weeks. Data shown is log₁₀ change of absolute bacteria abundance after 1-week (black triangle) or 4-weeks (pink triangle) of treatment. Solid black line and box represents median and interquartile range respectively. Difference in absolute bacterial abundance between 1-week of treatment and baseline and 4-weeks of treatment and baseline was assessed using Wilcoxon matched-pairs signed rank tests. Significant differences ($p \leq 0.05$) are represented by asterisks (* $p \leq 0.05$, ** $p \leq 0.01$, *** $p \leq 0.001$, **** $p \leq 0.0001$).

4.3.2 Effect of antimicrobial treatments on the density of HIV target cells in the foreskin

We focused our analysis on CD3+ cells (representing all T cells), CD3+CD4+CCR5+ cells (representing CD4+CCR5+ T cells), and CD3-CD4+CCR5+ cells (representing HIV target cells that are not T cells, this includes cells such as Langerhans cells, dendritic cells, and macrophages). The pixel-based algorithm was used to complement the cell segmentation algorithm. Using the pixel-based algorithm, we determined the percent coverage of total tissue area that was susceptible to HIV entry.

Based on this analysis strategy, we found that antimicrobial treatments reduced the abundance of HIV target cells in the foreskin, and this effect was limited to the inner foreskin (consistent with being caused by bacteria in the sub-preputial space) (**Figure 12**). The inner foreskin samples of participants in the topical clindamycin group and the topical metronidazole group had significantly lower density of CD3+ cells (T cells), CD3+CD4+CCR5+ cells (CD4+CCR5+ T cells), and CD3-CD4+CCR5+ cells (non-T cell HIV target cells) when compared to inner foreskin samples from men in the control group ($p < 0.05$). The percent coverage of CD4+CCR5+ area was also significantly lower in the inner foreskin samples from men in the clindamycin and metronidazole group when compared to control. The only topical antimicrobial treatments that had a significant effect on HIV target cells in the foreskin were clindamycin and metronidazole. The CD3+ cell density, CD3+CD4+CCR5+ cell density, CD3-CD4+CCR5+ cell density, and percent coverage of CD4+CCR5+ tissue area in the inner foreskin samples from the topical hydrogen peroxide group were not significantly different from those in the control group (**Figure 12A1, B1, C1, D1**). Interestingly, inner foreskin samples from men in the oral tinidazole were lower ($p < 0.05$) in the density of T cells and T cell subsets (CD3+ cells, CD3+CD4+CCR5+ cells) when compared to control. However, CD3- HIV target cell density (CD3-CD4+CCR5+ cells) and percent coverage of CD4+CCR5+ tissue area were not significantly different when compared to control ($p > 0.05$) (**Figure 12A1, B1, C1, D1**).

There was no significant difference in CD3+ cell density (T cells), CD3+CD4+CCR5+ cell density (CD4+CCR5+ T cells), CD3-CD4+CCR5+ cell density (CD3- HIV target cells) and the percent coverage of CD4+CCR5+ tissue area between any of the treatment groups and the control group in the outer foreskin (**Figure 12A2, B2, C2, D2**).

We did not find a significant difference in the proportion of CD3+CD4+ cells, CD3+CCR5+ cells, and CD3+CD4+CCR5+ cells in the inner foreskin tissue of the various treatment groups. Among all participants, CD3+CD4+ cell accounted for an average of 58.4% of all CD3+ cells, CD3+CCR5+ cells accounted for an average of 41.3% of all CD3+ cells, and CD3+CD4+CCR5+ cells accounted for an average of 33.1% of all CD3+ cells (**Table 7**).

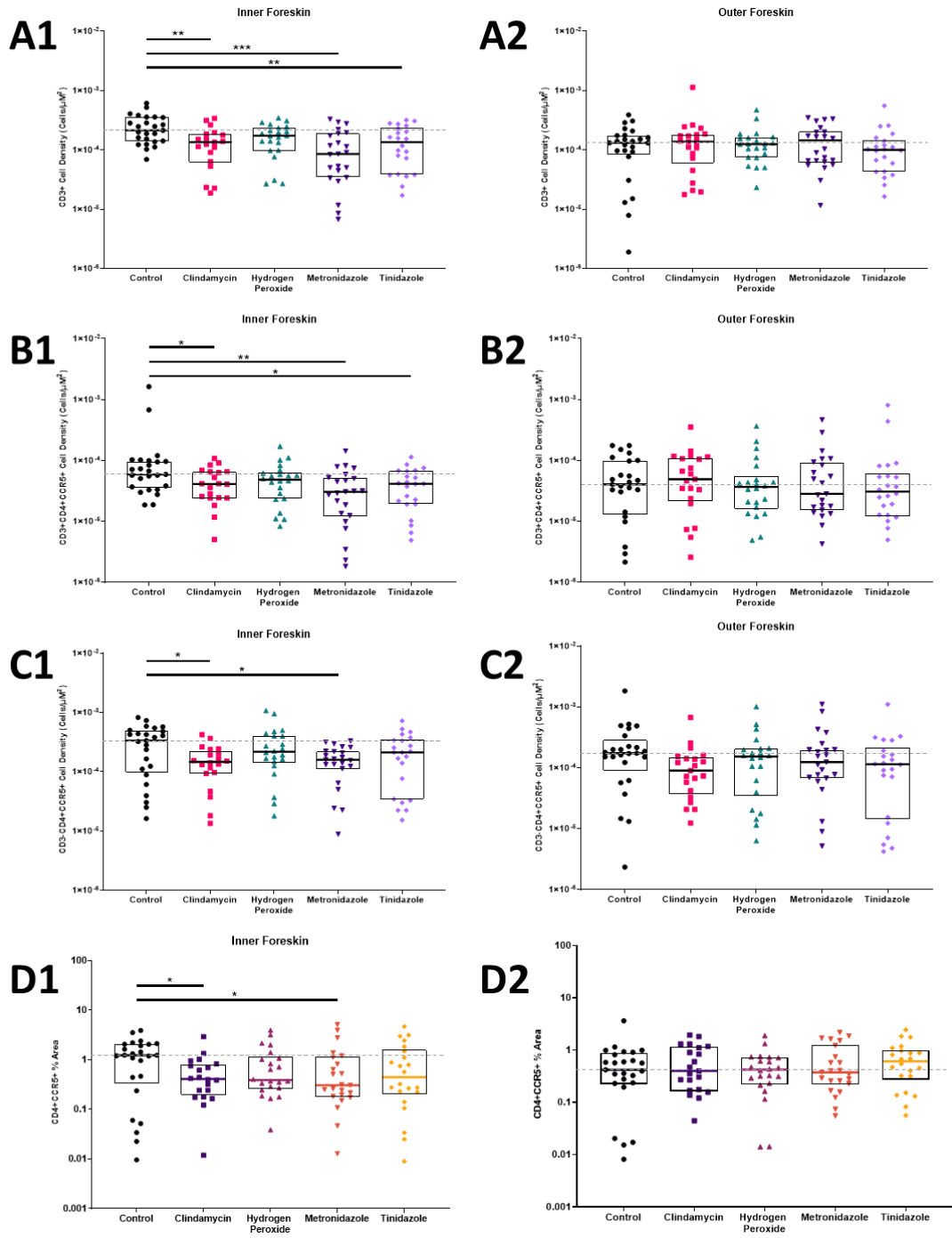


Figure 12: Effect of antimicrobial treatments on the abundance of HIV target cells in the foreskin. Foreskin tissue collected at time of circumcision from the randomized controlled trial were snap-frozen, cryosectioned at 8 μ m, and stained for CD3, CD4, CCR5, and nuclei for the identification of HIV target cells by immunofluorescent microscopy. Stained foreskin tissue sections were imaged at 200x total magnification and the tissue area within 300 μ m of the apical surface of the epidermis was analyzed using a deep-learning cell segmentation algorithm to determine the density of HIV target cells and an automated pixel-based algorithm to determine the percent coverage of HIV susceptible tissue area (CD4+CCR5+ area). Inner foreskin from men in the topical clindamycin and topical metronidazole groups had lower CD3+ cell density, CD3+CD4+CCR5+ cell density, CD3-CD4+CCR5+ cell density, and percent coverage of CD4+CCR5+ area when compared to those from control group men. Inner foreskin from men in the oral tinidazole group also had lower CD3+ cell density and CD3+CD4+CCR5+ cell density when compared to those from control group men. Results are presented as median with interquartile range (black line and box respectively). **(A1-A2)** CD3+ cell density, **(B1-B2)** CD3+CD4+CCR5+ cell density, **(C1-C2)** CD3-CD4+CCR5+ cell density, and **(D1-D2)** % coverage of CD4+CCR5+ tissue area in **(A1, B1, C1, D1)** inner foreskin and **(A2, B2, C2, D2)** outer foreskin samples. Difference in cell density or percent coverage of CD4+CCR5+ area between treatment groups and control group was assessed using two-tailed Mann-Whitney tests. Significant differences ($p \leq 0.05$) are represented by asterisks (* $p \leq 0.05$, ** $p \leq 0.01$, *** $p \leq 0.001$).

Table 7: Proportion of CD3+ cell subsets in the inner foreskin of study participants

	Proportion of CD3+ Cell Subsets*		
	CD3+CD4+ Cells	CD3+CCR5+ Cells	CD3+CD4+CCR5+ Cells
Control	49.9%	40.8%	29.3%
Topical Clindamycin	51.1%	41.2%	35.4%
Topical Hydrogen Peroxide	60.8%	42.5%	30.2%
Topical Metronidazole	63.9%	41.0%	36.2%
Oral Tinidazole	63.5%	40.8%	34.8%
All Participants	58.4%	41.3%	33.1%

Note: CD3+ cell subset proportions are displayed as mean percentages. Differences in CD3+ cell subset proportions between groups were evaluated using a Kruskal-Wallis test followed by a Dunn's multiple comparisons test. No significant differences were found ($p>0.05$).

*Proportion of CD3+ cell subset out of all CD3+ cells.

4.3.3 HIV target cell density is higher in the inner foreskin.

Evidence from previous studies have shown that the foreskin is enriched in HIV susceptible CD4 T cell subsets such as Th17 cells cell compared to peripheral blood and evidence suggests that the inner foreskin is more susceptible to HIV acquisition when compared to the outer foreskin (28,30,32). Several studies have also compared the composition of immune cells between the inner and outer foreskin and found that the inner foreskin had both an increased density of CD4+ T cells and increased levels of inflammatory cytokines (28–30). This evidence supports the idea that the anaerobic conditions of the sub-preputial space (space between inner foreskin and glans in non-erect penis) is conducive to the generation of pro-inflammatory environment that contributed to increased susceptibility to HIV infection.

We sought to examine if the difference in HIV target cell density in inner and outer foreskin samples from participants in our randomized controlled trial would align with these previous findings. To do this we compared the percent coverage of HIV susceptible tissue area and the density of HIV target cells (determined from automated analysis of immunofluorescent microscopy images) between the inner foreskin and outer foreskin samples from all participants in the trial. From our analysis we found that CD3+ cell density (T cells), CD3+CD4+CCR5+ cell density (CD4+CCR5+ T cells), CD3-CD4+CCR5+ cell density (CD3- HIV target cells), and the percent coverage of CD4+CCR5+ tissue area were all significantly higher in the inner foreskin ($p < 0.01$) (**Figure 13**).

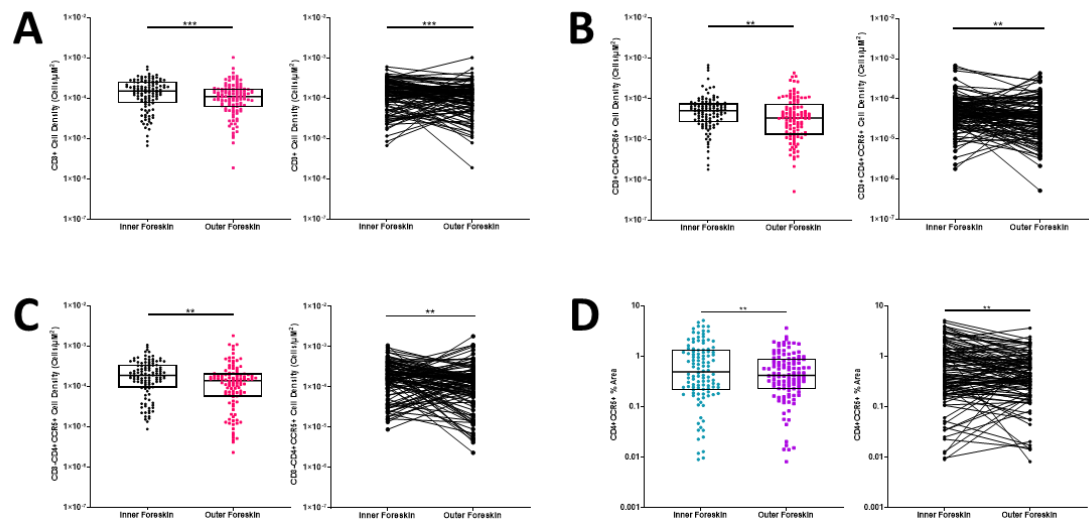


Figure 13: Higher abundance of HIV target cells in found in the inner foreskin.

Foreskin tissue collected at time of circumcision from the randomized controlled trial were snap-frozen, cryosectioned at $8\mu\text{m}$, and stained for CD3, CD4, CCR5, and nuclei for the identification of HIV target cells by immunofluorescent microscopy. Stained foreskin tissue sections were imaged at 200x total magnification and the tissue area within $300\mu\text{m}$ of the apical surface of the epidermis was analyzed using a deep-learning cell segmentation algorithm to determine the density of HIV target cells and an automated pixel-based algorithm to determine the percent coverage of HIV susceptible tissue area (CD4+CCR5+ area). Comparisons revealed that (A) CD3+ cells density, (B) CD3+CD4+CCR5+ cell density, (C) CD3-CD4+CCR5+ cell density, and (D) percent coverage of CD4+CCR5+ tissue area were all higher in the inner foreskin. Results are presented as median with interquartile range (black line and box respectively). Difference in cell density or percent coverage of CD4+CCR5+ area between inner foreskin and outer foreskin samples were assessed using Wilcoxon match-pairs signed rank tests. Significant differences ($p \leq 0.05$) are represented by asterisks (** $p \leq 0.01$, *** $p \leq 0.001$).

4.3.4 Soluble inflammatory molecules correlate with HIV target cells density

One way that anaerobic bacteria could modulate HIV susceptibility is by causing local inflammation in the inner foreskin which subsequently result in increased abundance of immune cells including HIV susceptible CD4+ T cells. Based on this idea, anaerobic bacteria previously associated with HIV risk would interact with the epithelial cells and innate immune system of the foreskin mucosa and promote the release of soluble mediators of inflammation in the foreskin.

Unpublished analysis performed by our collaborators have shown that the abundance of soluble inflammatory molecules including soluble E-Cadherin, IL-1 β , IL-8, and Resistin were reduced by topical clindamycin and metronidazole treatment. The results in section 4.3.2 of this thesis have also shown that the availability of HIV target cells in the inner foreskin is significantly lower in men in the topical clindamycin, topical metronidazole, and oral tinidazole groups (**Figures 12**). However, it is unclear if these observations are related. To answer this question, we correlated the levels of soluble inflammatory molecules in coronal sulcus swabs collected at the time of circumcision with CD3+ cell density, CD3+CD4+CCR5+ cell density, CD3-CD4+CCR5+ cell density, and the percent coverage of CD4+CCR5+ tissue area in the inner foreskin (**Figures 14-17**). Based on our analysis, we found that the levels of 4 out of 9 inflammatory molecules that we examined were positively correlated with the density of CD3+ cells, CD3+CD4+CCR5+ cells and CD3-CD4+CCR5+ cells in the inner foreskin ($p < 0.01$). These 4 molecules include soluble E-cadherin, IL-1 β , IL-8, and Resistin (**Figures 14-16**).

Of note, unpublished results from our collaborators have also shown that the reduction in the levels of only these 4 molecules from baseline to time of circumcision were associated with the reduction in total bacterial abundance and BASIC bacteria abundance. Interestingly, we did not find the percent coverage of CD4+CCR5+ tissue area in the inner foreskin to be significantly correlated with levels of any of the 9 inflammatory molecules we measured despite seeing a correlation between

CD3+CD4+CCR5+ cell density and CD3-CD4+CCR5+ cell density with inflammatory molecule levels (**Figures 15-17**). The levels of IL-1 α , MIP-1, MMP-9, TIMP1 and VEGF did not appear to be directly correlated to the abundance of HIV target cells in the inner foreskin ($p>0.05$).

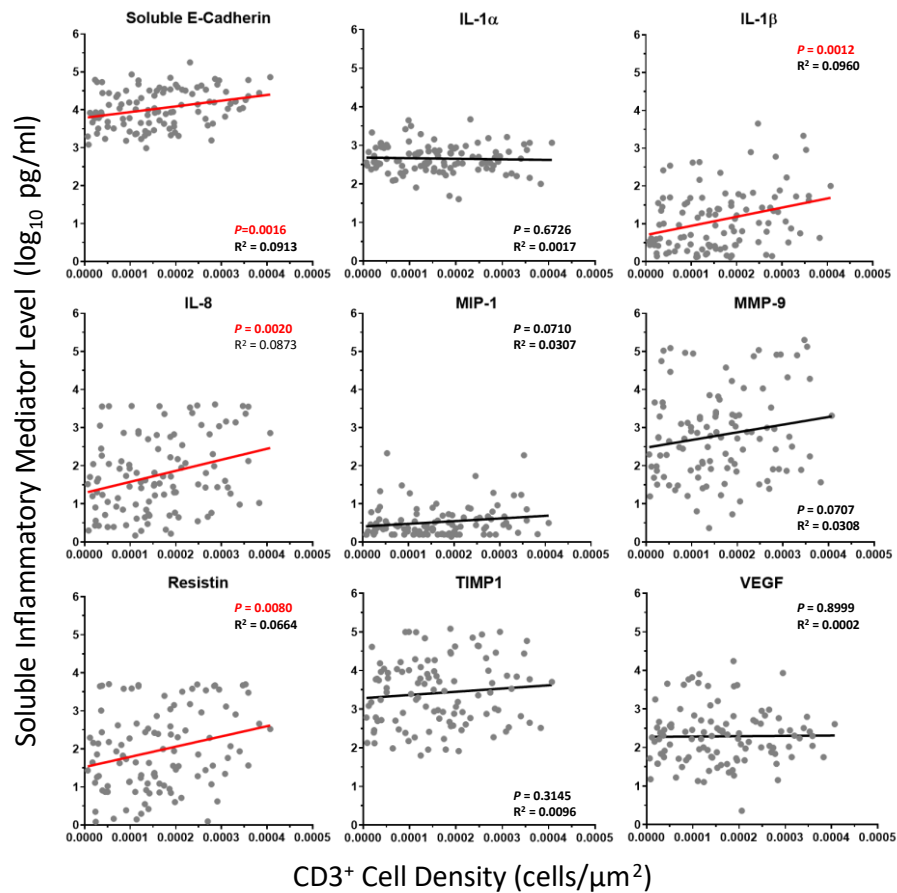


Figure 14: Inner foreskin CD3⁺ cell density is correlated with soluble inflammatory mediator levels in the coronal sulcus. Foreskin tissue collected from the randomized controlled trial were cryosectioned at 8 μ m and stained for CD3, CD4, CCR5, and nuclei for immunofluorescent microscopy analysis. Tiled full tissue sections scans were captured at 200x total magnification and a deep-learning cell segmentation algorithm was used to quantify CD3⁺ cells within 300 μ m of the apical surface of the epidermis in each image. Soluble inflammatory mediator levels in coronal sulcus swabs collected immediately before circumcision were measured using a chemiluminescent multiplex ELISA assay. Levels of soluble E-Cadherin, IL-1 β , IL-8 and Resistin were positively correlated with CD3⁺ cell density ($p < 0.01$). Trend lines represent simple linear regressions. Significant correlations are indicated by red trendlines and red p-values ($p < 0.05$).

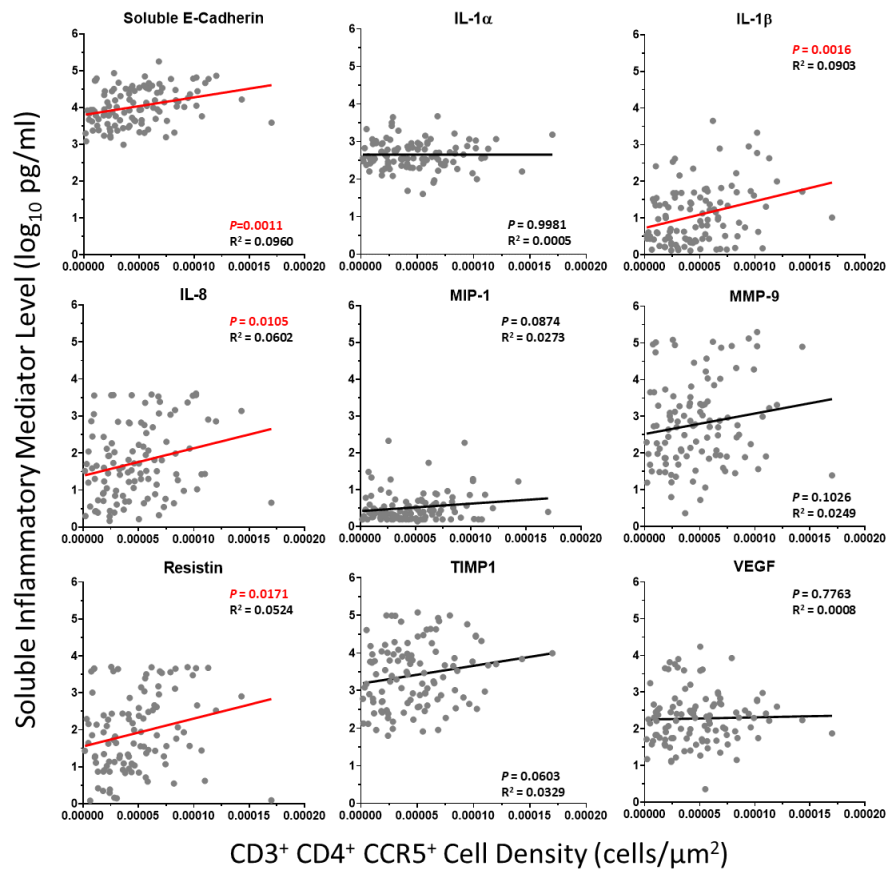


Figure 15: Inner foreskin CD3+CD4+CCR5+ cell density is correlated with soluble inflammatory mediator levels in the coronal sulcus. Foreskin tissue collected from the randomized controlled trial were cryosectioned at 8 μ m and stained for CD3, CD4, CCR5, and nuclei for immunofluorescent microscopy analysis. Tiled full tissue sections scans were captured at 200x total magnification and a deep-learning cell segmentation algorithm was used to quantify CD3+CD4+CCR5+ cells within 300 μ m of the apical surface of the epidermis in each image. Soluble inflammatory mediator levels in coronal sulcus swabs collected immediately before circumcision were measured using a chemiluminescent multiplex ELISA assay. Levels of soluble E-Cadherin, IL-1 β , IL-8 and Resistin were positively correlated with CD3+CD4+CCR5+ cell density ($p < 0.05$). Trend lines represent simple linear regressions. Significant correlations are indicated by red trendlines and red p-values ($p < 0.05$).

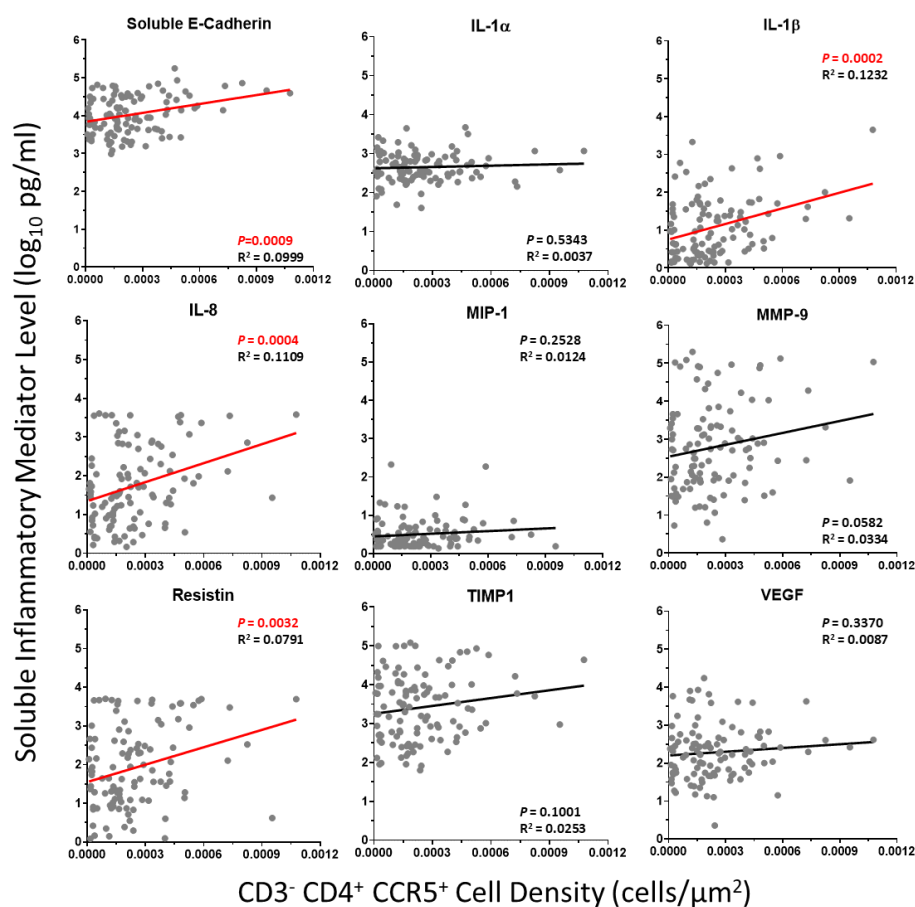


Figure 16: Inner foreskin CD3-CD4+CCR5+ cell density is correlated with soluble inflammatory mediator levels in the coronal sulcus. Foreskin tissue collected from the randomized controlled trial were cryosectioned at 8 μ m and stained for CD3, CD4, CCR5, and nuclei for immunofluorescent microscopy analysis. Tiled full tissue sections scans were captured at 200x total magnification and a deep-learning cell segmentation algorithm was used to quantify CD3-CD4+CCR5+ cells within 300 μ m of the apical surface of the epidermis in each image. Soluble inflammatory mediator levels in coronal sulcus swabs collected immediately before circumcision were measured using a chemiluminescent multiplex ELISA assay. Levels of soluble E-Cadherin, IL-1 β , IL-8 and Resistin were positively correlated with CD3-CD4+CCR5+ cell density ($p < 0.05$). Trend lines represent simple linear regressions. Significant correlations are indicated by red trendlines and red p-values ($p < 0.05$).

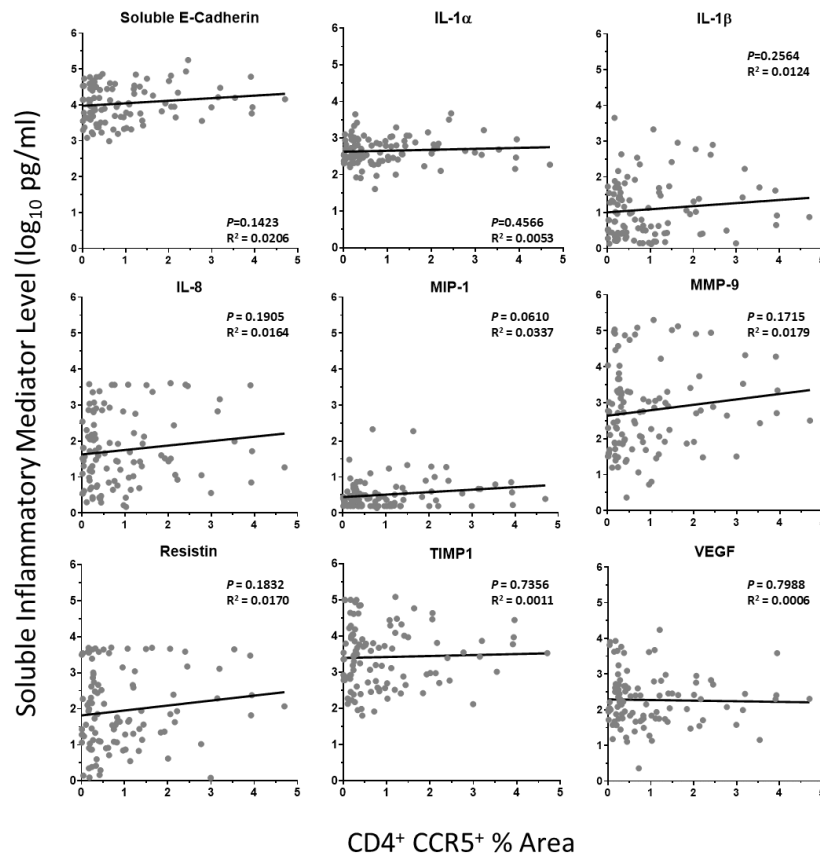


Figure 17: Percent coverage of inner foreskin CD4+CCR5+ tissue area is not correlated with soluble inflammatory mediator levels in the coronal sulcus. Foreskin tissue collected from the randomized controlled trial were cryosectioned at 8 μ m and stained for CD3, CD4, CCR5, and nuclei for immunofluorescent microscopy analysis. Tiled full tissue sections scans were captured at 200x total magnification and an automated pixel-based algorithm was used to quantify the CD4+CCR5+ tissue area within 300 μ m of the apical surface of the epidermis in each image. Soluble inflammatory mediator levels in coronal sulcus swabs collected immediately before circumcision were measured using a chemiluminescent multiplex ELISA assay. Abundance of all soluble inflammatory molecules measured were not correlated with CD4+CCR5+ tissue area ($p > 0.05$). Trend lines represent simple linear regressions. The p-value and R^2 value for the simple linear regressions are provided with each scatter plot.

4.3.5 High absolute abundance of BASIC species, but not overall bacterial load, is associated with HIV target cell density

Previous studies by our group have found BASIC species, but not overall bacterial load, to be associated with HIV seroconversion, increased penile abundance of inflammatory cytokines/chemokines, and increased abundance of CD4+ T cells in the foreskin (75). In unpublished analysis of the coronal sulcus swab samples from the RCT by our collaborators, it was found that the penile abundance of BASIC species was associated with penile soluble inflammatory marker abundance. Our analysis in section 4.3.4 of this thesis has also found that the abundance of penile soluble inflammatory markers was also associated with HIV target cell availability in the inner foreskin (**Figures 14-17**). Given these observations and results supporting that penile bacterial abundance, penile inflammatory marker abundance, and foreskin HIV target cell abundance are all reduced by antimicrobial treatments, we sought to determine if the difference in foreskin HIV target cell density between study participants could be explained by the difference in abundance of BASIC species (**Figure 18-19**).

We classified men from the randomized controlled trial into 4 groups: High BASIC (group 1, n = 28), Medium BASIC (group 2, n = 52), No BASIC (group 3, n = 35), and High Control (group 4, n = 28). Groups 1 to 3 were determined by sorting all participants based on the pooled absolute abundance (log₁₀ 16S RNA gene copies per swab) of BASIC species (median: 4.16438, IQR: 0, 5.14056) in coronal sulcus swabs collected at time of circumcision. Men in the top quartile for BASIC species absolute abundance were placed in the High BASIC species group (BASIC absolute abundance \geq 5.14056, n = 28). Men with no detectable BASIC bacteria were placed in the No BASIC group (BASIC absolute abundance = 0, n = 35). Remaining men were placed in the Medium BASIC group (0 < BASIC absolute abundance < 5.14056, n = 52). Group 4 (High Control) was determined by sorting all participants based on pooled absolute abundance (log₁₀ 16S RNA gene copies per swab) of control taxa bacteria (median: 4.75902, IQR: 4.05717, 5.39375) and then selecting the men in the top quartile for control taxa absolute abundance (control taxa absolute abundance > 5.39375, n = 28).

Total bacterial density of the High BASIC group and High Control group were not significantly different from each other; however, the absolute abundance of BASIC species was significantly higher in the High BASIC group when compared to the High Control group (**Figure 18**). Overall, we found that the abundance of BASIC bacteria was associated with the abundance of HIV target cell density (**Figure 18**). However, this relationship was only seen in the inner foreskin. The density of HIV target cells and the percent coverage of CD4+CCR5+ tissue area were similarly low in all 4 groups in the outer foreskin and matched the inner foreskin HIV target cell density and percent coverage of CD4+CCR5+ tissue area for the No BASIC group. Men in the High BASIC group had significantly higher CD3+ cell density, CD3+CD4+CCR5+ cell density, CD3-CD4+CCR5+ cell density, and percent coverage of CD4+CCR5+ tissue area compared to the No BASIC group ($p < 0.05$) (**Figure 19A-D**). Furthermore, similar to previous findings we also found that the relative proportions of specific T cell subsets were similar across all 4 groups in the inner foreskin. This suggests that BASIC bacteria were not inducing the recruitment of specific T cell subsets more than others. Rather, it seems that all T cells were recruited to the inner foreskin by BASIC bacteria in a generalized manner (**Figure 19E**).

Interestingly, inner foreskin CD3+ cell density (No BASIC median: 1.14×10^{-4} cells/ μm^2 , High Control median: 1.19×10^{-4} cells/ μm^2), CD3+CD4+CCR5+ cell density (No BASIC median: 3.83×10^{-5} cells/ μm^2 , High Control median: 3.72×10^{-5} cells/ μm^2), CD3-CD4+CCR5+ cell density (No BASIC median: 1.37×10^{-4} cells/ μm^2 , High Control median: 1.33×10^{-4} cells/ μm^2), and the percent coverage of CD4+CCR5+ tissue area (No BASIC median: 0.2493%, High Control median: 0.2925%) were very similar between the No BASIC group and High Control group. In fact, inner foreskin CD3+CD4+CCR5+ cell density, CD3-CD4+CCR5+ cell density, and percent coverage of CD4+CCR5+ tissue area were all significantly higher in the High BASIC group when compared to the High Control group (**Figure 19A-D**). Taken together, these results further support the idea that the abundance of BASIC bacteria rather than total bacteria density is associated with HIV target cell recruitment in the inner foreskin

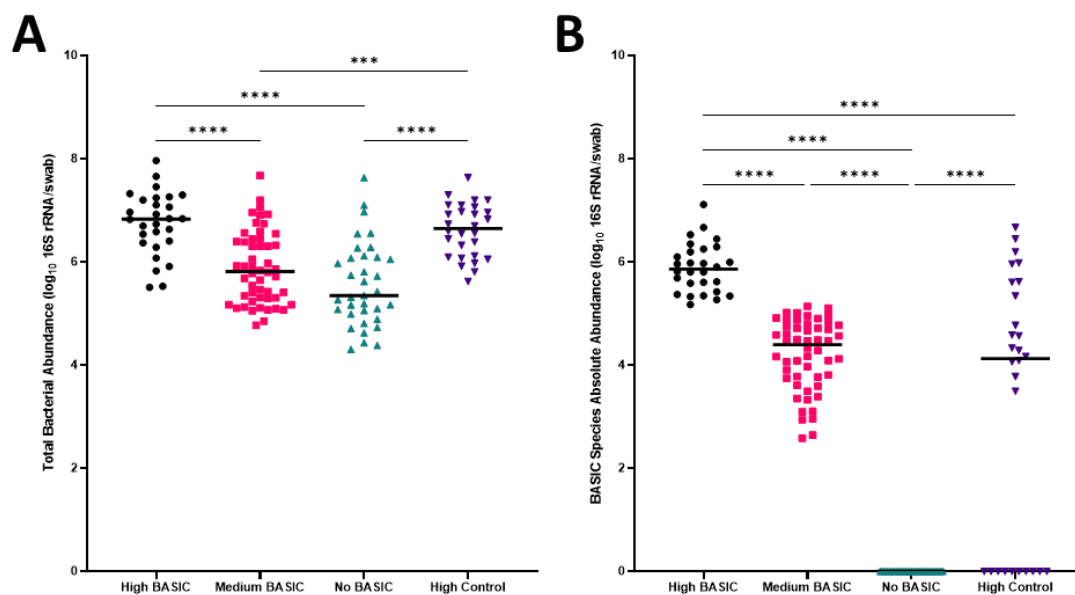


Figure 18: Men in the top quartile for abundance of BASIC species and men in the top quartile for abundance of control taxa have similar total bacterial abundance but differ in abundance for BASIC species. Men from the randomized controlled trial were sorted based on pooled absolute abundance of BASIC species then sorted based on pooled control taxa absolute abundance in coronal sulcus swabs collected at time of circumcision. Men in the top quartile for BASIC abundance were placed in the High BASIC group (n = 28), men with no detectable BASIC bacteria were placed in the No BASIC group (n = 35), and men with detectable BASIC bacteria but were not in the top quartile for BASIC abundance were placed in the medium BASIC group (n = 52). Men in the top quartile for control taxa abundance were placed in the High BASIC group. The total bacterial abundance (**A**) of High BASIC group men and High Control group men were not significantly different. However, BASIC species absolute abundance (**B**) was significantly higher in the High BASIC group men compared to the High Control group men. Differences in bacterial abundance were assessed using a Kruskal-Wallis test with a Dunn's multiple comparisons test. Significant differences ($p \leq 0.05$) are represented by asterisks (*** $p \leq 0.001$, **** $p \leq 0.0001$).

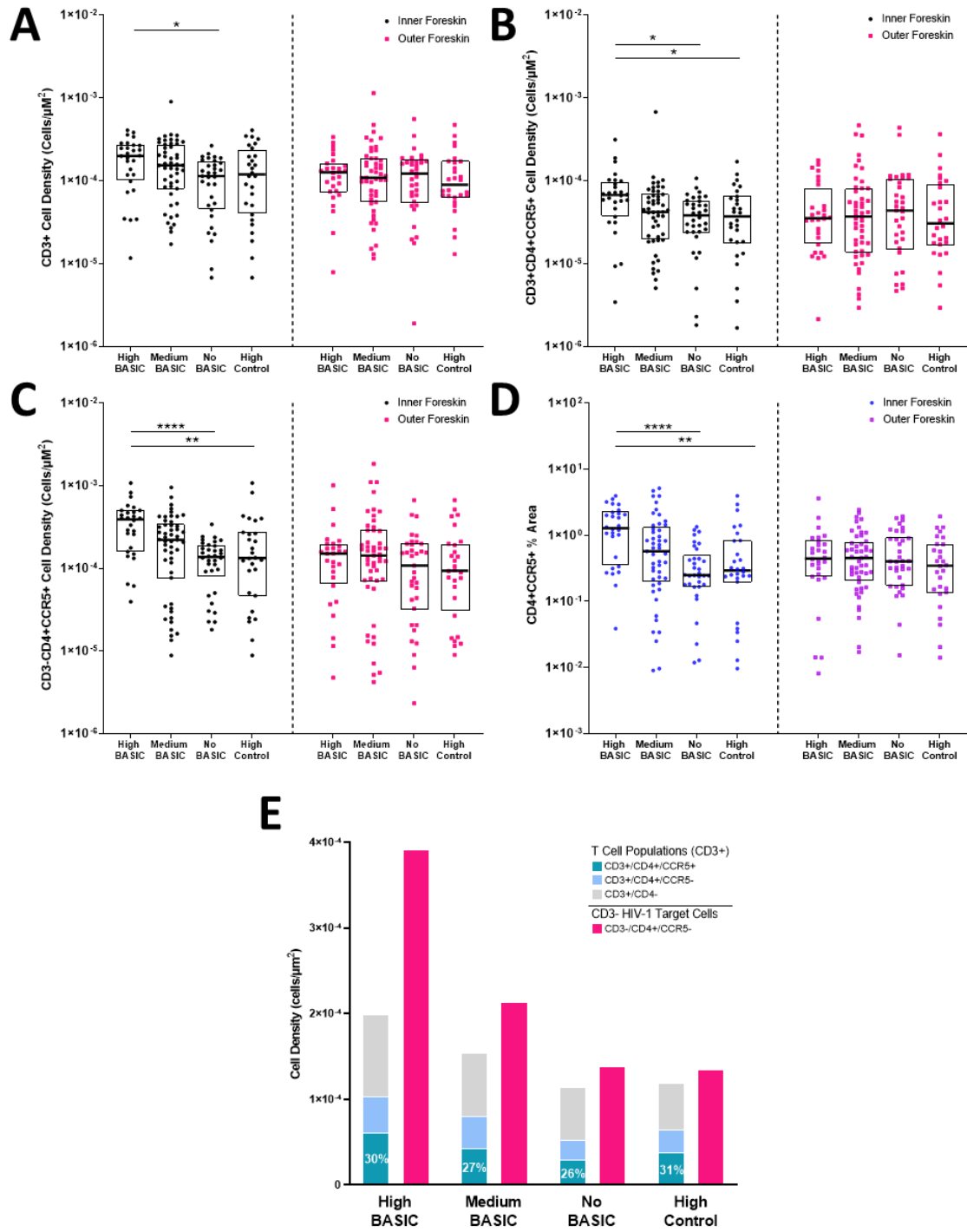


Figure 19: High abundance of BASIC species is associated with recruitment of HIV target cells to the inner foreskin without alterations in T cell subset distribution.

Participants in the randomized controlled trial were sorted into 4 groups based on BASIC species abundance and control taxa abundance: High BASIC group (n = 28), Medium BASIC group (n = 52), No BASIC group (n = 35), and High Control group (n=28). The **(A)** CD3⁺ cell density, **(B)** CD3⁺CD4⁺CCR5⁺ cell density, **(C)** CD3⁻CD4⁺CCR5⁺ cell density, and **(D)** percent coverage of CD4⁺CCR5⁺ tissue area in the inner and outer foreskin of men in each of the groups was determined through immunofluorescent microscopy and automated image analysis. Measurement of cell density and CD4⁺CCR5⁺ tissue was restricted to the area within 300 μ m of the apical surface of the epithelium. Lines and boxes in scatter plots **(A-D)** represent median and interquartile range respectively. **(E)** Proportions of T cell subsets in each of the groups in the inner foreskin. Differences in cell density or percent coverage of CD4⁺CCR5⁺ tissue area was determine using a Kruskal-Wallis test followed by a Dunn's multiple comparisons test. Significant differences ($p \leq 0.05$) are represented by asterisks (* $p \leq 0.05$, ** $p \leq 0.01$, *** $p \leq 0.0001$).

4.4 Discussion

Safe penile circumcision can reduce HIV susceptibility by up to 60% in men, however, many at risk men still choose to undergo this procedure and the mechanism behind how circumcision is protective against HIV infection is not fully understood (14–16,18). Previous studies have shown that specific species of penile anaerobic bacteria may be associated with local inflammation that leads to the recruitment of HIV susceptible immune cells in the penis (64,73,75). Thus, one way that circumcision could reduce HIV susceptibility in men is by increasing air exposure on the penis which eliminates these high-risk bacteria. If the abundance of penile anaerobes is indeed a determinant of HIV susceptibility, then targeted reduction of these bacteria using antimicrobials could potentially be a novel low-cost method for reducing HIV risk for men who choose to remain uncircumcised. However, it is still unclear if it would be possible to modify the penile microbiome using antimicrobials and how this would influence the availability of HIV target cells in the penis.

In this chapter we described the results of a randomized controlled trial looking at effect of antimicrobials on penile bacteria, inflammation, and HIV susceptibility in the foreskin (77). We provide evidence that antimicrobials can decrease the abundance of HIV target cells in the inner foreskin and provide evidence that supports the hypothesis that there is a causal effect between abundance of anaerobic species and HIV susceptibility (**Figures 12, 18, 19**). We found that the abundance of BASIC species rather than total bacterial density was correlated to abundance of HIV target cells in the inner foreskin (**Figures 18-19**). Additionally, the abundance of soluble inflammatory mediators at time of circumcision was also correlated with HIV target cell density in the inner foreskin (**Figures 14-17**).

Among the treatments examined in the randomized controlled trial, clindamycin and metronidazole appears to have the most potential as a microbiome-targeted intervention that can be used to reduce HIV susceptibility. Unpublished analysis by our collaborators have shown that these 2 treatments were able to reduce the abundance of

BASIC bacteria and soluble inflammatory molecules in the coronal sulcus. We have also showed in this thesis that HIV target cell availability is lower in the foreskin of men in the topical clindamycin and topical metronidazole groups (**Figure 12**). It is unsurprising that these treatments would have such a dramatic effect on the abundance of BASIC bacteria since these treatments are commonly used for the treatment of BV (76,77). BASIC species such as *Prevotella bivia* are commonly found in microbiome of women with BV. However, it is interesting that the penile abundance of BASIC bacteria was only significantly reduced by topical antimicrobials and that lower HIV target cell availability was seen in the topical clindamycin and metronidazole group men within the short duration of treatment application (4 weeks) (**Figures 11-12**). While we've seen that proportions of T cells expressing CD4 and CCR5 were similar between different treatment groups and BASIC bacteria recruited T cells in a generalized manner, future work should be done to further characterize the phenotype of CD3+ cell subsets that were reduced because of clearance of BASIC bacteria (**Table 7 & Figure 19**). It is possible that the lower availability of CD3+ cell subsets in the topical clindamycin and metronidazole group men can be explained by the reduction in the abundance resident memory T cells (T_{RM}). Resident memory T cells are a subset of memory T cells that persist long term in peripheral tissues including skin and genital mucosal tissue and respond rapidly to challenge by antigens (151–153). These cells are specific for pathogens and commensals commonly encountered (*Staphylococcus epidermidis*, HSV-1) at the site they reside in and accumulate in response to repeated antigen exposure. For instance, in mouse models it was seen that dendritic cells in the skin were capable of presenting antigen to local populations of HSV-specific T_{RM} to generate a recall immune response entirely contained within the skin (154–156). It is possible that topical antimicrobials, which were the most effective at reducing the penile abundance of BASIC bacteria in the trial, lowered the abundance of T_{RM} by reducing the availability of antigens that contributed to T_{RM} proliferation. Previous studies have also shown that T_{RM} progenitor cells generated by recent skin infection migrated in the greatest number into inflamed skin in an antigen independent manner (157). This supports the idea that the abundance of BASIC bacteria in the sub-preputial space may cause the recruitment of

HIV susceptible cells to the inner foreskin by inducing local inflammation. Consistent with previous findings, based on the results from the RCT we also found that CD3⁺ cell density, CD3⁺CD4⁺CCR5⁺ cell density, CD3⁻CD4⁺CCR5⁺ cell density, and percent coverage of CD4⁺CCR5⁺ tissue area was higher in the inner foreskin when compared to the outer foreskin (**Figure 13**).

In addition to CD3⁺ HIV target cells, the abundance CD3⁻CD4⁺CCR5⁺ cells in the inner foreskin were also reduced by antimicrobial treatments and were correlated with the penile abundance of BASIC species (**Figures 12 & 19**). Previous studies examining the relationship between bacteria associated with high HIV-risk with immune cell density in the foreskin have mostly focused on T lymphocytes (73,75). However, non CD3⁺ cells that express CD4⁺ and CCR5⁺ such as Langerhans cells are the first cells to encounter HIV virions that penetrate the foreskin in sexual transmission. While CD4⁺ T cells are the main reservoirs for productive HIV infection, the abundance of non CD3⁺ cells also play an important role in the spread the virus (29,39,97). Grouping of all CD3⁻ HIV target cells into the category of CD3⁻CD4⁺CCR5⁺ cells enabled us to gain a holistic understanding of the total abundance of non CD3⁺ cells that HIV virions can bind to. However, this grouping strategy also limits our understanding of the relationship between penile bacteria and the availability of specific CD3⁻ cell populations such as Langerhans cells and dendritic cells in the context of HIV infection. Future work should elaborate on the findings between CD3⁻ HIV target cell density in the inner foreskin and the abundance of BASIC bacteria in this thesis. This includes, but is not limited to, characterization of the composition of specific CD3⁻CD4⁺CCR5⁺ cell subsets, as well as, other innate immune cells that contribute to local inflammation in individuals with high or low penile abundance of BASIC species. More downstream work could also compare gene expression by HIV target cells between individuals with high or low abundance of BASIC species. This information will provide a better understanding of the immune profile and the mechanism by which HIV susceptible CD4⁺ T cells are recruited in the foreskin of individuals who have a high penile abundance of BASIC species.

In this thesis we have shown that men in the topical clindamycin, topical metronidazole and oral tinidazole groups all had significantly lower CD3+CD4+CCR5+ cell density in the inner foreskin compared to men in the control group (**Figure 12**). However, unpublished analysis completed by our collaborators have shown that only oral tinidazole reduced the infection of inner foreskin derived CD4+ T cells with a HIV pseudovirus in vitro. It appears that while reduction in the abundance of BASIC bacteria on the penis influenced the generalized recruitment of HIV target cells into the inner foreskin, the effect of oral tinidazole on in vitro viral entry could be mediated through a mechanism unrelated to the abundance of BASIC bacteria. Oral tinidazole could be modifying HIV susceptibility by directly affecting the cellular properties of HIV target cells. While men in the oral tinidazole group had lower abundance of CD3+ cells and CD3+CD4+CCR5+ cells in the inner foreskin when compared to control, oral tinidazole treatment did not significantly reduce the abundance of BASIC species after 1 or 4 weeks of treatment (**Figures 11-12**). Interestingly, in accordance with the in vitro viral entry results seen with oral tinidazole completed by our collaborators, a previous study has shown that oral metronidazole use significantly reduced ex-vivo HIV entry into cervical CD4+ T cells (158). Nitroimidazole compounds, which includes both tinidazole and metronidazole, function as antimicrobials through the disruption of nucleic acid synthesis in microbial cells (159,160). Several studies have investigated the potential cytotoxic or genotoxic properties that may affect human immune cells; however, these studies were often contradictory and had mixed conclusions (161–165). It is possible that oral metronidazole or tinidazole could be having a direct effect on proliferation or gene expression in CD4+ T cells which influences its susceptibility to HIV infection, however, more downstream studies are necessary to investigate if this is really the case. An immediate next step to follow-up on the results of the current study and to assess if oral tinidazole/metronidazole has a direct effect on CD4+ T cells could be to perform an infection assay to directly assess how various concentrations of oral metronidazole/tinidazole affects viral propagation of HIV in cultured CD4+ T cells.

As one of the outcomes of the RCT, our collaborators measured the abundance of 9 soluble molecules to broadly determine if antimicrobials can decrease the abundance of inflammatory markers and if the abundance of inflammatory markers are associated with both the abundance of BASIC bacteria and HIV target cells in the foreskin. These 9 soluble markers were selected based on their high abundance in the sub preputial space in healthy volunteers and because of their role in inflammation. Unpublished preliminary results from our collaborators have shown that soluble inflammatory can be reduced by antimicrobials and this reduction is associated with the reduction of penile bacteria. We have also shown that soluble inflammatory molecule levels in coronal sulcus swabs collected at time of circumcision is associated with HIV target cell density in the inner foreskin. However, we recognize that far more soluble inflammatory molecules are likely to be involved in facilitating the recruitment of HIV target cells into the inner foreskin. Future work could expand on the current panel of soluble inflammatory markers to gain a better understanding of the local inflammation associated with penile bacteria and how this inflammation is related to immune cell composition in the penis. Furthermore, at the time of writing this thesis, more penile microbiome analysis by our collaborators was still being completed and analysis of the effect of antimicrobials on epithelial integrity was still being completed by a member of our group. More sophisticated penile microbiome analysis could enable a better understanding of how bacterial species other than the BASIC species presented in this thesis and how co-association of bacteria influence HIV susceptibility. Results on the impact of antimicrobial treatment on epithelial integrity could also be paired with results from this thesis to investigate the relationship between epithelial integrity and HIV target cell abundance.

As a proof-of-concept, the current results from the randomized controlled trial have demonstrated that the penile microbiome can be altered using antimicrobials, and the resulting change in the abundance of BASIC bacteria is associated with decreased penile abundance of soluble inflammatory molecules and HIV target cells. However, more work should be done to investigate how long the effect of antimicrobials on HIV target cells can persist. It is very possible that both the abundance of BASIC species and

HIV target cells would return to levels seen prior to the application of antimicrobial treatment if treatment is discontinued. In the case of bacteria, it is well known that while the dysbiosis seen in bacterial vaginosis in women can be treated using antimicrobials, recurrence of bacterial vaginosis is very common (166,167). Based on unpublished results from our collaborators, we have seen that the abundance of BASIC bacteria after 1 week and 4 weeks of treatment with topical antimicrobials were both significantly lower than baseline. However, the abundance of BASIC bacteria after 1 week, which corresponded to a more intensive treatment regimen, was lower than the abundance of BASIC bacteria at time of circumcision. The abundance of BASIC bacteria on the penis appears to have rebounded through the less intensive treatment course from after week 1 to time of circumcision (**Figure 11**). The recurrence of BASIC bacteria following termination of treatment could be problematic for the feasibility of using antimicrobials as a potential tool for HIV prevention. Specifically, if resident memory T cells are in fact the main T cells reduced by decreased BASIC abundance. Based on previous studies, it is seen that T_{RM} tend to persist long-term in previous sites of inflammation. In the case of HSV, T_{RM} have been seen to persist in HSV ulcers even after viral clearance (156,157,168–171). In inflammatory lesions, while the abundance of T_{RM} can be reduced with anti-inflammatory therapy, T_{RM} abundance will return to previously observed levels when treatment is discontinued (154). Like these observations, it is possible that the abundance of HIV target cells in the foreskin will return to previously levels when antimicrobial treatment is discontinued. Future work should examine how long the effect of antimicrobial treatments on the penile microbiome and HIV target cells can be sustained after treatment to determine if antimicrobials can feasibly be used as a tool for HIV prevention.

In conclusion, the results presented in this chapter have shown that antimicrobials can reduce the penile abundance of HIV target cells. We have also provided evidence supporting the idea that there is a causal relationship between the abundance of bacteria previously associated with HIV risk and HIV susceptibility. We have shown that the abundance of bacteria associated with HIV risk and the penile levels of soluble

inflammatory molecules are associated with the abundance of HIV susceptible cells in the inner foreskin. The ability of antimicrobials to influence inflammation and HIV target cell density in the penis suggest that microbiome-based interventions could be a new possible strategy for HIV preventions.

Chapter 5

5 Overall Summary and Future Directions

In this thesis, I described select results from a randomized controlled trial looking at effect of antimicrobials on penile bacteria, inflammation, and HIV susceptibility in the Ugandan men. Specifically, this thesis focused on using IF microscopy analysis to measure the availability of HIV target cells in the foreskin tissue of participants enrolled in the RCT. To measure HIV target cell availability in the large number of foreskin sample images from the RCT in an automated fashion, I developed and validated a deep learning cell segmentation model that can quantify HIV target cells in foreskin tissue based on staining for CD3, CD4, CCR5, and nuclei. The performance of this model was comparable to manual counting and exceeded the performance of a conventional automated cell segmentation algorithm that uses image thresholding to quantify cells. Using the deep-learning model and a previously validated automated analysis algorithm that measured the tissue area susceptible to HIV entry (tissue area positive for CD4 and CCR5), we found that HIV target cell availability in the inner foreskin of men was significantly lower in the topical clindamycin, topical metronidazole, and oral tinidazole groups when compared to the control group. The effect of antimicrobials on HIV target cell abundance in the foreskin was limited to the inner foreskin and unpublished analysis of penile microbiome and soluble inflammatory molecule data from the RCT by our collaborators showed that topical antimicrobial treatments reduced the penile abundance of BASIC species bacteria and soluble inflammatory molecule levels. Furthermore, I found that the availability of HIV target cells in the inner foreskin was correlated to the penile abundance of soluble inflammatory molecules and BASIC species bacteria. These results support the hypothesis that antimicrobials can decrease the penile abundance of BASIC species, which is associated with the reduction in penile inflammation and HIV target cell availability in the foreskin. The results of this thesis have also shown as a proof-of-concept that microbiome-based interventions can be used to reduce HIV susceptibility in men. Overall, these results can contribute to development of new HIV

prevention strategies, which can be particularly useful to protect men who choose to remain uncircumcised.

To my knowledge, the deep-learning model described in chapter 3 of this thesis is the first report of any kind to use deep learning to quantify HIV target cell availability in genital mucosal tissue. The development of this model opens opportunities for future studies in our group and this work can be easily adapted by other groups who are looking for methods to accurately quantify immune cells in IF images of mucosal tissue. The trained deep learning model, the framework to train new deep learning models, and the annotated training data set used in this thesis are all available on public domains.

The trained model used in this study can be used without modification by our group or other investigators to quantify HIV target cells in foreskin tissues. The availability of this model is particularly useful for clinical studies investigating HIV susceptibility in men as large sample sets can be quickly analyzed in an objective manner. New deep learning models to identify other types of immune cells in mucosal tissues can be easily trained using our training framework. For example, the training framework described in chapter 3 is currently being used by students in our group to train new models to identify neutrophils, dendritic cells, and macrophages in the foreskin tissue of pediatric patients with phimosis. Additionally, previous studies have shown that the abundance of BASIC species are associated with the abundance of CD4+ T cells in the foreskin but results in this thesis have shown that both CD3+ HIV target cells and CD3- HIV target cells are associated with BASIC species abundance. In future work elaborating on the results of this thesis, new deep learning models can be trained to quantify other types of immune cells that are CD3- (for example Langerhans cells, macrophages etc.) to further characterized the exact subsets of CD3- immune cells that are associated with BASIC species abundance in the RCT samples. Manual annotation of training datasets is by far the most time-consuming step in the training of deep-learning algorithms. Open-access of the training dataset in this thesis can greatly speed up the development new deep-learning algorithms that utilize different techniques for HIV

target cell quantification since training images are very generalizable. Our deep-learning model currently only enables the quantification of HIV target cells, however, another aspect of HIV target cell availability that could be relevant for HIV susceptibility is the spatial distribution of target cells. Specifically, HIV target cells being closer to the surface of the epidermis would mean that they would be easier for virions to access. Improvements on the deep learning model used in this thesis could focus on measuring the distance of HIV target cells to the apical or basal edge of the epidermis.

References or Bibliography

1. Full report — In Danger: UNAIDS Global AIDS Update 2022 [Internet]. [cited 2022 Aug 29]. Available from: <https://www.unaids.org/en/resources/documents/2022/in-danger-global-aids-update>
2. Dehne KL, Dallabetta G, Wilson D, Garnett GP, Laga M, Benomar E, et al. HIV Prevention 2020: a framework for delivery and a call for action. *The Lancet HIV*. 2016 Jul 1;3(7):e323–32.
3. Baggaley R, Doherty M, Ball A, Ford N, Hirschall G. The Strategic Use of Antiretrovirals to Prevent HIV Infection: A Converging Agenda. *Clin Infect Dis*. 2015 Jun 1;60 Suppl 3:S159-160.
4. Rodger AJ, Cambiano V, Bruun T, Vernazza P, Collins S, Degen O, et al. Risk of HIV transmission through condomless sex in serodifferent gay couples with the HIV-positive partner taking suppressive antiretroviral therapy (PARTNER): final results of a multicentre, prospective, observational study. *The Lancet*. 2019 Jun 15;393(10189):2428–38.
5. Global HIV & AIDS statistics — 2020 fact sheet [Internet]. [cited 2021 Mar 27]. Available from: <https://www.unaids.org/en/resources/fact-sheet>
6. Teasdale CA, Abrams EJ, Yuengling KA, Lamb MR, Wang C, Vitale M, et al. Expansion and scale-up of HIV care and treatment services in four countries over ten years. *PLOS ONE*. 2020 Apr 16;15(4):e0231667.
7. Assefa Y, Alebachew A, Lera M, Lynen L, Wouters E, Van Damme W. Scaling up antiretroviral treatment and improving patient retention in care: lessons from Ethiopia, 2005-2013. *Globalization and Health*. 2014 May 27;10(1):43.
8. de Waal R, Lessells R, Hauser A, Kouyos R, Davies MA, Egger M, et al. HIV drug resistance in sub-Saharan Africa: public health questions and the potential role of real-world data and mathematical modelling. *J Virus Erad*. 4(Suppl 2):55–8.
9. Gregson J, Tang M, Ndembu N, Hamers RL, Rhee SY, Marconi VC, et al. Global epidemiology of drug resistance after failure of WHO recommended first-line regimens for adult HIV-1 infection: a multicentre retrospective cohort study. *The Lancet Infectious Diseases*. 2016 May 1;16(5):565–75.
10. Campbell C. Political will, traditional leaders and the fight against HIV/AIDS: a South African case study. *AIDS Care*. 2010;22 Suppl 2:1637–43.

11. Piot P, Russell S, Larson H. Good Politics, Bad Politics: The Experience of AIDS. *Am J Public Health*. 2007 Nov;97(11):1934–6.
12. Kurth AE, Celum C, Baeten JM, Vermund SH, Wasserheit JN. Combination HIV Prevention: Significance, Challenges, and Opportunities. *Curr HIV/AIDS Rep*. 2011 Mar;8(1):62–72.
13. HIV prevention 2025 road map — Getting on track to end AIDS as a public health threat by 2030 [Internet]. [cited 2022 Aug 29]. Available from: <https://www.unaids.org/en/resources/documents/2022/prevention-2025-roadmap>
14. Gray RH, Kigozi G, Serwadda D, Makumbi F, Watya S, Nalugoda F, et al. Male circumcision for HIV prevention in men in Rakai, Uganda: a randomised trial. *Lancet*. 2007;369(9562):657–66.
15. Bailey RC, Moses S, Parker CB, Agot K, Maclean I, Krieger JN, et al. Male circumcision for HIV prevention in young men in Kisumu, Kenya: a randomised controlled trial. *Lancet*. 2007;369(9562):643–56.
16. Auvert B, Taljaard D, Lagarde E, Sobngwi-Tambekou J, Sitta R, Puren A. Randomized, controlled intervention trial of male circumcision for reduction of HIV infection risk: the ANRS 1265 Trial. *PLoS Med*. 2005;2(11).
17. Stegman PM, Yee R, Davis J, Tchuente M, Linder R, Zembe L, et al. Estimating male circumcision coverage in 15 priority countries in sub-Saharan Africa. *J Int AIDS Soc*. 2021 Sep 21;24(Suppl 5):e25789.
18. Cork MA, Wilson KF, Perkins S, Collison ML, Deshpande A, Eaton JW, et al. Mapping male circumcision for HIV prevention efforts in sub-Saharan Africa. *BMC Medicine*. 2020 Jul 7;18(1):189.
19. Tobian AAR, Serwadda D, Quinn TC, Kigozi G, Gravitt PE, Laeyendecker O, et al. Male Circumcision for the Prevention of HSV-2 and HPV Infections and Syphilis. *New England Journal of Medicine*. 2009 03-26;360(13):1298–309.
20. Senkomago V, Backes DM, Hudgens MG, Poole C, Agot K, Moses S, et al. Acquisition and Persistence of Human Papillomavirus 16 (HPV-16) and HPV-18 Among Men With High-HPV Viral Load Infections in a Circumcision Trial in Kisumu, Kenya. *J Infect Dis*. 2015;211(5):811–20.
21. Van Howe RS. Sexually Transmitted Infections and Male Circumcision: A Systematic Review and Meta-Analysis. *ISRN Urol*. 2013 Apr 16;2013:109846.
22. Prodger JL, Gray R, Kigozi G, Nalugoda F, Galiwango R, Nehemiah K, et al. Impact of asymptomatic Herpes simplex virus-2 infection on T cell phenotype and function in the foreskin. *AIDS*. 2012;26(10):1319–22.

23. Looker KJ, Elmes JAR, Gottlieb SL, Schiffer JT, Vickerman P, Turner KME, et al. Effect of HSV-2 infection on subsequent HIV acquisition: an updated systematic review and meta-analysis. *The Lancet Infectious Diseases*. 2017 Dec 1;17(12):1303–16.
24. Boily MC, Baggaley RF, Wang L, Masse B, White RG, Hayes RJ, et al. Heterosexual risk of HIV-1 infection per sexual act: systematic review and meta-analysis of observational studies. *Lancet Infect Dis*. 2009 Feb;9(2):118–29.
25. Gray RH, Kigozi G, Serwadda D, Makumbi F, Nalugoda F, Watya S, et al. The effects of male circumcision on female partners' genital tract symptoms and vaginal infections in a randomized trial in Rakai, Uganda. *Am J Obstet Gynecol*. 2009;200(1):1–7.
26. Wawer MJ, Tobian AA, Kigozi G, Kong X, Gravitt PE, Serwadda D, et al. Effect of circumcision of HIV-negative men on transmission of human papillomavirus to HIV-negative women: a randomised trial in Rakai, Uganda. *Lancet*. 2011 Jan 11;2011;277(9761):209-18.
27. Freeman EE, Weiss HA, Glynn C JR, PL W, JA H, R.J. Herpes simplex virus 2 infection increases HIV acquisition in men and women: systematic review and meta-analysis of longitudinal studies. *Aids*. 2006;20(1):73–83.
28. Dinh MH, Anderson MR, McRaven MD, Cianci GC, McCoombe SG, Kelley ZL, et al. Visualization of HIV-1 interactions with penile and foreskin epithelia: clues for female-to-male HIV transmission. *PLoS Pathog*. 2015;11(3).
29. Zhou Z, Barry de Longchamps N, Schmitt A, Zerbib M, Vacher-Lavenu MC, Bomsel M, et al. HIV-1 Efficient Entry in Inner Foreskin Is Mediated by Elevated CCL5/RANTES that Recruits T Cells and Fuels Conjugate Formation with Langerhans Cells. *PLoS Pathog*. 2011 Jun 30;7(6):e1002100.
30. Lemos MP, Lama JR, Karuna ST, Fong Y, Montano SM, Ganoza C, et al. The Inner Foreskin of Healthy Males at Risk of HIV Infection Harbors Epithelial CD4+CCR5+ Cells and Has Features of an Inflamed Epidermal Barrier. *PLoS One*. 2014 Sep 30;9(9):e108954.
31. Prodger JL, Kaul R. The biology of how circumcision reduces HIV susceptibility: broader implications for the prevention field. *AIDS Research and Therapy*. 2017 Sep 12;14(1):49.
32. Prodger JL, Gray R, Kigozi G, Nalugoda F, Galiwango R, Hirbod T, et al. Foreskin T-cell subsets differ substantially from blood with respect to HIV co-receptor expression, inflammatory profile, and memory status. *Mucosal Immunol*. 2012;5(2):121–8.

33. Huang Y, Paxton WA, Wolinsky SM, Neumann AU, Zhang L, He T, et al. The role of a mutant CCR5 allele in HIV-1 transmission and disease progression. *Nature Medicine*. 1996 11;2(11):1240–3.
34. Hartley O, Martins E, Scurci I. Preventing HIV transmission through blockade of CCR5: rationale, progress and perspectives. *Swiss Medical Weekly*. 2018;148:w14580.
35. Joseph SB, Swanstrom R, Kashuba ADM, Cohen MS. Bottlenecks in HIV-1 transmission: insights from the study of founder viruses. *Nature reviews Microbiology*. 2015 07;13(7):414–25.
36. Zhang Z. Sexual Transmission and Propagation of SIV and HIV in Resting and Activated CD4+ T Cells. *Science*. 1999;286(5443):1353–7.
37. Powers KA, Poole C, Pettifor AE, Cohen MS. Rethinking the heterosexual infectivity of HIV-1: a systematic review and meta-analysis. *Lancet Infect Dis*. 2008 Sep;8(9):553–63.
38. McCoombe SG, Short RV. Potential HIV-1 target cells in the human penis. *Aids*. 2006;20(11):1491–5.
39. Fahrbach KM, Barry SM, Ayehunie S, Lamore S, Klausner M, Hope TJ. Activated CD34-derived Langerhans cells mediate transinfection with human immunodeficiency virus. *J Virol*. 2007 Apr 20;2007;81(13):6858–68:02472–06.
40. Cameron PU, Freudenthal PS, Barker JM, Gezelter S, Inaba K, Steinman RM. Dendritic cells exposed to human immunodeficiency virus type-1 transmit a vigorous cytopathic infection to CD4+ T cells. *Science*. 1992;257(5068):383–7.
41. Donoval BA, Landay AL, Moses S, Agot K, Ndinya-Achola JO, Nyagaya EA, et al. HIV-1 target cells in foreskins of African men with varying histories of sexually transmitted infections. *Am J Clin Pathol*. 2006;125(3):386–91.
42. Carnathan DG, Wetzel KS, Yu J, Lee ST, Johnson BA, Paiardini M, et al. Activated CD4+CCR5+ T cells in the rectum predict increased SIV acquisition in SIVGag/Tat-vaccinated rhesus macaques. *Proc Natl Acad Sci U S A*. 2015;112(2):518–23.
43. McKinnon LR, Nyanga B, Kim CJ, Izulla P, Kwatampora J, Kimani M, et al. Early HIV-1 infection is associated with reduced frequencies of cervical Th17 cells. *J Acquir Immune Defic Syndr*. 2015;68(1):6–12.
44. McKinnon LR, Nyanga B, Chege D, Izulla P, Kimani M, Huibner S, et al. Characterization of a human cervical CD4+ T cell subset coexpressing multiple markers of HIV susceptibility. *J Immunol*. 2011;187(11):6032–42.

45. El Hed A, Khaitan A, Kozhaya L, Manel N, Daskalakis D, Borkowsky W, et al. Susceptibility of Human Th17 Cells to Human Immunodeficiency Virus and Their Perturbation during Infection. *The Journal of Infectious Diseases*. 2010 03-15;201(6):843–54.
46. Alvarez Y, Tuen M, Shen G, Nawaz F, Arthos J, Wolff MJ, et al. Preferential HIV infection of CCR6+ Th17 cells is associated with higher levels of virus receptor expression and lack of CCR5 ligands. *J Virol*. 2013;87(19):10843–54.
47. Gosselin A, Monteiro P, Chomont N, Diaz-Griffero F, Said EA, Fonseca S, et al. Peripheral blood CCR4+CCR6+ and CXCR3+CCR6+CD4+ T cells are highly permissive to HIV-1 infection. *J Immunol*. 2010;184(3):1604–16.
48. Monteiro P, Gosselin A, Wacleche VS, El-Far M, Said EA, Kared H, et al. Memory CCR6+CD4+ T cells are preferential targets for productive HIV type 1 infection regardless of their expression of integrin beta7. *J Immunol*. 2011;186(8):4618–30.
49. Joag VR, McKinnon LR, Liu J, Kidane ST, Yudin MH, Nyanga B, et al. Identification of preferential CD4(+) T-cell targets for HIV infection in the cervix. *Mucosal Immunol*. 2016;9(1):1–12.
50. Goode D, Truong R, Villegas G, Calenda G, Guerra-Perez N, Piatak M, et al. HSV-2-driven increase in the expression of alpha4beta7 correlates with increased susceptibility to vaginal SHIV(SF162P3) infection. *PLoS Pathog*. 2014;10(12).
51. Martinelli E, Veglia F, Goode D, Guerra-Perez N, Aravantinou M, Arthos J, et al. The frequency of alpha(4)beta(7)(high) memory CD4(+) T cells correlates with susceptibility to rectal simian immunodeficiency virus infection. *J Acquir Immune Defic Syndr*. 2013;64(4):325–31.
52. Prodger JL, Hirbod T, Kigozi G, Nalugoda F, Reynolds SJ, Galiwango R, et al. Immune correlates of HIV exposure without infection in foreskins of men from Rakai, Uganda. *Mucosal Immunol*. 2014;7(3):634–44.
53. Zhang ZQ. Roles of substrate availability and infection of resting and activated CD4+ T cells in transmission and acute simian immunodeficiency virus infection. *Proceedings of the National Academy of Sciences*. 2004;101(15):5640–5.
54. Saba E, Grivel JC, Vanpouille C, Brichacek B, Fitzgerald W, Margolis L, et al. HIV-1 sexual transmission: early events of HIV-1 infection of human cervico-vaginal tissue in an optimized ex vivo model. *Mucosal Immunol*. 2010 Feb 12;2010;3(3):280-90.

55. Meditz AL, Haas MK, Folkvord JM, Melander K, Young R, McCarter M, et al. HLA-DR+ CD38+ CD4+ T lymphocytes have elevated CCR5 expression and produce the majority of R5-tropic HIV-1 RNA in vivo. *J Virol*. 2011 Aug 5;2011;85(19):10189-200:02529–10.
56. Narimatsu R, Wolday D, Patterson BK. IL-8 increases transmission of HIV type 1 in cervical explant tissue. *AIDS Res Hum Retroviruses*. 2005 Mar 30;2005;21(3):228-33.
57. Tang S, Patterson B, Levy JA. Highly purified quiescent human peripheral blood CD4+ T cells are infectible by human immunodeficiency virus but do not release virus after activation. *J Virol*. 1995 Sep 1;1995;69(9):5659-65.
58. Wang JH, Janas AM, Olson WJ, Wu L. Functionally distinct transmission of human immunodeficiency virus type 1 mediated by immature and mature dendritic cells. *J Virol*. 2007;81(17):8933–43.
59. Izquierdo-Useros N, Blanco J, Erkizia I, Fernandez-Figueras MT, Borrás FE, Naranjo-Gomez M, et al. Maturation of blood-derived dendritic cells enhances human immunodeficiency virus type 1 capture and transmission. *J Virol*. 2007;81(14):7559–70.
60. Novak RM, Donoval BA, Graham PJ, Boksa LA, Spear G, Hershov RC, et al. Cervicovaginal levels of lactoferrin, secretory leukocyte protease inhibitor, and RANTES and the effects of coexisting vaginoses in human immunodeficiency virus (HIV)-seronegative women with a high risk of heterosexual acquisition of HIV infection. *Clin Vaccine Immunol*. 2007;14(9):1102–7.
61. Levinson P, Kaul R, Kimani J, Ngugi E, Moses S, MacDonald KS, et al. Levels of innate immune factors in genital fluids: association of alpha defensins and LL-37 with genital infections and increased HIV acquisition. *AIDS*. 2008 Dec 31;2009;23(3):309-17.
62. Rebbapragada A, Wachihi C, Pettengell C, Sunderji S, Huibner S, Jaoko W, et al. Negative mucosal synergy between Herpes simplex type 2 and HIV in the female genital tract. *Aids*. 2007;21(5):589–98.
63. Kaul R, Rebbapragada A, Hirbod T, Wachihi C, Ball TB, Plummer FA, et al. Genital levels of soluble immune factors with anti-HIV activity may correlate with increased HIV susceptibility. *AIDS*. 2008 Sep 12;2008;22(15):2049-51.
64. Prodger JL, Gray RH, Shannon B, Shahabi K, Kong X, Grabowski K, et al. Chemokine Levels in the Penile Coronal Sulcus Correlate with HIV-1 Acquisition and Are Reduced by Male Circumcision in Rakai, Uganda. *PLOS Pathogens*. 2016 11-29;12(11):e1006025.

65. Hirbod T, Kong X, Kigozi G, Ndyababo A, Serwadda D, Procter JL, et al. HIV acquisition is associated with increased antimicrobial peptides and reduced HIV neutralizing IgA in the foreskin prepuce of uncircumcised men. *PLoS Pathog.* 2014;10(10).
66. Sewankambo N, Gray RH, Wawer MJ, Paxton L, McNaim D, Wabwire-Mangen F, et al. HIV-1 infection associated with abnormal vaginal flora morphology and bacterial vaginosis. *Lancet.* 1997;350(9077):546–50.
67. Atashili J, Poole C, Ndumbe PM, Adimora AA, Smith JS. Bacterial vaginosis and HIV acquisition: a meta-analysis of published studies. *AIDS.* 2008 Jul 11;2008;22(12):1493-501.
68. Cohen CR, Lingappa B JR, JM N, MO S, CA H, T D, et al. Bacterial vaginosis associated with increased risk of female-to-male HIV-1 transmission: a prospective cohort analysis among African couples. *PLoS Med.* 2012;9(6).
69. Thoma ME, Gray RH, Kiwanuka N, Aluma S, Wang MC, Sewankambo N, et al. The short-term variability of bacterial vaginosis diagnosed by Nugent Gram stain criteria among sexually active women in Rakai, Uganda. *Sex Transm Dis.* 2011;38(2):111–6.
70. Thoma ME, Gray RH, Kiwanuka N, Wang MC, Sewankambo N, Wawer MJ. The natural history of bacterial vaginosis diagnosed by gram stain among women in Rakai, Uganda. *Sex Transm Dis.* 2011;38(11):1040–5.
71. Martin HL, Richardson BA, Nyange PM, Lavreys L, Hillier SL, Chohan B, et al. Vaginal lactobacilli, microbial flora, and risk of human immunodeficiency virus type 1 and sexually transmitted disease acquisition. *J Infect Dis.* 1999 Nov 24;1999;180(6):1863-8.
72. Ñahui Palomino RA, Zicari S, Vanpouille C, Vitali B, Margolis L. Vaginal Lactobacillus Inhibits HIV-1 Replication in Human Tissues Ex Vivo. *Frontiers in Microbiology* [Internet]. 2017 05-19;8. Available from: <https://www.ncbi.nlm.nih.gov/pmc/articles/PMC5437121/>
73. Liu CM, Procter JL, Tobian AAR, Abraham AG, Kigozi G, Hungate BA, et al. Penile Anaerobic Dysbiosis as a Risk Factor for HIV Infection. *mBio* [Internet]. 2017 07-25;8(4). Available from: <https://www.ncbi.nlm.nih.gov/pmc/articles/PMC5527312/>
74. Cm L, Ba H, Aa T, J R, JI P, D S, et al. Penile Microbiota and Female Partner Bacterial Vaginosis in Rakai, Uganda [Internet]. *mBio.* 2015. Available from: <https://pubmed.ncbi.nlm.nih.gov/26081632/>

75. Prodger JL, Abraham AG, Tobian AAR, Park DE, Aziz M, Roach K, et al. Penile bacteria associated with HIV seroconversion, inflammation, and immune cells. *JCI Insight*. 6(8):e147363.
76. Prodger JL, Gray RH, Shannon B, Shahabi K, Kong X, Grabowski MK, et al. Penile chemokine levels correlate with HIV-1 acquisition and are reduced by male circumcision in Rakai, Uganda. *PloS Pathogens*. 2016;
77. Galiwango RM, Bagaya B, Mpendo J, Joag V, Okech B, Nanvubya A, et al. Protocol for a randomized clinical trial exploring the effect of antimicrobial agents on the penile microbiota, immunology and HIV susceptibility of Ugandan men. *Trials*. 2019 Jul 19;20(1):443.
78. Bradshaw CS, Sobel JD. Current Treatment of Bacterial Vaginosis-Limitations and Need for Innovation. *J Infect Dis*. 2016 Aug 15;214 Suppl 1:S14-20.
79. Faught BM, Reyes S. Characterization and Treatment of Recurrent Bacterial Vaginosis. *J Womens Health (Larchmt)*. 2019 Sep;28(9):1218–26.
80. Hanson JM, McGregor JA, Hillier SL, Eschenbach DA, Kreutner AK, Galask RP, et al. Metronidazole for bacterial vaginosis. A comparison of vaginal gel vs. oral therapy. *J Reprod Med*. 2000 Nov;45(11):889–96.
81. Paavonen J, Mangioni C, Martin MA, Wajszczuk CP. Vaginal clindamycin and oral metronidazole for bacterial vaginosis: a randomized trial. *Obstet Gynecol*. 2000 Aug;96(2):256–60.
82. Cardone A, Zarcone R, Borrelli A, Di Cunzolo A, Russo A, Tartaglia E. Utilisation of hydrogen peroxide in the treatment of recurrent bacterial vaginosis. *Minerva Ginecol*. 2003 Dec;55(6):483–92.
83. Armstrong NR, Wilson JD. Tinidazole in the treatment of bacterial vaginosis. *Int J Womens Health*. 2010 Aug 9;1:59–65.
84. Nord CE. Microbiological properties of tinidazole: spectrum, activity and ecological considerations. *Journal of Antimicrobial Chemotherapy*. 1982 Jan 1;10(suppl_A):35–42.
85. Nailor MD, Sobel JD. Tinidazole for bacterial vaginosis. *Expert Review of Anti-infective Therapy*. 2007 Jun 1;5(3):343–8.
86. Guay DRP. Topical clindamycin in the management of acne vulgaris. *Expert Opin Pharmacother*. 2007 Oct;8(15):2625–64.

87. Hossainian N, Slot DE, Afennich F, Van der Weijden GA. The effects of hydrogen peroxide mouthwashes on the prevention of plaque and gingival inflammation: a systematic review. *Int J Dent Hyg*. 2011 Aug;9(3):171–81.
88. Liu CM, Aziz M, Kachur S, Hsueh PR, Huang YT, Keim P, et al. BactQuant: An enhanced broad-coverage bacterial quantitative real-time PCR assay. *BMC Microbiology*. 2012;12(1).
89. Joag V, Sivro A, Yende-Zuma N, Imam H, Samsunder N, Abdool Karim Q, et al. Ex vivo HIV entry into blood CD4+ T cells does not predict heterosexual HIV acquisition in women. *PLoS One*. 2018;13(7):e0200359.
90. Fadrosch DW, Ma B, Gajer P, Sengamalay N, Ott S, Brotman RM, et al. An improved dual-indexing approach for multiplexed 16S rRNA gene sequencing on the Illumina MiSeq platform. *Microbiome*. 2014;2(1).
91. Galiwango RM, Yegorov S, Joag V, Prodger J, Shahabi K, Huibner S, et al. Characterization of CD4+ T cell subsets and HIV susceptibility in the inner and outer foreskin of Ugandan men. *Am J Reprod Immunol*. 2019 Jul;82(1):e13143.
92. Caporaso JG, Kuczynski J, Stombaugh J, Bittinger K, Bushman FD, Costello EK, et al. QIIME allows analysis of high-throughput community sequencing data. *Nat Methods*. 2010 May;7(5):335–6.
93. Cohen MS. Preventing sexual transmission of HIV. *Clin Infect Dis*. 2007 Dec 15;45 Suppl 4:S287-292.
94. Phillips DM, Zacharopoulos VR, Tan X, Pearce-Pratt R. Mechanisms of sexual transmission of HIV: does HIV infect intact epithelia? *Trends Microbiol*. 1994 Nov;2(11):454–8.
95. Reis Machado J, da Silva MV, Cavellani CL, dos Reis MA, Monteiro MLG dos R, Teixeira V de PA, et al. Mucosal immunity in the female genital tract, HIV/AIDS. *Biomed Res Int*. 2014;2014:350195.
96. Shen R, Richter HE, Smith PD. Interactions between HIV-1 and mucosal cells in the female reproductive tract. *Am J Reprod Immunol*. 2014 Jun;71(6):608–17.
97. Cavrois M, Neidleman J, Kreisberg JF, Greene WC. In vitro derived dendritic cells trans-infect CD4 T cells primarily with surface-bound HIV-1 virions. *PLoS Pathog*. 2007 Jan;3(1):e4.
98. Kijewski SD, Gummuluru S. A mechanistic overview of dendritic cell-mediated HIV-1 trans infection: the story so far. *Future Virol*. 2015 Mar;10(3):257–69.

99. Anahtar MN, Byrne EH, Doherty KE, Bowman BA, Yamamoto HS, Soumillon M, et al. Cervicovaginal bacteria are a major modulator of host inflammatory responses in the female genital tract. *Immunity*. 2015;42(5):965–76.
100. Schellenberg JJ, Plummer FA. The Microbiological Context of HIV Resistance: Vaginal Microbiota and Mucosal Inflammation at the Viral Point of Entry. *Int J Inflam*. 2012;2012:131243.
101. Lajoie J, Mwangi L, Fowke KR. Preventing HIV infection without targeting the virus: how reducing HIV target cells at the genital tract is a new approach to HIV prevention. *AIDS Res Ther*. 2017 Sep 12;14:46.
102. Hengel RL, Nicholson JK. An update on the use of flow cytometry in HIV infection and AIDS. *Clin Lab Med*. 2001 Dec;21(4):841–56.
103. Clift IC. Diagnostic Flow Cytometry and the AIDS Pandemic. *Lab Med*. 2015;46(3):e59-64.
104. Landay A, Ohlsson-Wilhelm B, Giorgi JV. Application of flow cytometry to the study of HIV infection. *AIDS*. 1990 Jun;4(6):479–97.
105. Prin-Mathieu C, Baty V, Faure G, Schumacher H, Kolopp-Sarda MN, May T, et al. Assessment by flow cytometry of peripheral blood leukocyte enzymatic activities in HIV patients. *J Immunol Methods*. 2001 Jun 1;252(1–2):139–46.
106. Pattanapanyasat K, Thakar MR. CD4+ T cell count as a tool to monitor HIV progression & anti-retroviral therapy. *Indian J Med Res*. 2005 Apr;121(4):539–49.
107. Barnett D, Walker B, Landay A, Denny TN. CD4 immunophenotyping in HIV infection. *Nat Rev Microbiol*. 2008 Nov;6(11 Suppl):S7-15.
108. Hunt PW, Brenchley J, Sinclair E, McCune JM, Roland M, Page-Shafer K, et al. Relationship between T Cell Activation and CD4+ T Cell Count in HIV-Seropositive Individuals with Undetectable Plasma HIV RNA Levels in the Absence of Therapy. *J Infect Dis*. 2008 Jan 1;197(1):126–33.
109. Cockerham LR, Siliciano JD, Sinclair E, O'Doherty U, Palmer S, Yukl SA, et al. CD4+ and CD8+ T Cell Activation Are Associated with HIV DNA in Resting CD4+ T Cells. *PLOS ONE*. 2014 Oct 23;9(10):e110731.
110. Brookner CK, Follen M, Boiko I, Galvan J, Thomsen S, Malpica A, et al. Autofluorescence patterns in short-term cultures of normal cervical tissue. *Photochem Photobiol*. 2000 Jun;71(6):730–6.

111. Baatz M, Zimmermann J, Blackmore CG. Automated analysis and detailed quantification of biomedical images using Definiens Cognition Network Technology. *Comb Chem High Throughput Screen*. 2009 Nov;12(9):908–16.
112. Maehara T, Munemura R, Shimizu M, Kakizoe N, Kaneko N, Murakami Y, et al. Tissue-infiltrating immune cells contribute to understanding the pathogenesis of Kimura disease. *Medicine (Baltimore)*. 2019 Dec 16;98(50):e18300.
113. Schindelin J, Arganda-Carreras I, Frise E, Kaynig V, Longair M, Pietzsch T, et al. Fiji: an open-source platform for biological-image analysis. *Nature Methods*. 2012 Jul;9(7):676–82.
114. Stirling DR, Swain-Bowden MJ, Lucas AM, Carpenter AE, Cimini BA, Goodman A. CellProfiler 4: improvements in speed, utility and usability. *BMC Bioinformatics*. 2021 Sep 10;22(1):433.
115. Bankhead P, Loughrey MB, Fernández JA, Dombrowski Y, McArt DG, Dunne PD, et al. QuPath: Open source software for digital pathology image analysis. *Sci Rep*. 2017 Dec 4;7(1):16878.
116. Diem K, Magaret A, Klock A, Jin L, Zhu J, Corey L. Image analysis for accurately counting CD4+ and CD8+ T cells in human tissue. *J Virol Methods*. 2015 Sep 15;222:117–21.
117. Lunde A, Glover JC. A versatile toolbox for semi-automatic cell-by-cell object-based colocalization analysis. *Sci Rep*. 2020 Nov 4;10(1):19027.
118. Tasnim H, Fricke GM, Byrum JR, Sotiris JO, Cannon JL, Moses ME. Quantitative Measurement of Naïve T Cell Association With Dendritic Cells, FRCs, and Blood Vessels in Lymph Nodes. *Front Immunol*. 2018 Jul 26;9:1571.
119. Walsh AJ, Skala MC. An automated image processing routine for segmentation of cell cytoplasm in high-resolution autofluorescence images. In: *Multiphoton Microscopy in the Biomedical Sciences XIV* [Internet]. SPIE; 2014 [cited 2022 Aug 29]. p. 161–6. Available from: <https://www.spiedigitallibrary.org/conference-proceedings-of-spie/8948/89481M/An-automated-image-processing-routine-for-segmentation-of-cell-cytoplasm/10.1117/12.2040644.full>
120. Kesler B, Li G, Thiemicke A, Venkat R, Neuert G. Automated cell boundary and 3D nuclear segmentation of cells in suspension. *Sci Rep*. 2019 Jul 15;9(1):10237.
121. Lee SMW, Shaw A, Simpson JL, Uminsky D, Garratt LW. Differential cell counts using center-point networks achieves human-level accuracy and efficiency over segmentation. *Sci Rep*. 2021 Aug 19;11(1):16917.

122. Yang L, Ghosh RP, Franklin JM, Chen S, You C, Narayan RR, et al. NuSeT: A deep learning tool for reliably separating and analyzing crowded cells. *PLoS Comput Biol*. 2020 Sep 14;16(9):e1008193.
123. Chen J, Zhang B. Segmentation of Overlapping Cervical Cells with Mask Region Convolutional Neural Network. *Comput Math Methods Med*. 2021 Oct 4;2021:3890988.
124. Neubeck A, Van Gool L. Efficient Non-Maximum Suppression. In: 18th International Conference on Pattern Recognition (ICPR'06). 2006. p. 850–5.
125. Schmidt U, Weigert M, Broaddus C, Myers G. Cell Detection with Star-convex Polygons. In 2018 [cited 2022 Aug 29]. p. 265–73. Available from: <http://arxiv.org/abs/1806.03535>
126. Buchanan LB, Shao Z, Jiang YC, Lai A, Hope TJ, Carias AM, et al. Quantitative Immunofluorescent Imaging of Immune Cells in Mucosal Tissues. *Methods Mol Biol*. 2022;2440:143–64.
127. AdaptiveThreshold --- ImageJ plugin - ImageJ plugins by Qingzong TSENG [Internet]. [cited 2022 Aug 29]. Available from: <https://sites.google.com/site/qingzongtseng/adaptivethreshold>
128. Arzt M, Deschamps J, Schmied C, Pietzsch T, Schmidt D, Tomancak P, et al. LABKIT: Labeling and Segmentation Toolkit for Big Image Data. *Frontiers in Computer Science* [Internet]. 2022 [cited 2022 Aug 29];4. Available from: <https://www.frontiersin.org/articles/10.3389/fcomp.2022.777728>
129. Mölder F, Jablonski KP, Letcher B, Hall MB, Tomkins-Tinch CH, Sochat V, et al. Sustainable data analysis with Snakemake [Internet]. *F1000Research*; 2021 [cited 2022 Aug 29]. Available from: <https://f1000research.com/articles/10-33>
130. O'Brien J, Hayder H, Peng C. Automated Quantification and Analysis of Cell Counting Procedures Using ImageJ Plugins. *J Vis Exp* [Internet]. 2016 Nov 17 [cited 2021 Mar 28];(117). Available from: <https://www.ncbi.nlm.nih.gov/pmc/articles/PMC5226253/>
131. Sofroniew N, Lambert T, Evans K, Nunez-Iglesias J, Bokota G, Winston P, et al. napari: a multi-dimensional image viewer for Python [Internet]. *Zenodo*; 2022 [cited 2022 Aug 29]. Available from: <https://zenodo.org/record/6598542>
132. de Chaumont F, Dallongeville S, Chenouard N, Hervé N, Pop S, Provoost T, et al. Icy: an open bioimage informatics platform for extended reproducible research. *Nat Methods*. 2012 Jul;9(7):690–6.

133. Korfhage N, Mühling M, Ringshandl S, Becker A, Schmeck B, Freisleben B. Detection and segmentation of morphologically complex eukaryotic cells in fluorescence microscopy images via feature pyramid fusion. *PLOS Computational Biology*. 2020 Sep 8;16(9):e1008179.
134. Mandal S, Uhlmann V. Splinedist: Automated Cell Segmentation With Spline Curves. In: 2021 IEEE 18th International Symposium on Biomedical Imaging (ISBI). 2021. p. 1082–6.
135. Zafar MM, Rauf Z, Sohail A, Khan AR, Obaidullah M, Khan SH, et al. Detection of tumour infiltrating lymphocytes in CD3 and CD8 stained histopathological images using a two-phase deep CNN. *Photodiagnosis Photodyn Ther*. 2022 Mar;37:102676.
136. Abas FS, Shana'ah A, Christian B, Hasserjian R, Louissaint A, Pennell M, et al. Computer-assisted quantification of CD3+ T cells in follicular lymphoma. *Cytometry A*. 2017 Jun;91(6):609–21.
137. Su H, Yin Z, Huh S, Kanade T. Cell segmentation in phase contrast microscopy images via semi-supervised classification over optics-related features. *Med Image Anal*. 2013 Oct;17(7):746–65.
138. Negahbani F, Sabzi R, Pakniyat Jahromi B, Firouzabadi D, Movahedi F, Kohandel Shirazi M, et al. PathoNet introduced as a deep neural network backend for evaluation of Ki-67 and tumor-infiltrating lymphocytes in breast cancer. *Sci Rep*. 2021 Apr 19;11(1):8489.
139. Sadanandan SK, Ranefall P, Le Guyader S, Wählby C. Automated Training of Deep Convolutional Neural Networks for Cell Segmentation. *Sci Rep*. 2017 Aug 10;7:7860.
140. Lee MY, Bedia JS, Bhate SS, Barlow GL, Phillips D, Fantl WJ, et al. CellSeg: a robust, pre-trained nucleus segmentation and pixel quantification software for highly multiplexed fluorescence images. *BMC Bioinformatics*. 2022 Jan 18;23(1):46.
141. Stringer C, Wang T, Michaelos M, Pachitariu M. Cellpose: a generalist algorithm for cellular segmentation. *Nat Methods*. 2021 Jan;18(1):100–6.
142. Maylaa T, Windal F, Benhabiles H, Maubon G, Maubon N, Vandenhoute E, et al. An Evaluation of Computational Learning-based Methods for the Segmentation of Nuclei in Cervical Cancer Cells from Microscopic Images. *Curr Comput Aided Drug Des*. 2022;18(2):81–94.

143. Mela CA, Liu Y. Application of convolutional neural networks towards nuclei segmentation in localization-based super-resolution fluorescence microscopy images. *BMC Bioinformatics*. 2021 Jun 15;22(1):325.
144. Kromp F, Bozsaky E, Rifatbegovic F, Fischer L, Ambros M, Berneder M, et al. An annotated fluorescence image dataset for training nuclear segmentation methods. *Sci Data*. 2020 Aug 11;7(1):262.
145. Wagner M, Reinke S, Hänsel R, Klapper W, Braumann UD. An image dataset related to automated macrophage detection in immunostained lymphoma tissue samples. *Gigascience*. 2020 Mar 1;9(3):giaa016.
146. von Chamier L, Laine RF, Jukkala J, Spahn C, Krentzel D, Nehme E, et al. Democratising deep learning for microscopy with ZeroCostDL4Mic. *Nat Commun*. 2021 Apr 15;12(1):2276.
147. Rasse TM, Hollandi R, Horvath P. OpSeF: Open Source Python Framework for Collaborative Instance Segmentation of Bioimages. *Front Bioeng Biotechnol*. 2020;8:558880.
148. Jones J, Sullivan PS, Curran JW. Progress in the HIV epidemic: Identifying goals and measuring success. *PLoS Med*. 2019 Jan 18;16(1):e1002729.
149. Bekker LG, Alleyne G, Baral S, Cepeda J, Daskalakis D, Dowdy D, et al. Advancing global health and strengthening the HIV response in the era of the Sustainable Development Goals: the International AIDS Society—Lancet Commission. *Lancet*. 2018;392(10144):312–58.
150. Nguyen PT, Gilmour S, Le PM, Onishi K, Kato K, Nguyen HV. Progress toward HIV elimination goals: trends in and projections of annual HIV testing and condom use in Africa. *AIDS*. 2021 Jul 1;35(8):1253–62.
151. Mackay LK, Rahimpour A, Ma JZ, Collins N, Stock AT, Hafon ML, et al. The developmental pathway for CD103(+)CD8+ tissue-resident memory T cells of skin. *Nat Immunol*. 2013 Dec;14(12):1294–301.
152. Wakim LM, Woodward-Davis A, Liu R, Hu Y, Villadangos J, Smyth G, et al. The molecular signature of tissue resident memory CD8 T cells isolated from the brain. *J Immunol*. 2012 Oct 1;189(7):10.4049/jimmunol.1201305.
153. Clark RA, Chong B, Mirchandani N, Brinster NK, Yamanaka KI, Dowgiert RK, et al. The vast majority of CLA+ T cells are resident in normal skin. *J Immunol*. 2006 Apr 1;176(7):4431–9.

154. Wakim LM, Waithman J, van Rooijen N, Heath WR, Carbone FR. Dendritic cell-induced memory T cell activation in nonlymphoid tissues. *Science*. 2008 Jan 11;319(5860):198–202.
155. Jiang X, Clark RA, Liu L, Wagers AJ, Fuhlbrigge RC, Kupper TS. Skin infection generates non-migratory memory CD8+ TRM cells providing global skin immunity. *Nature*. 2012 Feb 29;483(7388):227–31.
156. Liu L, Zhong Q, Tian T, Dubin K, Athale SK, Kupper TS. Physical disruption of skin during poxvirus immunization is critical for the generation of highly protective T cell-mediated immunity. *Nat Med*. 2010 Feb;16(2):224–7.
157. Mackay LK, Stock AT, Ma JZ, Jones CM, Kent SJ, Mueller SN, et al. Long-lived epithelial immunity by tissue-resident memory T (TRM) cells in the absence of persisting local antigen presentation. *Proc Natl Acad Sci U S A*. 2012 May 1;109(18):7037–42.
158. Joag V, Obila O, Gajer P, Scott MC, Dizzell S, Humphrys M, et al. Impact of Standard Bacterial Vaginosis Treatment on the Genital Microbiota, Immune Milieu, and Ex Vivo Human Immunodeficiency Virus Susceptibility. *Clin Infect Dis*. 2019 May 15;68(10):1675–83.
159. Edwards DI. Nitroimidazole drugs--action and resistance mechanisms. I. Mechanisms of action. *J Antimicrob Chemother*. 1993 Jan;31(1):9–20.
160. Fung HB, Doan TL. Tinidazole: a nitroimidazole antiprotozoal agent. *Clin Ther*. 2005 Dec;27(12):1859–84.
161. López Nigro MM, Carballo MA. Genotoxicity and cell death induced by tinidazole (TNZ). *Toxicol Lett*. 2008 Jul 30;180(1):46–52.
162. López Nigro MM, Gadano AB, Carballo MA. Evaluation of genetic damage induced by a nitroimidazole derivative in human lymphocytes: Tinidazole (TNZ). *Toxicol In Vitro*. 2001 Jun;15(3):209–13.
163. Boechat N, Carvalho AS, Salomão K, de Castro SL, Araujo-Lima CF, Mello FV, et al. Studies of genotoxicity and mutagenicity of nitroimidazoles: demystifying this critical relationship with the nitro group. *Mem Inst Oswaldo Cruz*. 2015 Jun;110(4):492–9.
164. Hernández Ceruelos A, Romero-Quezada LC, Ruvalcaba Ledezma JC, López Contreras L. Therapeutic uses of metronidazole and its side effects: an update. *Eur Rev Med Pharmacol Sci*. 2019 Jan;23(1):397–401.

165. Buschini A, Ferrarini L, Franzoni S, Galati S, Lazzaretti M, Mussi F, et al. Genotoxicity Reevaluation of Three Commercial Nitroheterocyclic Drugs: Nifurtimox, Benznidazole, and Metronidazole. *J Parasitol Res.* 2009;2009:463575.
166. Vodstrcil LA, Muzny CA, Plummer EL, Sobel JD, Bradshaw CS. Bacterial vaginosis: drivers of recurrence and challenges and opportunities in partner treatment. *BMC Med.* 2021 Sep 2;19(1):194.
167. Hay null. Recurrent Bacterial Vaginosis. *Curr Infect Dis Rep.* 2000 Dec;2(6):506–12.
168. Gebhardt T, Wakim LM, Eidsmo L, Reading PC, Heath WR, Carbone FR. Memory T cells in nonlymphoid tissue that provide enhanced local immunity during infection with herpes simplex virus. *Nat Immunol.* 2009 May;10(5):524–30.
169. Shin H, Iwasaki A. A vaccine strategy protects against genital herpes by establishing local memory T cells. *Nature.* 2012 Nov 15;491(7424):463–7.
170. Zhu J, Koelle DM, Cao J, Vazquez J, Huang ML, Hladik F, et al. Virus-specific CD8⁺ T cells accumulate near sensory nerve endings in genital skin during subclinical HSV-2 reactivation. *J Exp Med.* 2007 Mar 19;204(3):595–603.
171. Zhu J, Peng T, Johnston C, Phasouk K, Kask AS, Klock A, et al. Immune Surveillance by CD8 α ⁺ Skin Resident T Cells in Human Herpesvirus Infection. *Nature.* 2013 May 23;497(7450):494–7.

Curriculum Vitae

Name: Zhongtian (Eric) Shao

Post-secondary Education and Degrees: The University of Western Ontario
London, Ontario, Canada
2020-2022 Master of Science (MSc)
(Microbiology and Immunology)

The University of Western Ontario
London, Ontario, Canada
2016-2020 Bachelor of Medical Sciences (BMSc)
(Honours Specialization in Microbiology and Immunology)

Honours and Awards: CIHR - Canada Graduate Scholarship - Master's
2021-2022

Related Work Experience Teaching Assistant - MICROIMM3610 (Microbiology Laboratory)
The University of Western Ontario
2021-2022

Publications:

Buchanan LB, Shao Z, Jiang YC, Lai A, Hope TJ, Carias AM, et al. Quantitative Immunofluorescent Imaging of Immune Cells in Mucosal Tissues. *Methods Mol Biol.* 2022;2440:143–64.

Mohammadi A, Bagherichimeh S, Choi Y, Fazel A, Tevlin E, Huibner S, Shao Z, Zuanazzi D, Prodger JL, Good SV, Tharao W, Kaul R. Insertive condom-protected and condomless vaginal sex both have a profound impact on the penile immune correlates of HIV susceptibility. *PLoS Pathog.* 2022 Jan 4;18(1):e1009948. doi: 10.1371/journal.ppat.1009948. PMID: 34982799; PMCID: PMC8769335.